

การศึกษาผลของการดูซับต่อปฏิกิริยาการย่อยสลายที่เร่งด้วยแสงของสารปราบวัชพืช
ชนิดพินิลยูเรียบนซิงค์ออกไซด์



นางสาวสุทธาภรณ์ มีผล

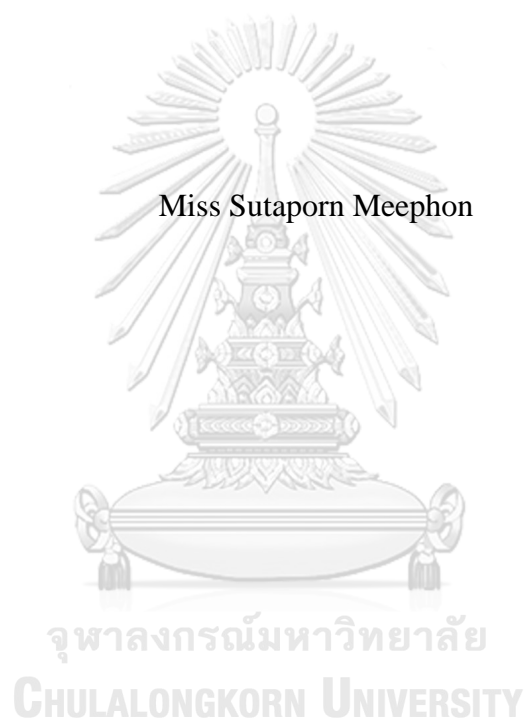
บทคัดย่อและแฟ้มข้อมูลฉบับเต็มของวิทยานิพนธ์ตั้งแต่ปีการศึกษา 2554 ที่ให้บริการในคลังปัญญาจุฬาฯ (CUIR)
เป็นแฟ้มข้อมูลของนิสิตเจ้าของวิทยานิพนธ์ ที่ส่งผ่านทางบัณฑิตวิทยาลัย

The abstract and full text of theses from the academic year 2011 in Chulalongkorn University Intellectual Repository (CUIR)
are the thesis authors' files submitted through the University Graduate School.

วิทยานิพนธ์นี้เป็นส่วนหนึ่งของการศึกษาตามหลักสูตรปริญญาวิทยาศาสตรดุษฎีบัณฑิต
สาขาวิชาวิศวกรรมเคมี ภาควิชาวิศวกรรมเคมี
คณะวิศวกรรมศาสตร์ จุฬาลงกรณ์มหาวิทยาลัย
ปีการศึกษา 2560
ลิขสิทธิ์ของจุฬาลงกรณ์มหาวิทยาลัย

THE EFFECT OF ADSORPTION ON PHOTOCATALYTIC DEGRADATION OF
PHENYL UREA HERBICIDES ON ZINC OXIDE

Miss Sutaporn Meephon



A Dissertation Submitted in Partial Fulfillment of the Requirements
for the Degree of Doctor of Engineering Program in Chemical Engineering

Department of Chemical Engineering

Faculty of Engineering

Chulalongkorn University

Academic Year 2017

Copyright of Chulalongkorn University

Thesis Title THE EFFECT OF ADSORPTION ON
PHOTOCATALYTIC DEGRADATION OF
PHENYL UREA HERBICIDES ON ZINC
OXIDE

By Miss Sutaporn Meephon

Field of Study Chemical Engineering

Thesis Advisor Associate Professor Varong Pavarajarn, Ph.D.

Accepted by the Faculty of Engineering, Chulalongkorn University in
Partial Fulfillment of the Requirements for the Doctoral Degree

.....
Dean of the Faculty of Engineering
(Associate Professor Associate Professor Supot Teachavorasinskun,
D.Eng.)

THESIS COMMITTEE

..... Chairman
(Associate Professor Tawatchai Charinpanitkul, D.Eng.)

..... Thesis Advisor
(Associate Professor Varong Pavarajarn, Ph.D.)

..... Examiner
(Chalida Klaysom, Ph.D.)

..... Examiner
(Akawat Sirisuk, Ph.D.)

..... Examiner
(Assistant Professor Thanyada Rungrotmongkol, Ph.D.)

..... External Examiner
(Chanchana Thanachayanont, Ph.D.)

สุทธาภรณ์ มีผล : การศึกษาผลของการดูดซับต่อปฏิกิริยาการย่อยสลายที่เร่งด้วยแสงของสารปราบวัชพืชชนิดฟิโนลยูเรียบนซิงค์ออกไซด์ (THE EFFECT OF ADSORPTION ON PHOTOCATALYTIC DEGRADATION OF PHENYL UREA HERBICIDES ON ZINC OXIDE) อ.ที่ปรึกษาวิทยานิพนธ์หลัก: รศ. ดร.วรงค์ ปวารจารย์, 137 หน้า.

ผลของการดูดซับต่อปฏิกิริยาการย่อยสลายที่เร่งด้วยแสงถูกศึกษาโดยใช้ซิงค์ออกไซด์ที่มีลักษณะพื้นฐานและพื้นผิวภายนอกต่างกันเป็นตัวเร่งปฏิกิริยา พื้นผิวมีขั้วซิงค์และพื้นผิวมีขั้วออกซิเจนเป็นระนาบหลักที่ครอบคลุมบริเวณด้านบนและล่างของซิงค์ออกไซด์ชนิดอนุภาค ในขณะที่พื้นผิวไม่มีขั้วผสมเป็นระนาบหลักด้านข้างของซิงค์ออกไซด์ชนิดแท่งขนาดนาโน พื้นผิวเหล่านี้ส่งผลต่อพฤติกรรมดูดซับของสารปราบวัชพืชชนิดฟิโนลยูเรีย ได้แก่ ไคยอรอน ลินูรอน และ ไดคลอโรนิลีน และส่งผลต่ออัตราการย่อยสลายที่เร่งด้วยแสงและสารมัธยันตร์ที่เกิดในระหว่างกระบวนการย่อยสลาย ความสามารถในการดูดซับของซิงค์ออกไซด์ชนิดอนุภาคมากกว่าของซิงค์ออกไซด์ชนิดแท่งขนาดนาโนประมาณสองเท่า แม้ว่าพื้นที่ผิวของซิงค์ออกไซด์ชนิดอนุภาคน้อยกว่าพื้นที่ผิวของซิงค์ออกไซด์ชนิดแท่งขนาดนาโนถึงสิบเท่าก็ตาม ทั้งนี้เป็นเพราะปริมาณตำแหน่งดูดซับที่มากกว่าและความชอบในการดูดซับของพื้นผิวมีขั้ว อย่างไรก็ตามขอบเขตของปฏิกิริยาการย่อยสลายที่เร่งด้วยแสงบนทั้งสองรูปแบบของซิงค์ออกไซด์ไม่มีความแตกต่างกันอย่างมีนัยสำคัญ นอกจากนี้ลักษณะการดูดซับของสารปราบวัชพืชบนพื้นผิวของซิงค์ออกไซด์ยังส่งผลต่อประสิทธิภาพในการย่อยสลายอีกด้วย สารมัธยันตร์ที่ถูกตรวจพบแม้ที่ระยะเวลาทำปฏิกิริยาที่สั้นที่สุดขึ้นอยู่กับพฤติกรรมดูดซับของสารปราบวัชพืช การเข้าทำปฏิกิริยาของไฮดรอกซิลเรดิคัลเกิดขึ้นที่ตำแหน่งที่ถูกดูดซับ ดังนั้นการวางตัวที่แตกต่างกันจะส่งผลทำให้เกิดสารมัธยันตร์ที่มีความหลากหลาย ความเป็นพิษของสารมัธยันตร์ถูกประเมินและพบว่าสารมัธยันตร์ที่เกิดบนซิงค์ออกไซด์ชนิดแท่งขนาดนาโนมีความเป็นพิษน้อยกว่าที่เกิดบนซิงค์ออกไซด์ชนิดอนุภาค

ภาควิชา วิศวกรรมเคมี

ลายมือชื่อนิสิต

สาขาวิชา วิศวกรรมเคมี

ลายมือชื่อ อ.ที่ปรึกษาหลัก

ปีการศึกษา 2560

5571422721 : MAJOR CHEMICAL ENGINEERING

KEYWORDS: ZINC OXIDE, ADSORPTION, POLAR SURFACE, NON-POLAR SURFACE, PHOTOCATALYTIC DEGRADATION, INTERMEDIATE, 137 TOXICITY

SUTAPORN MEEPHON: THE EFFECT OF ADSORPTION ON PHOTOCATALYTIC DEGRADATION OF PHENYL UREA HERBICIDES ON ZINC OXIDE. ADVISOR: ASSOC. PROF. VARONG PAVARAJARN, Ph.D., pp.

The effect of adsorption on photocatalytic degradation was studied by using zinc oxide with different morphologies and exposed surfaces as the photocatalyst. Polar zinc-terminated surface and polar oxygen-terminated surface are dominating planes on the top and bottom of a crystal of ZnO conventional particles, while non-polar surface is the main plane on the side of ZnO nanorods. These surfaces affect the adsorption behavior of phenylurea herbicides, i.e. diuron, linuron and 3,4-dichloroaniline. Consequently, they cause the difference in photocatalytic degradation rate and intermediate products formed during the degradation. The adsorption capacity of ZnO conventional particles is about twice as high as that of ZnO nanorods although the surfaces area of the ZnO conventional particles is one order of magnitude less than that of ZnO nanorods because of the greater amount of adsorption sites and affinity of the polar surfaces. However, the extents of the photocatalytic degradation achieved by two forms of ZnO are insignificantly different. In addition, the adsorption configuration of the herbicides on the surface of ZnO also affects the performance in degradation. The intermediates detected even at the shortest residence time investigated depend on the adsorption behavior of the herbicides. The attack of hydroxyl radicals occur on adsorbed position. Therefore, the different alignment on the surface results in variation in intermediates. The toxicity of intermediates were assessed and were found that intermediates produced on ZnO nanorods is less toxic than that on ZnO powder.

Department: Chemical Engineering Student's Signature

Field of Study: Chemical Engineering Advisor's Signature

Academic Year: 2017

ACKNOWLEDGEMENTS

The author would like to express her highest gratitude to Assoc. Prof. Dr. Varong Pavarajarn, her research advisor, for his patient guidance, inspiration, assistance and valuable support throughout her research study. Besides her advisor, the author would like to thank Asst. Prof. Thanyada Rungrotmongkol for her extensive knowledge, technical advice and support in molecular simulation.

Most of all, the author would like to express her highest gratitude to her beloved family for their useful advice, encouragement and continuous support during her Ph.D. study. Special thanks should be given to Mr. Hattachai Aeowjaroenlap for his support in workstation and resources for modelling and simulation tasks.

Finally, grateful thanks to all academic staffs, technical staffs and colleagues at Center of Excellence in Particle Technology, Department of Chemical Engineering, Chulalongkorn University for their assistance and valuable advice.

CONTENTS

	Page
THAI ABSTRACT	iv
ENGLISH ABSTRACT.....	v
ACKNOWLEDGEMENTS.....	vi
CONTENTS.....	vii
LIST OF FIGURES	x
LIST OF TABLES	xiv
Chapter 1 INTRODUCTION.....	1
Chapter 2 THEORY AND LITERATURE REVIEWS.....	3
2.1 Herbicides	3
2.1.1 Diuron.....	3
2.1.2 Linuron	4
2.1.3 3, 4-dichloroaniline (DCA)	7
2.2 Catalyst	8
2.2.1 ZnO.....	8
2.2.2 Synthesis of ZnO	12
2.2.2.1 Sol-gel method	12
2.2.2.2 Hydrothermal method.....	14
2.3 Adsorption	15
2.3.1 Adsorption isotherm.....	16
2.3.2 Modeling of the isotherm	18
2.4 Photocatalytic degradation reaction.....	20
2.5 Intermediates from photocatalytic degradation of diuron and linuron	24
2.6 Simulation of adsorption.....	29
2.7 Toxicity.....	32
Chapter 3 EXPERIMENTAL	33
3.1 Materials	33
3.2 Preparation of ZnO catalyst	33
3.2.1. ZnO powder.....	33

	Page
3.2.2. ZnO nanorods	33
3.2.3 ZnO thin film.....	34
3.3 Characterizations of ZnO.....	34
3.4 Experimental adsorption.....	35
3.4.1 Experimental adsorption.....	35
3.4.2 Simulated calculation	36
3.5 Photocatalytic degradation in micro-reactor.....	36
3.6 Toxicity test	38
3.6.1 Phytotoxicity test.....	38
3.6.2 Cytogenotoxicity test.....	38
Chapter 4 RESULTS AND DISCUSSION	40
4.1 Characterization of ZnO catalyst.....	40
4.2 Adsorption studies	46
4.2.1. Effect of surfaces of ZnO.....	46
4.2.2. Effect of pH.....	60
4.2.3 Adsorption in aqueous system.....	67
4.3 Photocatalytic degradation.....	75
4.3.1 Effect of morphology of ZnO.....	76
4.3.2 Effect of pH.....	79
4.4 Photodegraded intermediated	80
4.4.1 Effect of surface on photodegraded intermediates	80
4.4.2 Effect of pH on Photodegraded intermediates	84
4.5 Toxicity test	88
4.5.1. Effect of surface on toxicity	88
4.5.2 Effect of pH on toxicity.....	95
Chapter 5 CONCLUSIONS.....	102
5.1 Summary of findings	102
5.2 Conclusions.....	102
5.3 Recommendations.....	103

	Page
REFERENCES	104
APPENDIX A.....	115
APPENDIX B.....	117
APPENDIX C.....	120
APPENDIX D.....	123
APPENDIX E.....	124
APPENDIX F.....	136
VITA.....	137



LIST OF FIGURES

Figure 2.1 The structure of zinc oxide; cubic rocksalt (a), cubic zinc blende (b) and hexagonal wurtzite (c) [21]. The black balls represent Zn atoms and the gray balls represent O atoms.	9
Figure 2.2 The morphology of ZnO particle. The end faces are corresponding to the zinc-terminated and oxygen-terminated surface and the side faces are corresponding to the mixed-terminated ZnO (1010) surfaces [14]. The gray balls represent Zn atoms and the red balls represent O atoms.	11
Figure 2.3 The mixed terminated ZnO (1010)-surface (a) and the mixed terminated ZnO (1120)-surface (b) [14]. The gray balls represent Zn atoms and the red balls represent O atoms.	11
Figure 2.4 The zinc-terminated ZnO (0001)-surface (a) and the oxygen-terminated ZnO (000 $\bar{1}$)-surface (b) [14]. The gray ball represent Zn atoms and the red ball represent O atoms.	12
Figure 2.5 The sol-gel process diagram of ZnO preparation.	13
Figure 2.6 The category of adsorption isotherm; the “C” isotherm (a), the “L” isotherm (b), the “H” isotherm (c) and the “S” isotherm (d) [41].	17
Figure 2.7 Photocatalysis mechanism scheme of semiconductor catalyst.....	21
Figure 2.8 Pathway and intermediates formed in photo-oxidative process of diuron [49]......	24
Figure 2.9 Degradation pathways of linuron in both Vis/TiO ₂ /H ₂ O ₂ and UV/TiO ₂ systems (dash line represent reactants that could more one step to reach the products) [51]......	26
Figure 2.10 configuration for the adsorbed octyltrihydroxysilane (a), butyltrihydroxysilane (b), aminopropyltrihydroxysilane (c) and thiolpropylhydroxysilane (d) [53]......	30
Figure 2.11 configuration of octyltrihydroxysilane (a) and aminopropyltrihydroxysilane (b) on the polar zinc oxide [53]......	31
Figure 2.12 The optimized adsorption structure of urea molecule on the mixed-terminated zinc oxide (1010) surface; the side view of M1 (a), the side view of M2 (b) and the top view of M2 (c) [54]......	31
Figure 3.1 The scheme of micro-reactor setup.	37
Figure 3.2 The setup of photocatalytic degradation in micro-reactor.....	37

Figure 4.1 The FESEM images and selected area electron diffraction (inserted image) of sol-gel synthesized catalyst (a) and hydrothermal synthesized catalyst (b).....	41
Figure 4.2 The X-ray diffraction of ZnO nanorods (a) and ZnO powder (b).	41
Figure 4.3 The Zeta potential plot of ZnO powder (black dots and line) and ZnO nanorods (white dots and black line).	42
Figure 4.4 Nitrogen adsorption isotherm of ZnO powder (black dots and line) and ZnO nanorods (white dots and black line).....	43
Figure 4.5 The absorbance spectra of ZnO powder (a) and ZnO nanorods (b).	44
Figure 4.6 The high resolution XPS spectra of Zn 2p (1) and O 1s (2) of ZnO powder (a) and ZnO nanorods (b).....	46
Figure 4.7 Freundlich isotherm fitting of diuron (a), linuron (b) and DCA (c).....	48
Figure 4.8 The adsorption models of diuron (a), linuron (b) and DCA (c) on mixed-terminated surface.....	50
Figure 4.9 The electron distribution on diuron (a), linuron (b) and DCA (c) where the red and blue color indicate the most negative and positive part on molecule, respectively.	52
Figure 4.10 The space-filling model of diuron (a), linuron (b) and DCA (c) on mixed-terminated surface.....	55
Figure 4.11 The adsorption models of diuron (a), linuron (b) and DCA (c) on zinc-terminated surface.	57
Figure 4.12 The adsorption models of diuron (a), linuron (b) and DCA (c) on oxygen-terminated surface.....	59
Figure 4.13 The adsorption models at pH4 of DCA on mixed-terminated surface (a), oxygen-terminated surface (b), diuron on mixed-terminated surface (c) and oxygen-terminated surface (c).	63
Figure 4.14 The adsorption models at pH10 of DCA on mixed-terminated surface (a), oxygen-terminated surface (b), diuron on mixed-terminated surface (c) and zinc-terminated surface (d).	65
Figure 4.15 The adsorption models of diuron (a), linuron (b) and DCA (c) on mixed-terminated surface.....	68
Figure 4.16 The adsorption models of diuron (a), linuron (b) and DCA (c) on zinc-terminated surface.	69
Figure 4.17 The adsorption models of diuron (a), linuron (b) and DCA (c) on oxygen-terminated surface.....	70

Figure 4.18 The adsorption models at pH4 of DCA on mixed-terminated surface (a), oxygen-terminated surface (b), diuron on mixed-terminated surface (c) and oxygen-terminated surface (c).	71
Figure 4.19 The adsorption models at pH10 of DCA on mixed-terminated surface (a), oxygen-terminated surface (b), diuron on mixed-terminated surface (c) and zinc-terminated surface (d).	72
Figure 4.20 The photocatalytic degradation of diuron (black), linuron (red) and DCA (blue) on ZnO powder (solid) and ZnO nanorods (dash).	77
Figure 4.21 The photocatalytic degradation of diuron on ZnO powder (solid line) and ZnO nanorods (dash line) at pH4 (black) and pH10 (red).	79
Figure 4.22 The detected intermediated from degradation of linuron at shortest residence time (1 min) on ZnO nanorods (red arrow) and ZnO powder (blue arrow). The common detected intermediates on both catalyst are presented on purple arrow.	80
Figure 4.23 The detected intermediated from degradation of diuron at shortest residence time (1 min) on ZnO nanorods (red arrow) and ZnO powder (blue arrow).	82
Figure 4.24 The intermediates formed arranged by residence time of diuron on ZnO nanorods (red box), ZnO powder (blue box) and both ZnO (purple box).	83
Figure 4.25 The intermediates formed arranged by residence time of linuron on ZnO nanorods (red box), ZnO powder (blue box) and both ZnO (purple box).	84
Figure 4.26 The detected intermediated from degradation of diuron at shortest residence time (1 min) pH4 on ZnO nanorods (red arrow) and ZnO powder (blue arrow). The common detected intermediates on both catalyst are presented on purple arrow.	85
Figure 4.27 The detected intermediated from degradation of diuron at shortest residence time (1 min) pH10 on ZnO nanorods (red arrow) and ZnO powder (blue arrow). The common detected intermediates on both catalyst are presented on purple arrow.	86
Figure 4.28 The intermediates formed arranged by residence time of diuron on ZnO nanorods (red box), ZnO powder (blue box) and both ZnO (purple box) at pH4.	87
Figure 4.29 The intermediates formed arranged by residence time of diuron on ZnO nanorods (red box), ZnO powder (blue box) and both ZnO (purple box) at pH10.	87

Figure 4.30 Phytotoxicity assessment of the degraded products from the photocatalytic degradation of diuron (striped orange bar) and DCA (striped green bar), compared with standard diuron (orange bar) and DCA (green bar).....	88
Figure 4.31 The abnormally population representative cells treated in different degraded solution of diuron in each dividing step. Treated cells in control DI water are normal cells.	93
Figure 4.32 The abnormally population representative cells treated in different degraded solution of DCA in each dividing step. Treated cells in control DI water are normal cells.	94
Figure 4.33 Phytotoxicity assessment of the degraded products from the photocatalytic degradation of diuron at pH 4 (striped red bar) and pH 10 (striped purple bar), compared with standard diuron at pH 4 (red bar) and pH 10 (purple bar).	95
Figure 4.34 The abnormally population representative cells treated in different degraded solution of diuron in each dividing step. Treated cells in control DI water are normal cells	100
Figure A1 The calibration curve of 3,4-dichloroaniline.	115
Figure A2 The calibration curve of diuron.	115
Figure A3 The calibration curve of linuron.	116
Figure B1 The variation of initial orientation of linuron on mixed-terminated surface.	117
Figure B2 The variation of initial orientation of diuron on mixed-terminated surface.....	118
Figure B3 The variation of initial orientation of 3,4-dichloroaniline.	119
Figure C1 The interaction of diuron on mixed-terminated surface.	120
Figure C2 The interaction of diuron on zinc-terminated surface.....	121
Figure C3 The interaction of diuron on oxygen-terminated surface.....	122
Figure D1 The adsorption of water on mixed-terminated surface.	123
Figure D2 The adsorption of water on zinc-terminated surface.	123
Figure D3 The adsorption of water on oxygen-terminated surface.	123

LIST OF TABLES

Table 2.1 Physical and chemical properties of diuron.	4
Table 2.2 The physical and chemical properties of linuron.	6
Table 2.3 The physical and chemical properties of 3,4-dichloroaniline.	8
Table 2.4 Physical and chemical properties of wurtzite ZnO [24].	10
Table 2.5 The comparison between the physisorption and the chemisorption [40]. ...	16
Table 2.6 The formula of adsorption model [42].	20
Table 2.7 The possible intermediate products from the photocatalytic degradation of diuron and linuron using ZnO and TiO ₂ as catalyst.	27
Table 2.8 The interaction energy of the silane molecules.	29
Table 4.1 The fitted parameters for Freundlich isotherm model.	49
Table 4.2 The adsorption energy from calculation.	51
Table 4.3 The fitted parameters for Freundlich isotherm model at various pH.	61
Table 4.4 The adsorption energy from calculation at various pH.	66
Table 4.5 The occupied surface area of herbicides on ZnO surface in water-soluble system.	73
Table 4.6 The adsorption energy of herbicides on ZnO surfaces in water-soluble system.	74
Table 4.7 The mitotic index, the number of chromosomal aberration and the aberration index of degraded products from diuron and DCA degradation.	91
Table 4.8 The mitotic index, the number of chromosomal aberration and the aberration index of degraded products from diuron at pH4 and pH10.	98
Table E1 Mass fraction of intermediates from degradation of linuron.	124
Table E2 Mass fraction of intermediates from degradation of diuron at pH7.	128
Table E 3 Mass fraction of intermediates from degradation of diuron at pH4 and pH10.	131

Chapter 1

INTRODUCTION

The environmental impacts in agricultural regions are caused by leaching of residual herbicides into the ground and water i.e., diuron (3-(3,4-dichlorophenyl)-1,1-dimethylurea) and linuron (3-(3,4-dichlorophenyl)-1-methoxy-1-methylurea). They are herbicides in phenyl urea family which is widely used in many countries [1-3]. Due to the stability and long half-life in environment, diuron and linuron can damage the ecosystem and cause the harmful to organisms [4].

Although several process are applied to resolve these problems [5, 6], in present, photocatalytic degradation has been still effective technique to remove undesired organic compounds. Equal or higher energies than catalyst's bandgap energy is induced to generate electron-hole pairs. In aqueous solution, the photogenerated electrons (e^-) and holes (h^+) normally transfer and react with oxygen and water molecules on catalyst surface to produce superoxide and hydroxide radicals ($O_2^{\bullet-}$ and OH^{\bullet}), respectively [7, 8]. These highly strong oxidizing radicals attack on organic compounds which results to several intermediates. Many studies have been reported different intermediates formed on the same catalyst [9-11] and some are more toxic than their parent [12, 13]. Therefore, this effect should be seriously taken into account in order to eliminate diuron and linuron and choose the most environmentally safe ways. Besides, elimination of them in different conditions may exhibit different toxicities such as acidic and basic conditions.

It is commonly known that the adsorption is dependent on the characteristic of surface and certainly, it affects the variation of intermediates formed during the degradation processes. Photocatalytic degradation is surface reaction so, herbicides adsorb on catalyst and are then attacked by active radicals. This work dedicates on the substantiation that the formation of variation intermediates is depended on the adsorption of herbicides on different surfaces. The wurtzite zinc oxide (ZnO) which is chosen for photocatalyst due to its appropriate properties consists of two types of surface; (i) zinc-terminated (0001) and oxygen-terminated ($000\bar{1}$) of polar surface which only zinc and oxygen atoms stay on the plane, respectively and are located on

both ends of column and (ii) mixed-terminated $(10\bar{1}0)$ of non-polar surface with the alternate arrangement of zinc and oxygen atoms on the plane which are on the side of hexagonal crystal [14].

ZnO is synthesized by different methods to provide different forms and surfaces, i.e. ZnO powder and ZnO nanorods. Moreover, 3, 4-dichloroaniline (DCA) which has same aromatic structure as diuron and linuron is also interestingly studied for the effect of molecular structure on adsorption and photocatalytic degradation.

The aim of this study is to study the effect of surface, molecular structure and pH on adsorption behavior, photocatalytic degradation of diuron, linuron and DCA and the formation of intermediates in degradation of diuron and linuron using ZnO as a catalyst.

This thesis consists of five chapters as follows;

Chapter 1 Introduction of this research.

Chapter 2 The literature review and thesis related theory i.e. physical and chemical properties of herbicides and ZnO, catalyst synthesis technique, adsorption process, photocatalytic degradation, the formation in photocatalytic degradation, molecular simulation and toxicity test.

Chapter 3 Chemical and experimental equipment and procedures.

Chapter 4 Results and discussion.

Chapter 5 Overall conclusions.

Chapter 2

THEORY AND LITERATURE REVIEWS

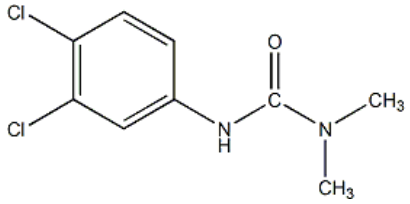
2.1 Herbicides

2.1.1 Diuron

Diuron (N-(3, 4-dichlorophenyl)-N, N-dimethylurea (C₉H₁₀Cl₂N₂O)) which is classified into phenylurea family is suitably applied for many plants. Normally, it is used by combination with other herbicides for the higher performance such as bromacil, sodium chlorate and copper sulfate. Dissolved diuron in soil can be easily taken up by root system and rapidly translocated to other parts of plant by transpiration system. Diuron effectively affects the growth of weeds by inhibiting their photosynthesis. However many plant species have the physiological adaptation to endure this group of herbicide. In term of effect on aquatic organism, diuron is moderately toxic to fish and aquatic invertebrates (LC₅₀ (48hr) is in range between 4.3-42 mg/L in fish and 1-2.5 mg/L in aquatic invertebrates). Moreover, diuron also has widespread application in non-agricultural part especially as the complement in material used in construction [15]. There has been reported the statewide used of diuron in California which is up to 1,300,000 pounds in 2002 [16].

Diuron is available in wetttable powder, flowable, pelleted or tableted, granular, liquid suspension and soluble concentrate formulations. Physical appearance of diuron is a white crystalline and odorless solid. Other physical-chemical properties are shown in Table 2.1. Diuron is stable in neutral media, moisture and oxidation state at normal temperature. In addition, it can be decomposed at 180-190°C and can be hydrolyzed by strong acidic and alkaline.

Table 2.1 Physical and chemical properties of diuron.

Properties	Data
Chemical structure	
Molecular formula	C ₉ H ₁₀ Cl ₂ N ₂ O
Molecular weight*	233.10 g/mole
Melting point	158 – 159°C
Boiling point	180 °C
Water solubility*	36.4 ppm (25° C)
Vapor pressure*	6.90 x10 ⁻⁸ mm Hg (25° C)
Density	1.48g/cm ³
Aerobic soil degradation*	372 days
Anaerobic soil degradation*	995 days
Soil photolysis half-life*	173 days
Henry's law constant*	5.10 x 10 ⁻¹⁰ atm m ³ mol ⁻¹ (25°C)

* DPR Pesticide Chemistry Database, 2003.

2.1.2 Linuron

Linuron (3-(3,4-dichlorophenyl)-1-methoxy-1-methylurea (C₉H₁₀Cl₂N₂O)) which is another herbicide in phenylurea family was first registered as a pesticide in the U.S. in 1966. Using linuron for inhibition the growth of weed can be done by two ways; (i) pre-emergence control which linuron is added to soil and the roots of weed then take it up and (ii) post-emergence control which linuron is directly sprayed to leaves and is then adsorbed and translocated to other parts of plant [17]. It has been

reported that the total quantity of produced and imported linuron is used in agriculture in California. For human, linuron can cause toxic in slightly low level by oral, dermal and inhalation routes. For aquatic organism, linuron is found to be moderated toxic to fish which it affects the fish length in early-life even in the lowest dose used. Furthermore, it cause the high toxic to aquatic invertebrates such as sheepshead minnow, oysters and mysid shrimp [18].

Generally, linuron with the half-life range between 38-67 days can be degraded in nature environment i.e. photolysis, hydrolysis and biotic processes. However, the higher toxic of transformed products, the stability of linuron in water and the long-time in degradation are the reason that render these natural degraded ways are ineffective. It found that only low amount of linuron is successful eliminated [18]. The physical and chemical properties of linuron is showed in Table 2.2.

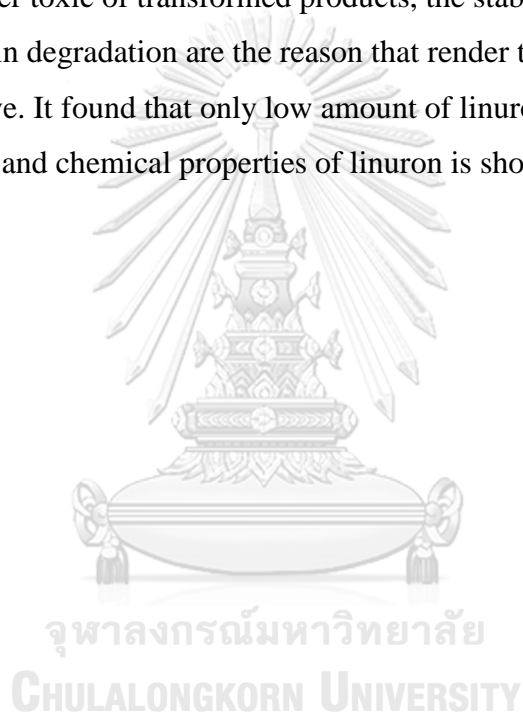
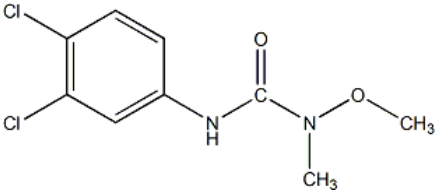


Table 2.2 The physical and chemical properties of linuron.

Properties	Data
Chemical structure	
Molecular formula ^a	C ₉ H ₁₀ Cl ₂ N ₂ O
Molecular weight ^a	249.10 g/mole
Melting point ^b	86 -91°C
Boiling point	
Water solubility ^a	81 mg/L (25° C)
Vapor pressure ^b	1.5 x 10 ⁻⁵ mm Hg
Density	
Flammability [19]	Not capable of burning.
Henry's law constant ^c	1.97 x 10 ⁻⁹ atm m ³ mol ⁻¹
Solubility in organic solvents [19]	acetone 395 g/l, 20°C acetonitrile 152 g/l, 20°C dichloromethane 463 g/l, 20°C dimethyl sulfoxide >500 g/l, 20°C ethyl acetate 292 g/l, 20°C hexane 2.3 g/l, 20°C methanol 170 g/l, 20°C 2-propanol 18 g/l, 20°C toluene 75 g/l, 20°C

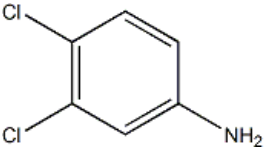
^a Kidd and James 1991^b US EPA 1995^c Hazardous Substances Data Bank

2.1.3 3, 4-dichloroaniline (DCA)

3,4-dichloroaniline (DCA) is used for an intermediate in many chemicals synthesis i.e. phenylurea herbicides (such as diuron and linuron), propanil herbicide and an azo dye for polyester fabrics. In addition, DCA can also be formed by biodegradation of several phenylurea, phenylcarbanates and acylanilide herbicides. Normally, DCA has not been used directly or without chemical transformation. It has been reported that the production of DCA in Western Europe is up to 13,500-15,500 tons/annum and the exported amount is 3,750-4,600 tons/annum in 1996-1998 [20]. The physical and chemical properties of 3,4-dichloroaniline are showed in Table 2.3.

When DCA is released to soil or sediment during using of herbicides, it will be mobile for a few hours and DCA-humic acid-complexes will be formed under the environment conditions after 1-2 days. For the human health, DCA can be absorbed through the gastrointestinal system, skin and lungs. The total daily intake of DCA for oral exposure via drinking water, fish and from plants has been calculated to amount up to about 4×10^{-3} mg/kg bw/day. Moreover, under unprotected condition, the level of 26-260 mg/person/day is available expose to worker. For mammals, DCA can cause acute dermal toxicity to rabbits and acute inhalation to rats. For the effect of DCA in short and long term tests with fish, Daphnids are the most responsive species to DCA which their LC_{50} values are found to be 0.23 mg/l for 48-hour and 0.16 mg/l for 96-hour [20].

Table 2.3 The physical and chemical properties of 3,4-dichloroaniline.

Properties	Data
Chemical structure	
Molecular formula	C ₆ H ₅ Cl ₂ N
Molecular weight ^a	162.02 g/mole
Melting point ^b	69-71 °C
Boiling point ^b	272 °C
Water solubility ^b	0.06 g/100 mL
Vapor pressure	0.0±0.6 mm Hg at 25°C
Density ^b	1.34 g/cm ³
Flammability ^c	> 600 °C at 1013 hPa
Solubility in organic solvents ^c	DMSO ≥ 100 g/L at 22 °C Acetone ≥ 100 g/ at 22 °C Ethanol ≥ 100 g/ at 22 °C

^a PPDB Pesticide Properties Database

^b World of chemicals

^c HCS The Hazard Communication Standard

2.2 Catalyst

2.2.1 ZnO

Zinc Oxide (ZnO) is a metal oxide compound. It is found that ZnO is used as a component material in many products in daily life such as white pigment in painting and coloring paper, antiseptic in wound-treatment in medical area, front electrode from transparent conducting oxide layers, sensor for hydrogen and carbon hydrides, accelerator for Sulphur-induced vulcanization and rubber improvement in chemical

process. By its unique properties, ZnO has been developed for value adding in versatile applications. For example, ZnO which has the high mobility is used instead of amorphous silicon and GaN to produce an active channel in invisible thin film transistors and UV emitting phosphor, respectively. Besides, it is also used for heterogeneous composite catalyst i.e. Cu/ZnO/Al₂O₃ in methanol synthesis process which is the important industry.

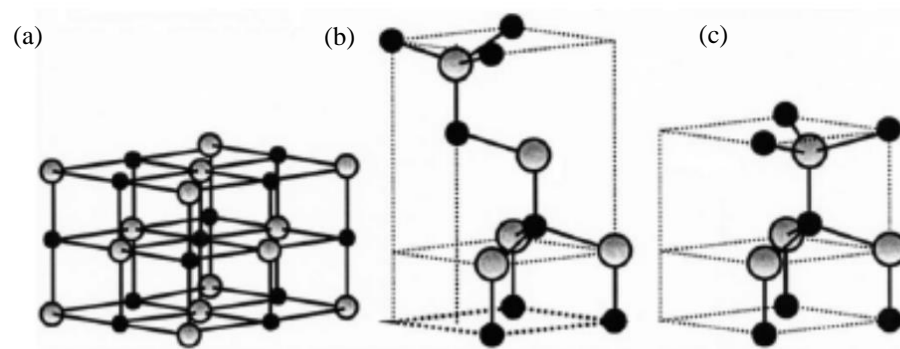


Figure 2.1 The structure of zinc oxide; cubic rocksalt (a), cubic zinc blende (b) and hexagonal wurtzite (c) [21]. The black balls represent Zn atoms and the gray balls represent O atoms.

The bandgap of ZnO is 3.4 eV. ZnO consists of three structure as shown in Figure 2.1; (i) zincblende is formed by the growth of ZnO on cubic substrate, (ii) rocksalt is obtained at high pressure condition and (iii) wurtzite is stable phase at ambient condition [22, 23]. Each structure of ZnO is suitable for special applications, but in this research, wurtzite with the lattice spacing $a = b = 0.325$ nm and $c = 0.521$ nm is interesting due to the appropriate property of photocatalyst. Table 2.4 shows the physical and chemical properties of wurtzite ZnO.

Table 2.4 Physical and chemical properties of wurtzite ZnO [24].

Properties	Data
Molecular formula	ZnO
Molecular weight	81.38 g/mole
Lattice parameters at 300 K*	
a	0.32469 nm
c	0.52069 nm
a/c	1.602
Density	5.606 g cm ⁻³
Melting point	1970-1975 °C (decompose)
Thermal conductivity	130 W/m K
Energy gap	3.4 eV
Relative dielectric constant	8.66
Excitation binding energy	60 meV
Appearance	White solid
Synonyms	Zinc white, Zinc flower, Calamine, C.I. pigment, white 4
Solubility*	Insoluble in water and alcohols Soluble in acid and bases
Physicochemical stability	Stable under normal conditions of handling and storage.

* NIOSH National Institute for Occupational Safety and Health

The surfaces of ZnO in wurtzite phase can classify into two main types; (i) non-polar consists of mixed-terminated (10 $\bar{1}$ 0)-surface and mixed-terminated (11 $\bar{2}$ 0)-surface and (ii) polar surfaces consists of zinc-terminated ZnO (0001)-surface and oxygen-terminated ZnO (000 $\bar{1}$)-surface as shown in Figure 2.2.

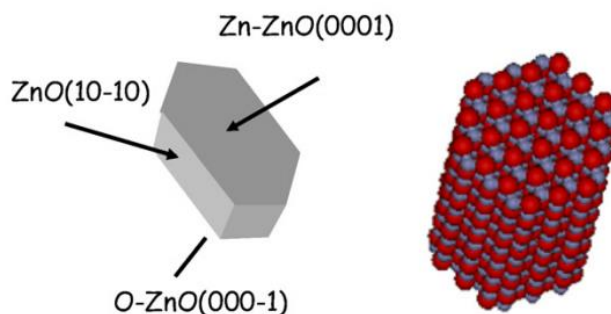


Figure 2.2 The morphology of ZnO particle. The end faces are corresponding to the zinc-terminated and oxygen-terminated surface and the side faces are corresponding to the mixed-terminated ZnO ($10\bar{1}0$) surfaces [14]. The gray balls represent Zn atoms and the red balls represent O atoms.

There are equal number of zinc (Zn) and oxygen (O) atoms on surface of mixed-terminated. Due to the balance of Zn and O atoms, non-polar surfaces have no electrostatic instabilities and have lower surface free energy than the polar surfaces. The mixed-terminated ($10\bar{1}0$)-surface is the most favorable surface which can be found on side of ZnO column. In contrast, there is a few study in the ZnO ($11\bar{2}0$) surface because there is a limitation in synthesis of this surface. The characteristic of both mixed-terminated surfaces are shown in Figure 2.3. In addition, it found that the surface free energy which is indicator for disruption of intermolecular on surface of the ($10\bar{1}0$)-surface is slightly larger than that of the ($11\bar{2}0$)-surface [14].

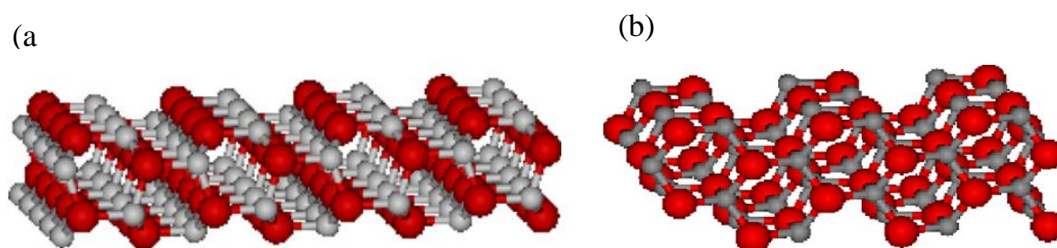


Figure 2.3 The mixed terminated ZnO ($10\bar{1}0$)-surface (a) and the mixed terminated ZnO ($11\bar{2}0$)-surface (b) [14]. The gray balls represent Zn atoms and the red balls represent O atoms.

The polar surfaces of ZnO are shown in Figure 2.4. The zinc-terminated ZnO (0001)-surface and the oxygen-terminated ZnO ($000\bar{1}$)-surface are appeared on the top and bottom of ZnO crystalline consisted only of zinc and oxygen atoms on the plane, respectively. It is found that most metal oxides undergo a structural rearrangement but there is not observation in polar surface of ZnO polar surface [14].

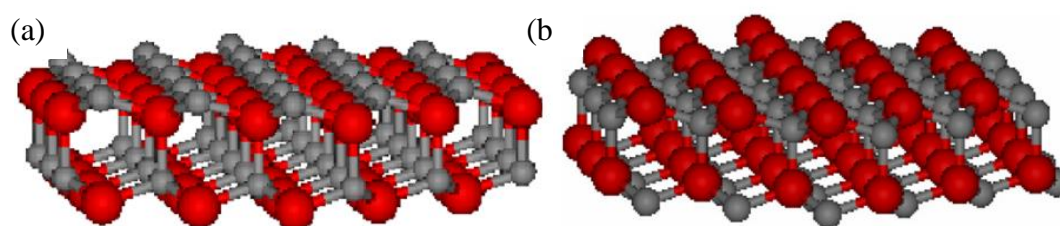


Figure 2.4 The zinc-terminated ZnO (0001)-surface (a) and the oxygen-terminated ZnO ($000\bar{1}$)-surface (b) [14]. The gray ball represent Zn atoms and the red ball represent O atoms.

2.2.2 Synthesis of ZnO

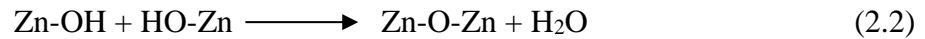
2.2.2.1 Sol-gel method

There are many researches that reported several methods of catalyst synthesis. For instance, vapor transport which vapor of zinc and oxygen are transported and reacted with each other, decomposition of ZnO which is operated at high temperature (up to 1400°C), heating up zinc powder under oxygen flowing to form ZnO nanostructure at moderate temperature ($500\text{-}700^{\circ}\text{C}$) [25, 26] or electrodeposition which is suitable for the porous ZnO [23]. It can be seen that these preparations have been complicated to operate and control the ratio between zinc and oxygen to form desired ZnO nanostructure. Apart from mentioned, sol-gel techniques is widely interested due to highly effective, stable and pure catalyst [27-32]. Therefore, it is chosen to prepare catalyst in this work. The reaction of sol-gel process is followed by Equation 2.1-2.3 and its diagram is shown in Figure 2.5.

Hydrolysis:



Condensation:



Whereas, Zn is zinc metal and OAc is acetate (alkoxyl group)

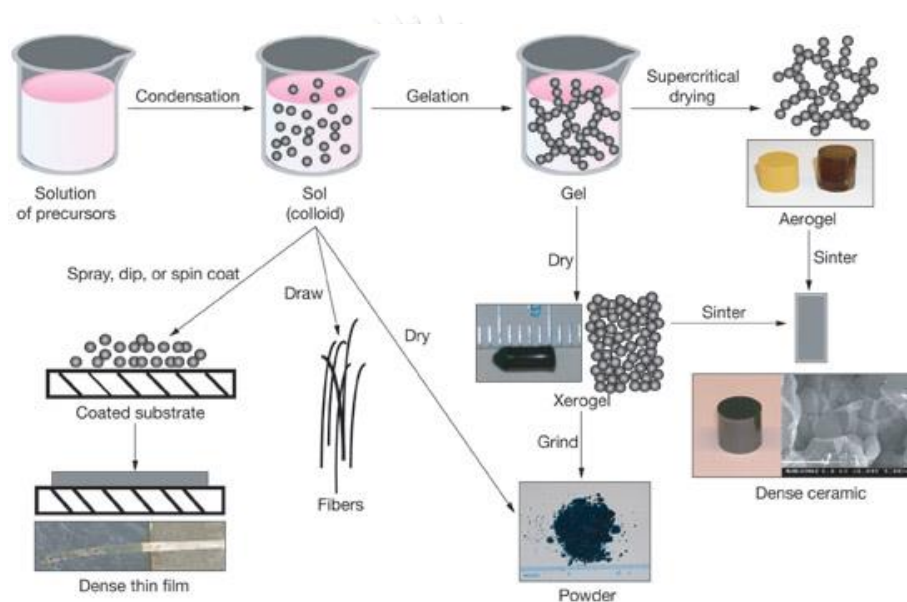


Figure 2.5 The sol-gel process diagram of ZnO preparation.

(*Novel Materials from Solgel Chemistry, 2005*)

Firstly, metal-alkoxide is hydrolyzed to obtain metal-hydroxide as a precursor solution. Secondly, the network between metal and oxygen is formed by cross-link in condensation step. When Zn-O-Zn is bonded, the colloid is observed. The sol is then aged for a period of time which result to three-dimensional linkage. Thirdly, the solvent is removed from the interconnected network, Zn-OH bonds is eliminated and the gel is obtained. Finally, the gel is heated up at high temperature in densification step. The densification temperature depends on the dimension of pore network [33].

In addition the basic concept, There are many effects in synthesized process on the properties of catalysts were studied. For example, *Hhosand Zal et al.* [34]

studied the effect of annealing temperature on particles size and band gap energy of ZnO nanoparticles which prepared by sol-gel method. Zinc acetate, pure water and diethanolamine were mixed to produce precursor solution. After the produced gel was dried, it was annealed in high temperature, i.e. 600°C, 650°C and 750°C for 1 hr. The results shows that product from sol-gel synthesis are ZnO in wurtzite phase and their shapes are nearly hexagonal plates. The particles size increase and their band gap energy decrease when the annealed temperature increase. *Seema Rani et al.* [30] report the effect of pH on crystallized size and morphology of ZnO powder synthesized by sol-gel technique. Zinc acetate dehydrate was mixed with methanol to form the sol solution. The pH values of transparent sol were varied between 6 and 11 by 0.1 N of NaOH. The largest crystallized size was found on ZnO powder formed from the sol solution at pH9. The sol solution at pH6 produces amorphous ZnO, while the crystalized size of ZnO was increased when the pH was increased from 6 to 9. The pH value higher than 9, the crystalized size was decreased again. Moreover, they found that the band gap energy of ZnO was decreased when pH was increased. *Kuo-Feng Lin et al.* [35] demonstrated the effect of concentration of precursor on the size of ZnO which was prepared by simple sol-gel method. The concentration of zinc acetated in diethylene glycol as the precursor solution was varied including 0.04, 0.06, 0.08, 0.1, 0.16 and 0.32 M. The size of ZnO was decreased and their band gap energy was increased when the concentration of zinc acetate was decreased.

2.2.2.2 Hydrothermal method

Hydrothermal is one common technique for synthesis of various nanomaterials via solution route. Nanoparticles can be synthesized into special composition, morphology and propertied which other techniques cannot prepare. Moreover, these characteristics can be easily varied by adjusting some factors such as temperature, pH, reaction time and concentration of reactants. This synthesis refers to the chemical reaction under high temperature and pressure condition within special sealed container called autoclave. Water used as a medium in reaction is important key in reaction. At high operated temperature (100-1000°C) and pressure condition, the properties of solvent of water is significantly changed such as density and viscosity will be lower and vapor pressure and ion product will be higher. Therefore, the ionic

reaction rate is accelerated and the mobility of ions is increased. This results in the higher reactivity compared with solid-state reaction [36, 37].

Normally, products from hydrothermal method is single crystals and have the high purity. Particles are formed by large influence of the growth rate. The diffusion to crystal growth is neglected due to the fast transfer of reactant in low viscosity of water-medium at hydrothermal conditions. In addition, hydrothermal techniques can be applied in synthesis of some crystals with special valence which other failed to produce by other techniques [36].

In case of ZnO, it was successfully synthesized by hydrothermal method especially for nanorods shape even in very small size. *Chen et al.* [38] vary the different concentration of zinc acetate (2, 5 and 10 mM) and reaction time (0.5-6 hr) in formation of ZnO nanostructure. The best condition to produce the ZnO nanorods with 10 ± 2 and 100 nm in diameter and length, respectively was 1mM of reactant and 3 hr of reaction time. In addition, increasing the concentration which was related to larger size of ZnO results in the red shift of absorption edge. However, the uniform of ZnO size was lacked when the concentration of zinc acetate reaches 10 mM. One-dimensional nanostructure ZnO with up to 5 μm can also be successfully prepared by *Lepot et al.* [39]. They found that even the reaction time in hydrothermal was varied from 6 to 9 hr, the particle size was not different. However, the obtained ZnO from hydrothermal with DI water as solvent achieved 5 μm in length and only 50-200 nm in diameter.

2.3 Adsorption

Adsorption is the changed concentration of substance on surface of adsorbent. Direct contact between adsorbent and adsorbate leads to the adsorption process. Generally, the substance with the low surface free energy can easily adsorb on surface while, adsorption process either difficult or cannot occur if the substance has high surface free energy. The adsorption capacity depends on many factors such as temperature, pressure and interaction potential energy between adsorbent and adsorbate.

Adsorption process can be classified into two types; (i) physical adsorption (physisorption) and (ii) chemical adsorption (chemisorption). Table 2.5 show the comparison between physisorption and chemisorption.

Table 2.5 The comparison between the physisorption and the chemisorption [40].

Parameters	chemisorption	physisorption
The energy of adsorption	50-400 kJ mol ⁻¹	≤ 20 kJ mol ⁻¹
Temperature	High	low
The interaction of molecules	Chemical bond	Van de Waals
Reversibility	Most irreversible	Reversible
Adsorption of gas onto the solid	Occur in some systems	Occur almost system
The layer of adsorption	Monolayer	Monolayer and Multilayer
Activation energy	Related	Not related

2.3.1 Adsorption isotherm

Adsorption isotherm of gas phase is the relation between the amount of adsorbed adsorbate at any temperature and the total pressure at equilibrium condition. Adsorption of liquid phase on solid surface, its isotherm is the relation between the amount of adsorbed adsorbate [Q] and the concentration of solution at equilibrium at any constant temperatures [C]. Isotherm can be classified into four types as seen in Figure 2.6 which represent the different adsorption behavior as followed [41];

a) The “C” isotherm

The graph is linear curve which intercept at origin point. This manner of graph means that the ratio between concentration of substance remaining in solution and concentration of adsorbed substance on solid surface is equal at any concentrations. It is usually applied to approximate in case of the low observed concentration.

b) The “L” isotherm

This isotherm indicates that the ratio between concentration of substance remaining in solution and concentration of adsorbed substance on solid surface is decreased when the concentration of solute increases.

c) The “H” isotherm

The characteristic of this graph is the high slope at initial part.

d) The “S” isotherm

The graph is sigmoidal so, there is an inflection point. It means that at least two opposite mechanisms include in adsorption process such as non-polar organic compounds adsorb on clays.

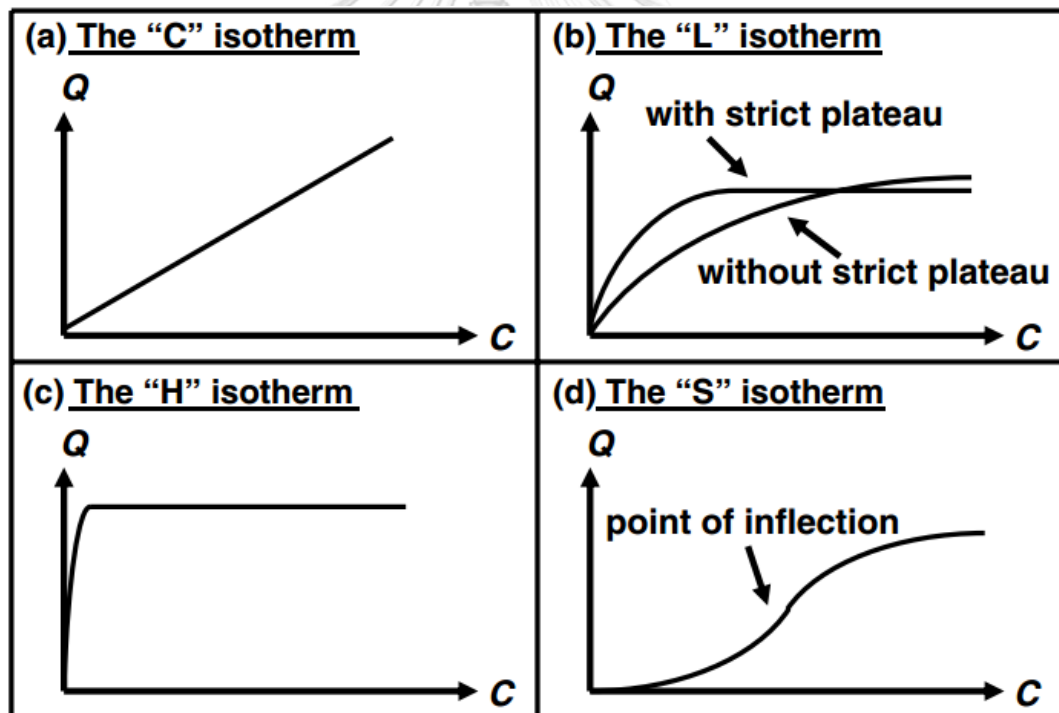


Figure 2.6 The category of adsorption isotherm; the “C” isotherm (a), the “L” isotherm (b), the “H” isotherm (c) and the “S” isotherm (d) [41].

2.3.2 Modeling of the isotherm

a) Langmuir isotherm model

This model is based on three assumptions; (i) adsorbates directly contacts with surface of adsorbent and form strong attraction, (ii) there are specific surface on adsorbent for adsorption of adsorbates and (iii) there is only one layer of adsorbed adsorbates on surface.

b) Freundlich isotherm model

This model can be applied to the multilayer of adsorption and is related to non-ideal and reversible process. The stronger adsorption sites will be first occupied by adsorbates and the adsorption curve then exponentially decrease which results to the competition in adsorption. Freundlich isotherm is usually applied to the heterogeneous system especially for the adsorption of organic compounds.

c) Dubinin-Radushkevich isotherm model

This model is used to explain the adsorption of subcritical vapor onto micropores. In addition, Gaussian energy is also brought to express the adsorption mechanism onto heterogeneous surface. This model is suitable for solute with high activity at moderate concentration. Furthermore, it can be applied to distinguish the difference between physisorption and chemisorption of metal ions. However, it lacks the precision to predict the Henry's law at low pressure.

d) Temkin isotherm model

Temkin model is suitable for the gas phase equilibrium especially for the adsorption of hydrogen onto platinum electrodes in acidic solution. It is focus only on the interaction between adsorbent and adsorbate by negligence the effect of concentration.

e) Flory-Huggins isotherm model

This model is used to express the coverage of adsorbate onto surface of adsorbent, the feasibility and the spontaneous nature of adsorption process.

f) Hill isotherm model

The assumption of this model is based on a cooperative phenomenon. The binding of ligand on one site of macromolecule may affect the other binding sites on the same macromolecule.

g) Redlich-Peterson isotherm model

This model is a hybrid model between Langmuir and Freundlich isotherm model. It can be applied for the wide range of concentration either homogeneous or heterogeneous system.

h) Sips isotherm model

This model is a combined model between Langmuir and Freundlich isotherm model that can predict heterogeneous adsorption. At the low concentration of adsorbate, the formula of this model is reduced to the Freundlich model. At the high concentration of adsorbate and the adsorption on surface is monolayer, it will be followed by Langmuir isotherm model.

i) Toth isotherm model

Toth isotherm model is developed to improve the deficiency of Langmuir model. It is suitable for heterogeneous adsorption which is satisfying at both low and high-boundary concentration.

j) Koble-Corrigan isotherm model

This model is a combined model between Langmuir and Freundlich model and can be represented the adsorption data at equilibrium condition.

k) Khan isotherm model

Khan isotherm model is a generalized model for pure solution.

l) Radke-Prausnitz isotherm model

It is a correlation model with exponential presentation.

m) Brunauer-Emmett-Teller isotherm model

Brunauer-Emmett-Teller (BET) is the theoretical model to represent the multilayer of gas-solid equilibrium systems.

From all isotherm model, the model from a) to f) are the two parameters model. The model from g) to l) are the three parameter model and the Brunauer-Emmett-Teller model is the physisorption isotherm [42, 43]. The list of equation isotherm models are showed in Table 2.6.

Table 2.6 The formula of adsorption model [42].

Isotherm	Nonlinear form	Linear form	Plot
Langmuir	$q_e = \frac{Q_0 b C_e}{1 + b C_e}$	$\frac{C_e}{q_e} = \frac{1}{b Q_0} + \frac{C_e}{Q_0}$ $\frac{1}{q_e} = \frac{1}{Q_0} + \frac{1}{b Q_0 C_e}$ $q_e = Q_0 - \frac{Q_0^2}{b C_e}$ $\frac{Q_0}{C_e} = b Q_0 - b q_e$	$\frac{C_e}{q_e}$ vs C_e $\frac{1}{q_e}$ vs $\frac{1}{C_e}$ q_e vs $\frac{Q_0}{b C_e}$ $\frac{Q_0}{C_e}$ vs q_e
Freundlich	$q_e = K_F C_e^{1/n}$	$\log q_e = \log K_F + \frac{1}{n} \log C_e$	$\log q_e$ vs $\log C_e$
Dubinin–Radushkevich	$q_e = (q_s) \exp(-k_{ad} \varepsilon^2)$	$\ln(q_e) = \ln(q_s) - k_{ad} \varepsilon^2$	$\ln(q_e)$ vs ε^2
Tempkin	$q_e = \frac{RT}{b_T} \ln A_T C_e$	$q_e = \frac{RT}{b_T} \ln A_T + \left(\frac{RT}{b_T}\right) \ln C_e$	q_e vs $\ln C_e$
Flory–Huggins	$\frac{\theta}{C_0} = K_{FH}(1 - \theta)^{n_{FH}}$	$\log\left(\frac{\theta}{C_0}\right) = \log(K_{FH}) + n_{FH} \log(1 - \theta)$	$\log\left(\frac{\theta}{C_0}\right)$ vs $\log(1 - \theta)$
Hill	$q_e = \frac{q_{sH} C_e^{n_H}}{K_D + C_e^{n_H}}$	$\log\left(\frac{q_e}{q_{sH} - q_e}\right) = n_H \log(C_e) - \log(K_D)$	$\log\left(\frac{q_e}{q_{sH} - q_e}\right)$ vs $\log(C_e)$
Redlich–Peterson	$q_e = \frac{K_R C_e}{1 + a_R C_e^g}$	$\ln\left(K_R \frac{C_e}{q_e} - 1\right) = g \ln(C_e) + \ln(a_R)$	$\ln\left(K_R \frac{C_e}{q_e} - 1\right)$ vs $\ln(C_e)$
Sips	$q_e = \frac{K_S C_e^{\beta_S}}{1 + a_S C_e^{\beta_S}}$	$\beta_S \ln(C_e) = -\ln\left(\frac{K_S}{q_e}\right) + \ln(a_S)$	$\ln\left(\frac{K_S}{q_e}\right)$ vs $\ln(C_e)$
Toth	$q_e = \frac{K_T C_e}{(a_T + C_e)^{1/T}}$	$\ln\left(\frac{q_e}{K_T}\right) = \ln(C_e) - \frac{1}{T} \ln(a_T + C_e)$	$\ln\left(\frac{q_e}{K_T}\right)$ vs $\ln(C_e)$
Koble–Corrigan	$q_e = \frac{A C_e^n}{1 + B C_e^n}$	$\frac{1}{q_e} = \frac{1}{A C_e^n} + \frac{B}{A}$	-
Khan	$q_e = \frac{a_2 b_1 C_e}{(1 + b_1 C_e)^{n_K}}$	-	-
Radke–Prausnitz	$q_e = \frac{a_{RP} r_R C_e^{\beta_R}}{a_{RP} + r_R C_e^{\beta_R - 1}}$	-	-
BET	$q_e = \frac{q_s C_{BET} C_e}{(C_s - C_e) [1 + (C_{BET} - 1) C_e / C_s]}$	$\frac{C_e}{q_e(C_s - C_e)} = \frac{1}{q_s C_{BET}} + \frac{(C_{BET} - 1) C_e}{q_s C_{BET} C_s}$	$\frac{C_e}{q_e(C_s - C_e)}$ vs $\frac{C_e}{C_s}$
FHH	$\ln\left(\frac{C_e}{C_s}\right) = -\frac{q}{RT} \left(\frac{a_3}{q_e d}\right)^r$	-	-
MET	$q_e = q_s \left(\frac{k}{\ln(C_s/C_e)}\right)^{1/3}$	-	-

2.4 Photocatalytic degradation reaction

Photocatalytic process is a technology for degradation of organic contaminant compounds in environmental control. Sunlight or UV light, which is available in abundance, can be the energy source to initiate the photo-decomposition of pollutants. The end products of this treatment process are usually harmless compounds such as carbon dioxide, water and inorganic ions such as acids, chloride and nitrate.

Photocatalytic process has been widely used as an alternative physical-chemical process for the elimination of toxic and hazardous organic substances in wastewater, drinking water and air. In this process, a semi-conductor activated by ultra-violet (UV) radiation is used as a catalyst to eliminate organic contaminants.

The photocatalysis can be defined as the acceleration of photoreaction on semiconductor catalyst. This catalyst can be activated by the absorption of greater energy than its band gap's energy. When the contaminants are presented in aqueous phase and the semiconductor is solid, this process can be called heterogeneous photocatalysis process. The generations of electron-hole pairs are represented in Equation 2.4. In aqueous solution, water molecules adsorb on surface of catalyst and are oxidized by photo-generated holes giving to hydroxyl radicals ($\text{OH}\cdot$). Because the process is usually carried out in aerobic conditions, the species which are reduced by photo-generated electrons is oxygen resulting to generation of superoxide radical ($\text{O}_2^{\cdot-}$) as following Equation 2.5-2.7. Adsorbed organic pollutants are subsequently oxidized by these strong oxidizing radicals as shown in Figure 2.7.

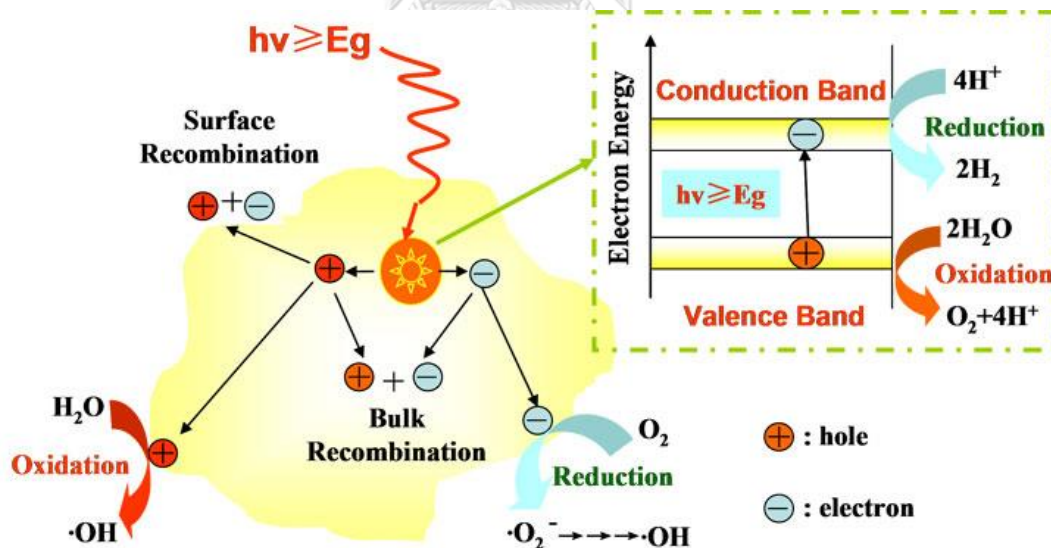
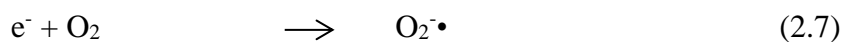
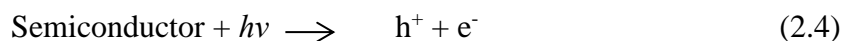


Figure 2.7 Photocatalysis mechanism scheme of semiconductor catalyst.

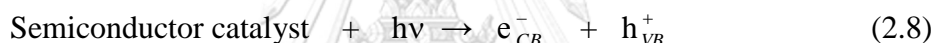
(*Prof. Jin's Laboratory, material-oriented Chemical Engineering*)



There is evidence that OH• radicals are the main reactive oxidant during the photocatalytic degradation by observation of detected intermediates of halogenated aromatic compounds. They are typically hydroxyl structures which are found when similar aromatics react with a known source of OH• radicals (*Environment Photochemistry, 1999*).

The mechanism of the photocatalytic degradation of aqueous organic compound in aqueous phase on semiconductor catalyst can be expressed by the series of advanced oxidation process as following [44].

1. Absorption of efficient photons



2. Oxygen ionosorption (first step of oxygen reduction)



3. Neutralization of OH⁻ groups by photoexcited holes



4. Neutralization of O₂^{•-} by protons



5. Transient hydrogen peroxide formation



6. Decomposition of H₂O₂ and second reduction of oxygen



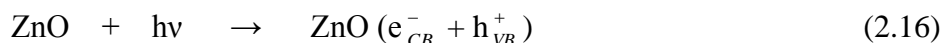
7. Oxidation of the organic reactant via successive attack by OH• radical



8. Direct oxidation by reaction with holes



The mechanisms of photocatalytic degradation on ZnO powder can be expressed by applying the research of Daneshvar [45]. The photocatalytic degradation of organic in solution is initiated by photo-excitation of semiconductor catalyst and is then followed by the transfer of electron-hole pairs to surface of catalyst as in Equation 2.16.



The high oxidative potential of the hole (h_{VB}^+) in the catalyst permits the direct oxidation of herbicide into the reactive intermediates followed by Equation 2.17.

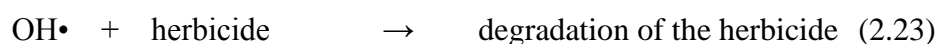
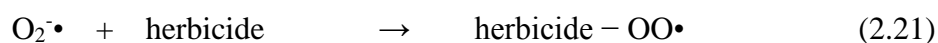
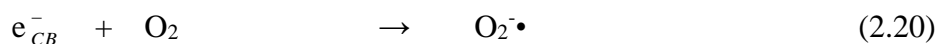


High reactive hydroxyl radicals can also be formed either by the decomposition of water (Equation 18) or by the reaction of the hole with OH^- (Equation 2.19).



The hydroxyl radical is an extremely strong, non-selective oxidant that brings about the degradation of organic chemicals as well [46, 47].

Electron in the conduction band (e_{CB}^-) can reduce molecular oxygen to superoxide anion (Equation 2.20). This radical, in the presence of organic scavengers, may form organic peroxides (Equation 2.21) or hydrogen peroxide (Equation 2.22). Electrons in the conduction band are also responsible for the production of hydroxyl radicals, which have been indicated as the primary cause of organic matter mineralization (Equation 2.23) [47, 48].



2.5 Intermediates from photocatalytic degradation of diuron and linuron

During irradiation process, diuron and linuron are degraded and several intermediate products will be formed. These products are either lower and higher molecular weight or may be more toxic than their parents. It is hence interested not only to control the degradation of parent compound but also to identify the intermediate compounds formed and assess their toxicity to environment. For example, *Hana Mestankova et al.* [49] studied the toxicity and the pathway of diuron using TiO_2 as catalyst. It was found that 3,4-dichloroaniline was the major product that had high toxicity and was easily degraded by hydroxyl radicals. The toxicity of intermediate products were compared with their parent compound. The toxicity of intermediate product was lower toxicity toward the photosynthetic organism than their parent. The loss of methyl group and decrease of aromaticity in diuron degradation process lead to a decrease in toxicity. During the process, the products formed exhibit lower toxicity toward the algae. Figure 2.8 show the diuron degradation pathway in this work.

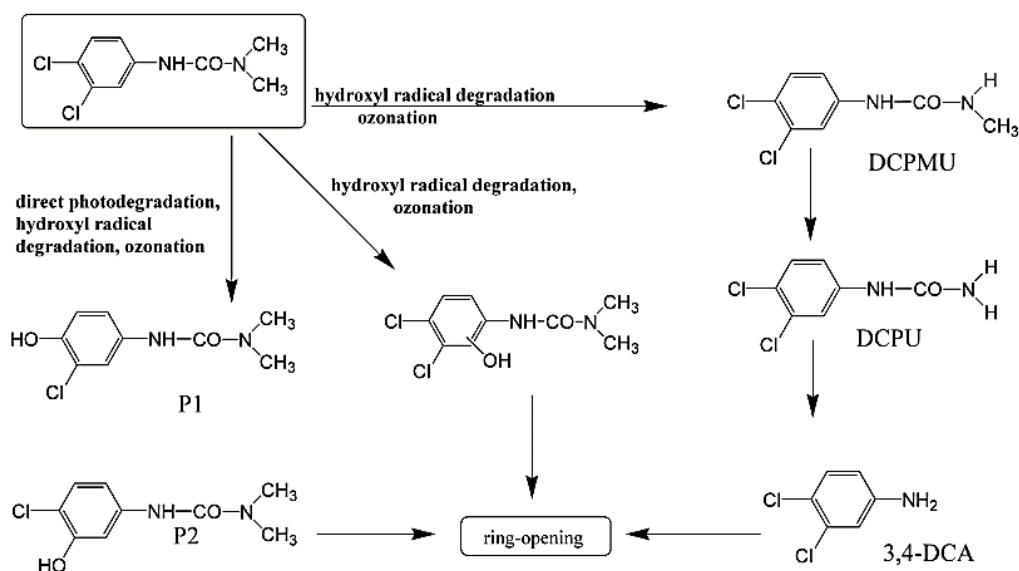


Figure 2.8 Pathway and intermediates formed in photo-oxidative process of diuron [49].

The variation of intermediated are formed in many reaction route. Therefore, there are many researches studying the formation of intermediates by proposing many possible mechanisms of degradation processes. *Moises Canle Lopez et al.* [50] studied mechanisms of UV degradation of phenylurea herbicides. In the absence of TiO_2 , the irradiation of diuron mainly yielded hydroxychloro derivatives, probably through photohydrolysis reaction. In the presence of TiO_2 (Degussa P-25), the photocatalytic degradation of diuron is proceeded by several pathway;

- (1) The oxidation of methyl group at side chain
- (2) Chlorine substitution on aromatic ring
- (3) Hydroxylation of aromatic ring
- (4) Dechlorination

Y. F. RAO and W. CHU [51] studied the reaction and mechanism of linuron degradation on TiO_2 under visible irradiation with assistance of H_2O_2 . It was found that hydroxyl radicals play an important key to degrade the organic compounds. Pathway of degradation of linuron is showed in Figure 2.9. The mechanism of degradation includes the attraction of hydroxyl radical on Cl atom, N-terminus methyl and methoxyl group.

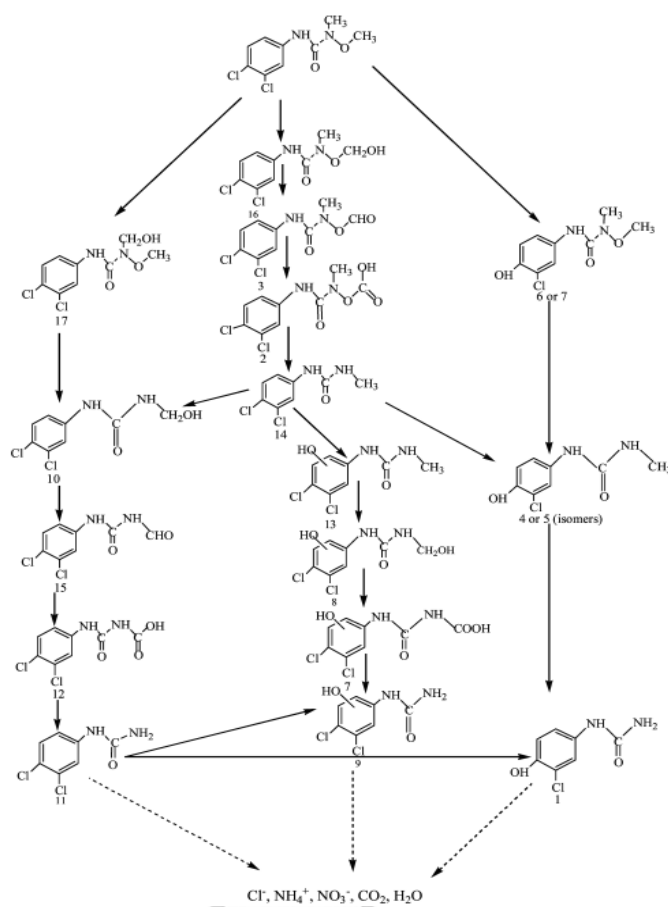


Figure 2.9 Degradation pathways of linuron in both Vis/TiO₂/H₂O₂ and UV/TiO₂ systems (dash line represent reactants that could more one step to reach the products)

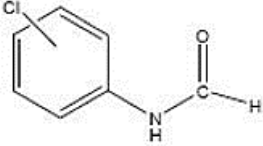
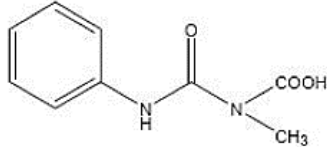
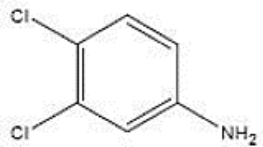
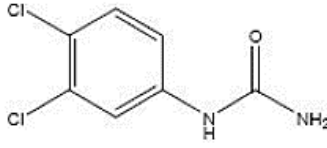
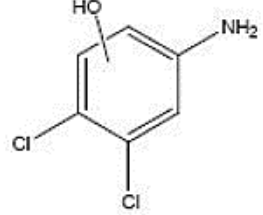
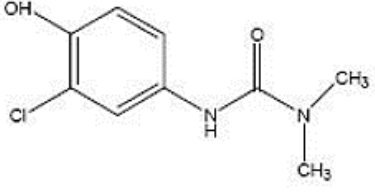
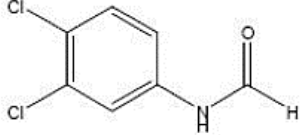
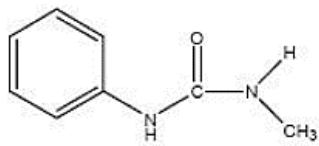
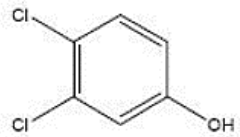
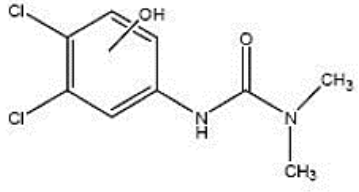
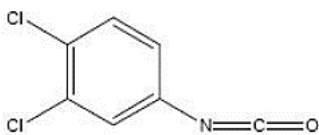
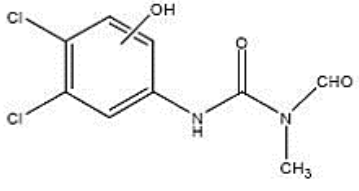
[51].

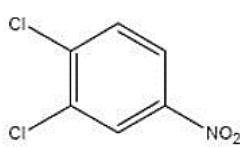
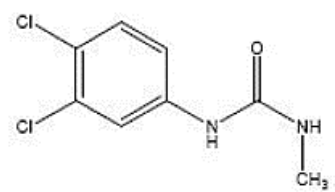
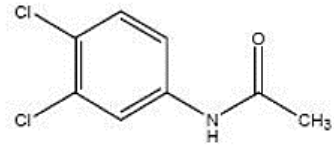
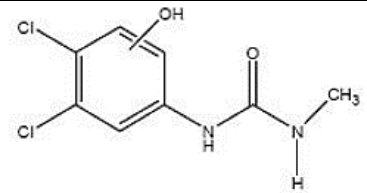
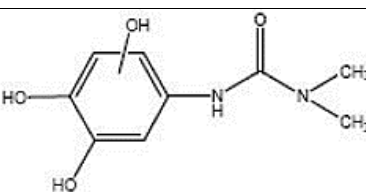
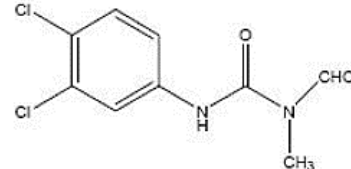
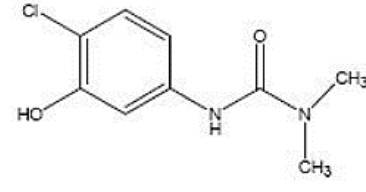
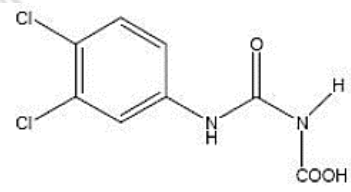
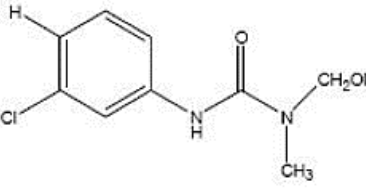
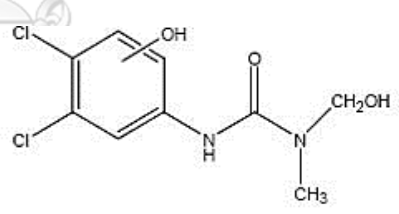
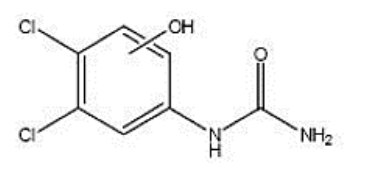
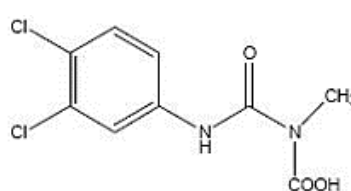
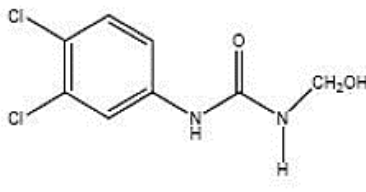
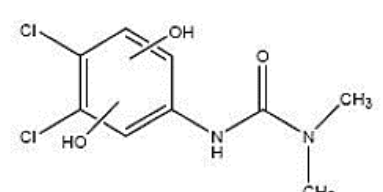
จุฬาลงกรณ์มหาวิทยาลัย

CHULALONGKORN UNIVERSITY

Table 2.7 reports the possible intermediates in photocatalytic degradation of linuron and diuron [52] from many literatures.

Table 2.7 The possible intermediate products from the photocatalytic degradation of diuron and linuron using ZnO and TiO₂ as catalyst.

Structures	
	
	
	
	
	
	

 <chem>Clc1cc(Cl)cc([N+](=O)[O-])c1</chem>	 <chem>CC(=O)Nc1cc(Cl)cc(Cl)c1</chem>
 <chem>CC(=O)Nc1cc(Cl)cc(Cl)c1</chem>	 <chem>CC(=O)Nc1cc(Cl)cc(Cl)c1</chem>
 <chem>CC(=O)Nc1cc(O)cc(O)c1O</chem>	 <chem>CC(=O)Nc1cc(Cl)cc(Cl)c1</chem>
 <chem>CC(=O)Nc1cc(Cl)ccc1O</chem>	 <chem>CC(=O)Nc1cc(Cl)cc(Cl)c1</chem>
 <chem>CC(=O)Nc1cc(Cl)ccc1O</chem>	 <chem>CC(=O)Nc1cc(Cl)cc(Cl)c1</chem>
 <chem>CC(=O)Nc1cc(Cl)ccc1O</chem>	 <chem>CC(=O)Nc1cc(Cl)cc(Cl)c1</chem>
 <chem>CC(=O)Nc1cc(Cl)cc(Cl)c1</chem>	 <chem>CC(=O)Nc1cc(Cl)cc(Cl)c1</chem>

2.6 Simulation of adsorption

Simulation will show the adsorption behavior of interested molecules on solid surface. Material Studio is molecular visualization software from Accelrys, Inc. It can simulate crystalline and amorphous materials, edit and optimize the structure, study powder diffraction and predict polymorph. This program is widely used in most researches, especially for the study of adsorption mechanism on solid surface. For example, *Andreas Kornherr et al.* [53] compared the adsorption of organosilanes on reconstructed and ideal polar zinc oxide surface. The process was operated at ambient temperature (298K). The size of simulation box was 3.3×3.4×6.8 nm which comprised 810 atoms of Zn and O. The interface was devoid from boundary effect. The first liquid layer contained one silane and 250 isopropanol molecules and second layer contained 150 isopropanol molecule. The results showed octyltrihydroxysilane and butyltrihydroxysilane adsorbed in orthogonal orientation while, thiolpropylhydroxysilane and aminopropyltrihydroxysilane adsorbed in parallel orientation as show in Figure 2.10. The interaction energy of silane molecules are showed in Table 2.8. The interaction of silane molecules on reconstruction surface which is less polar is weaker than that on the ideal surface.

Table 2.8 The interaction energy of the silane molecules.

Silane molecule	The interaction energy (kJ mol ⁻¹)	
	reconstruction	Ideal surface
octyltrihydroxysilane	-76	-192
aminopropyltrihydroxysilane	-104	-138
thiolpropylhydroxysilane	-118	-133

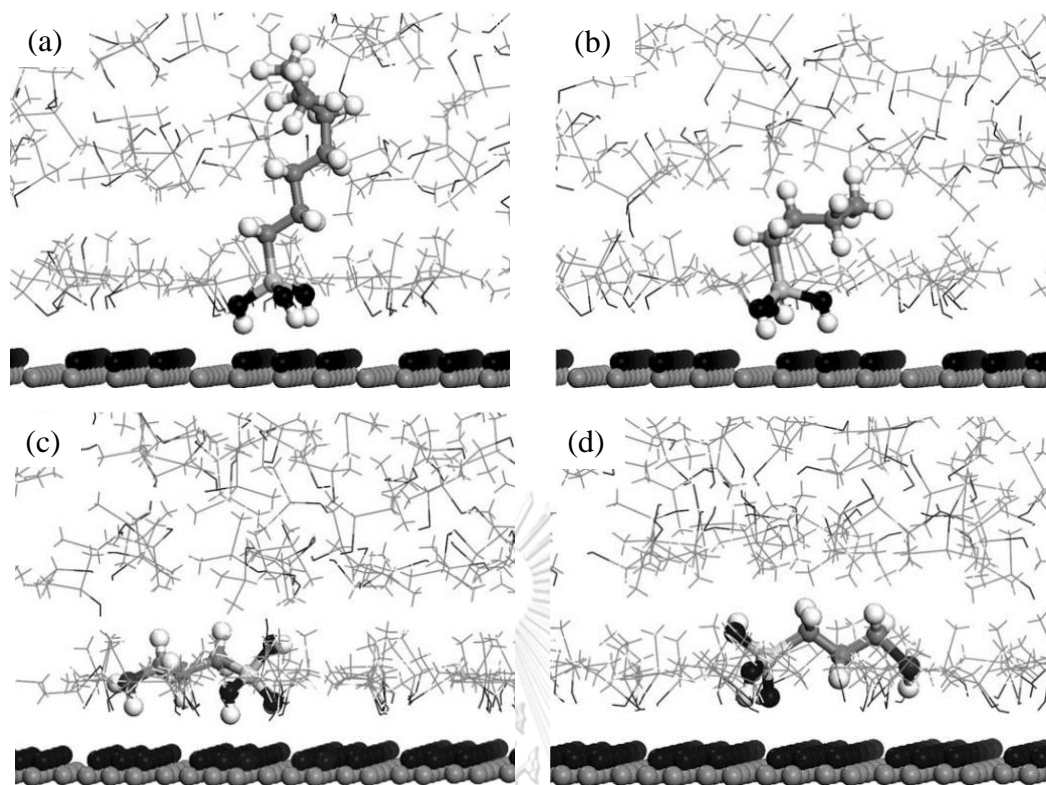


Figure 2.10 configuration for the adsorbed octyltrihydroxysilane (a), butyltrihydroxysilane (b), aminopropyltrihydroxysilane (c) and thiolpropylhydroxysilane (d) [53].

In addition, they studied the first step of the adsorption of silane molecules on polar zinc oxide surface. The simulation box consists of 50 silane and 100 isopropanol in the first layer and 150 isopropanol in the second layer. At the beginning of adsorption, most of silane molecules adsorbed on surface in orthogonal orientation and some of them adsorbed in parallel as shown in Figure 2.11. The interaction between polar surface and unpolar tail of octyl group is van der Waals, while that and polar tail i.e. aminopropyl or thiolpropyl is dipole-ion interaction. The adsorption proceeded, the competition of trihydroxy and amino groups occurred, so the adsorbed configuration of silane was a mixture of parallel and orthogonal. When the thiol group with lower polarity was taken place, the interaction between this group and polar surface was weaker compared with amino group.

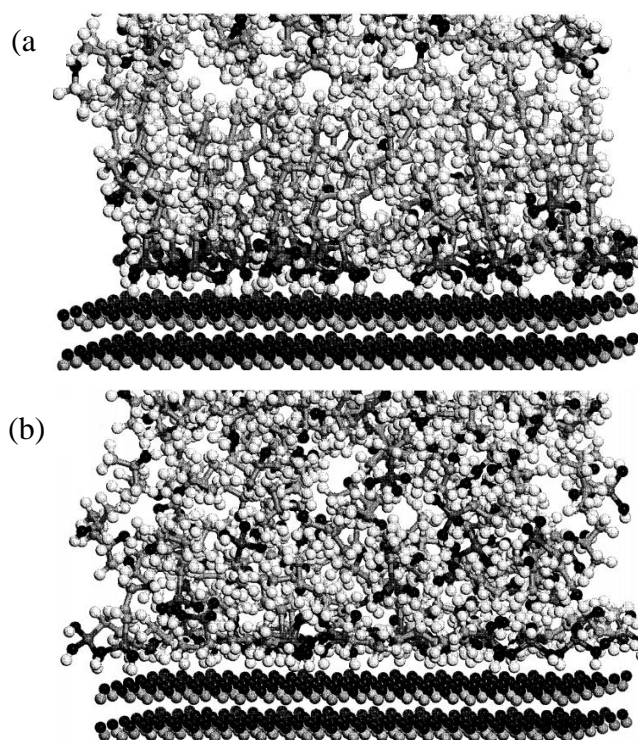


Figure 2.11 configuration of octyltrihydroxysilane (a) and amonopropyltrihydroxysilane (b) on the polar zinc oxide [53].

Yangyan Gao *et al.* [54] studied the adsorption of urea on the mixed-terminate zinc oxide surface. The result showed that urea could adsorb on either Zn or O atom. The adsorption energy of stable structure (M1) is exothermic with 37.2 kcal/mol as in Figure 2.12a. The metastalble structures (M2) of urea as shown in Figure 2.12b and c show the parallel orientation with 33.2 kcal/mol of the adsorption energy.

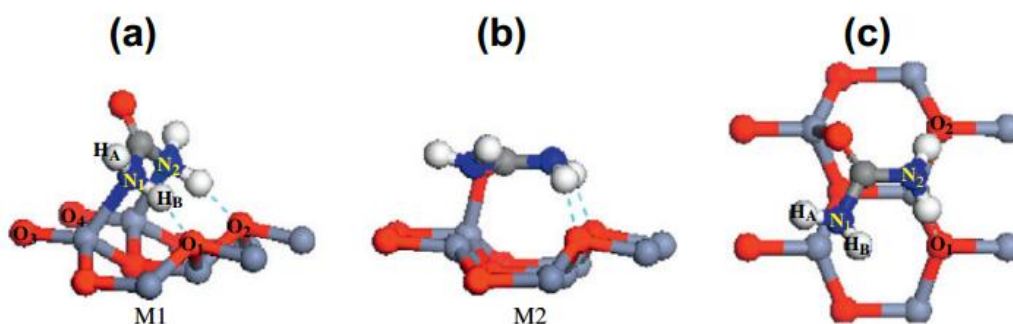


Figure 2.12 The optimized adsorption structure of urea molecule on the mixed-terminated zinc oxide ($10\bar{1}0$) surface; the side view of M1 (a), the side view of M2 (b) and the top view of M2 (c) [54].

2.7 Toxicity

Toxicology is a branch of science which study the effect of toxins and poisons including their treatments. Toxicants are generally classified based on the chemical nature, the mode of action or class. Based on class of toxicants, it can be classified into two types; (i) exposur class such as food, air, water and soil and (ii) use class such as drug agriculture chemicals, pesticides and cosmetic. Toxicity test are used to evaluate specific adverse effect or specific end point such as cardiotoxicity, irritation and cancer [55].

Merkulov et al. [56] studied the efficiency of photocatalytic degradtion, intermediate products and their toxicity of pharmaceuticals (i.e. propranolol and amitriptyline) and pesticides (i.e. sulcotrione and clomazone) using TiO_2 and TiO_2 /polyaniline composite as catalysts. The results showed phaemaceticals can be removed from environment water up to 30% on TiO_2 within 60 min of irradiation time. Meanwhile, about 90% of pesticides were also transformed on TiO_2 within 60 min of irradiation time. In addition, both initial solution and reaction mixture (after irradiation time) of pharmaceicals and pesticides are not affected cell growth inhibition higher than 50%.

Armakovic et al. [57] investigated the detailed degradation of 4-amino-6-chlorobenzene-1,3-disulfonamide (ASBA) used hydrochlorothiazode (HCTZ) as a contaminants in solution. It was found that photocatalytic degradation was the effective process to degrade ASBA by employing TiO_2 Degussa P25 catalyst. HCTZ was transformed to ABSA even in short time of hydrolysis. After 240 min of photocatalytic degradation time, 65% of ASBA was mineralized which NH^+ was found to be predominant presence in water. Toxicity assesments showed the mixture of intermediates during photocatalytic process exerted only mild cell growth while the mixture from photolysis did not affect cell growth.

Chapter 3

EXPERIMENTAL

3.1 Materials

Phenyl urea i.e. Diuron (3-(3,4-dichlorophenyl)-1,1-dimethyl urea, 99.5% purity), linuron (3-(3,4-dichlorophenyl)-1-methoxy-1-methylurea, 99.5% purity) and 3,4-dichloroaniline (99.5% purity) were purchased from Sigma-Aldrich. Acetonitrile used as mobile-phase for HPLC was HPLC grade (99.9% purity). Other chemicals used in this research were AR grade. The soda-lime glasses for catalyst coating and micro-reactor fabrication were firstly washed by sonication in distilled water, ethanol and acetone, respectively for 1 hr in each solution before using in experiment.

3.2 Preparation of ZnO catalyst

3.2.1. ZnO powder

ZnO powder was prepared via sol-gel techniques. Firstly, 3.29 g of zinc acetate was dissolve in 20 ml of ethanol to produce precursor solution. Secondly, 0.26 ml of distilled water, 0.18 ml of hydrochloric acid, 1.58 ml of diethanolamine and 5 ml of ethanol were mixed together and were slowly dropped into the precursor solution under a stirring. The solution was continuously stirred for 2 hrs to achieve the transparent sol and was then aged at room temperature for 24 hrs. Fourthly, the transparent ZnO sol was dried at 80°C for 24 hrs to form the gel and was again aged at room temperature for 3 days. Lastly, the ZnO gel was calcined at 500°C for 4 hrs in furnace with 10°C/min of heating rate. After calcination, solid of ZnO powder was formed.

3.2.2. ZnO nanorods

ZnO nanorods was synthesized by hydrothermal method. Firstly, a precursor solution was prepared by dissolving 1.1 g of zinc acetate in 4 ml of distilled water. Secondly, 6 ml of 8 M sodium hydroxide solution was slowly dropped in precursor

solution. Thirdly, 2 ml of mixture between zinc acetate and sodium hydroxide were mixed with 5 ml of polyethylene glycol and 20 ml of ethanol. Fourthly, this mixture was transferred to Teflon-lined autoclave and was heated to 140°C for 1 hr. Lastly, the white crystalline product was washed by ethanol and distilled water for several times to remove residual ions and organic composition and was then dried at 60°C overnight.

3.2.3 ZnO thin film

For the photocatalytic degradation of phenyl urea in micro-reactor, catalysts were coated on the glass by spin coating method. 1 g of ZnO powder and ZnO nanorods were separately suspended in 20 ml of ethanol under stirring for 30 min. The catalyst loading was controlled by the amount of droplet of catalyst mixtures on the rotated glass with the rate of 55 drops/min and 40 drops/min for ZnO nanorods and ZnO powder, respectively. ZnO catalysts will be spread over the glass by centrifugal force and was dried at 60°C overnight. The film of both ZnO catalysts on glasses with only approximate weight at 7 mg were chosen to use.

3.3 Characterizations of ZnO

After synthesis, both ZnO powder and ZnO nanorods were characterized by X-ray diffraction (XRD, Bruker AXS D8 Advance) to confirm the phase of catalysts. The diffraction angle (2θ) was recorded in the range of 20-80 degree with 0.04 degree in scan step. The morphology of catalysts were observed by field emission scanning microscopy (FESEM, JSM-7610F) and transmission electron microscopy (TEM, 2100). The FESEM was operated in high resolution and high vacuum, so the samples had to be dried before characterization. The surface area was calculated by Brunauer-Emmett-Teller model (BET, BELmax 00092). The samples weight were about 0.4 g and the adsorption temperature was 77 K. The band gap energy was calculated by Tauc plot method [58] which the wavelength was obtained from UV-visible near infrared spectrometer (UV-VIS-NIR, Cary 5000). The measurement scans the wavelength from 200 to 800 nm with 1 nm in scan step. The defects on surfaces were

verified by X-ray photoelectron spectroscopy (XPS, Kratos Axis ultra DLD). The charges on surfaces were evaluated by Zetasizer (Nanoseries S4700). The 0.1 g of catalysts were separately immersed in 10 ml of DI water and were adjusted pH by 0.1 M of HCl and 0.1 M of NaOH. The detached catalysts from the glass into solution phase were characterized by inductively coupled plasma optical emission spectrometry (ICP-OES, PerkinElmer Optima7000DV) before using. DI water was supplied to micro-reactor with the highest used flow rate (5.8 ml/hr) for 6 hr which was the real reaction time in experiments. The outlet stream will be tested.

3.4 Experimental adsorption

3.4.1 Experimental adsorption

Adsorption of diuron, linuron and DCA were carried out in batches in the dark for 6 hrs to completely reach equilibrium. The adsorption system was completely isolated from surrounding by sealing with parafilm and aluminium foil. Therefore, the systems were not affected by external environment, i.e. dissolution of CO₂ into solution which was resulted to the change of pH. The initial concentration of herbicides were separately prepared between 1 and 25 ppm. The pH of each concentration was adjusted to 4, 7 and 10 by 0.1 M of HCl and 0.1 M of NaOH. The catalyst content was 1 mg per 1 ml of solution. The experimental temperature was maintained at 25±2°C. The samples were collected at 0, 1, 3, 5, 10, 15, 20, 30, 40, 50, 60, 80, 100, 120, 150, 180, 240, 300 and 360 min and were then analyzed for the concentration by reverse-phase high performance liquid chromatography (HPLC, Shimadzu Class 10VP) with reverse phase C18 column (Luna 5µ C18, 250×4.6 mm, Phenomenex, USA). 70% (v/v) of acetonitrile with HPLC grade and 30% (v/v) of DI water were used for mobile phase. The flow rate of mobile phases were 1.5 ml/min and the wavelength of UV detector was 254 nm.

3.4.2 Simulated calculation

The adsorption mechanism of diuron, linuron and DCA were simulated using DFT calculation in Dmol³ program available in Material Studio 6.0 package (from Accelrys Inc.). The ZnO surfaces i.e. mixed-terminated (10 $\bar{1}$ 0)-surface, zinc-terminated (0001)-surface and oxygen-terminated (000 $\bar{1}$)-surface were investigated. The generalized gradient approximation (GGA) with Perdew and Wang (PW91) function was used. DNP was set up as basis set and the cutoff radius was 4.4 Å. The electron basis set was used for all element except Zn atom, which was treated by effective core potential. Electron density, Electrostatics and population analysis were chosen in properties of calculation for electron density mapping and charge distribution of phenyl urea compounds. The maximum energy change were 1×10^{-5} Hartree, the maximum force were 2×10^{-3} Hartree/Å and the maximum displacement for the geometry optimization were 5×10^{-3} Å. The adsorption energy was calculated by Equation 3.1.

$$\Delta E_{\text{ads}} = E_{\text{ZnO/phenyl urea}} - (E_{\text{ZnO}} + E_{\text{phenyl urea}}) \quad (3.1)$$

where $E_{\text{ZnO/phenyl urea}}$ = the energy of adsorption system (herbicide on surface)

E_{ZnO} = the energy of surface.

$E_{\text{phenyl urea}}$ = the energy of molecule of herbicide.

The molecular herbicide was applied in system with up to 5 Å of distance from surface in planar configuration and were allowed to freely adsorb on fixed surface. In acidic condition, surface was protonated by proton on oxygen atom. In basic condition, hydroxyl anion was left to cover on zinc atom. Due to the repulsive between anions, their alignment on surface were optimized to obtain the stable orientation.

3.5 Photocatalytic degradation in micro-reactor

Micro-reactor was fabricated for photocatalytic degradation which ZnO catalysts were deposited on one piece of glass. Another piece of blank glass was drilled for inlet-outlet stream. A Teflon sheet and Aluminium foil with predetermined

opening were placed between glasses to create micro-channel (250 micrometers) as shown in Figure 3.1.

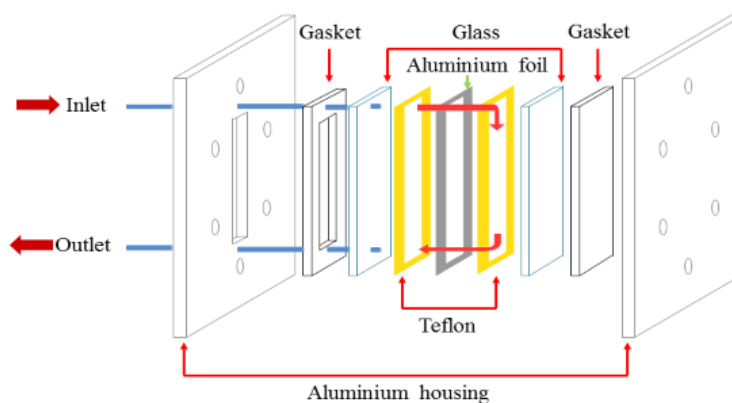


Figure 3.1 The scheme of micro-reactor setup.

The microstructure was then mounted by stainless steel housing [59] and was irradiated from outside micro-reactor by a 40 W mercury lamp (Philips F40T12/BL) with the spectrum 350-410 nm of wavelength. The length of light source is 120cm and micro-reactor will be placed at the center of UV light for the uniform energy. The length between the light source and the micro-reactor is about 10 cm. The experimental setup was shown in Figure 3.2.

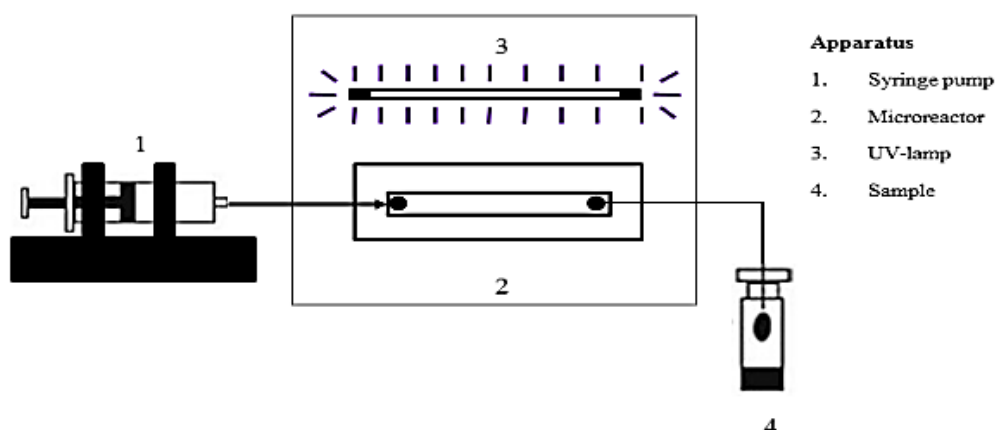


Figure 3.2 The setup of photocatalytic degradation in micro-reactor.

The UV adsorption were measured by an ILT1700 Research Radiometer (International Light Technologies) with SED005 GaAsP UV detector. It was found that some light source was absorbed by soda lime glass. The light intensity measured at the micro-reactor locates was 3.18×10^{-6} W/cm² and that measured through the glass was 2.63×10^{-7} W/cm².

Solution of herbicide with 10 ppm of initial concentration was supplied to micro-reactor for 1 hr for equilibrium adsorption before irradiation. The pH of solution was adjusted to 4, 7 and 10 by 0.1M of HCl and 0.1M of NaOH. The residence times were controlled by adjusting the flowrate, i.e. 5.8, 1.2, 0.6 and 0.4 ml/hr for the residence time of 1, 5, 10 and 15 min, respectively. The samples were collected every hour and were analyzed for the concentration by reverse-phase high performance liquid chromatography (HPLC, Shimadzu Class 10VP). The intermediates structures were identified by liquid chromatography equipped with tandem mass spectroscopy (LC-MS/MS, Thermo Finning, LCQ Advantage). Reverse phase C18 column was used with 70% (v/v) of acetonitrile and 30% (v/v) of DI water as mobile phase. The ion source was operated in positive mode.

3.6 Toxicity test

3.6.1 Phytotoxicity test

For the toxicity studies, seed of mung bean (*Vigna radiate*) were used in Phytotoxicity test. Four surface-sterilized seed were placed on the Petri dish lined with filter paper. 2 ml of test solution including DI water, herbicide solutions and degraded herbicides were added to the dish. They were controlled at 28 °C of temperature and 90% humidity in the dark for 72 h. After that, the level toxicity was indicated by the term of inhibition of seeds. The sprouting length in herbicides solution were compared to those in control DI water.

3.6.2 Cytogenotoxicity test

Cytogenotoxicity was evaluated using *Allium cepa* chromosome aberration test. *A. cepa* bulbs were kept in water for 72h in the dark after their dried and over

scales roots were removed. Approximately 15mm in length of roots were then exposed to DI water, herbicides and degraded herbicides for 3h. The root tips in different solution were cut, placed on glass slide, fixed in Carnoy's solution for 90min, hydrolyzed in HCl for 10min, washed and stained with 1% aceto-orcein for 5min [60]. They were observed for cell division by a light microscope. The mitotic index (MI) and aberration index (ARD) can be calculated by followed equation:

$$MI (\%) = \frac{\text{number of dividing cells}}{\text{total cells}} \times 100 \quad (3.2)$$

$$ARD (\%) = \frac{\text{number of chromosomal aberrations cells}}{\text{total cells}} \times 100 \quad (3.3)$$



Chapter 4

RESULTS AND DISCUSSION

4.1 Characterization of ZnO catalyst

Synthesized catalysts were prepared by two different techniques to provide catalysts with different forms and surfaces. Figure 4.1 indicates that the morphologies of both catalysts are significantly different which are induced to different surfaces. Catalyst synthesized by sol-gel method are hexagonal-shaped particles with large fraction of end surfaces (Figure 4.1a). The particles size is in range between 400 and 600 nm. Meanwhile, the shape of products from hydrothermal process are long hexagonal prism which most of exposed area are the side surface (Figure 4.1b). The length of prism is in range between 300 and 500 nm, while the diameter is about 50 nm. The results from selected area electron diffraction (inserted figure) indicate that both forms of catalyst are single crystals. Therefore, they confirm that surface on powder particles are mainly polar surface which correspond to zinc-terminated and oxygen-terminated surface, while that on nanorods almost are mixed-terminated of non-polar surface. The surfaces on both ZnO powder and ZnO nanorods are considered to confirm the dominant type of surface. For ZnO powder, polar surface on both ends of column is about 4 times higher than non-polar surface of the side of column. Due to their long shape, non-polar surface is one order of magnitude higher than polar surface, for ZnO nanorods.

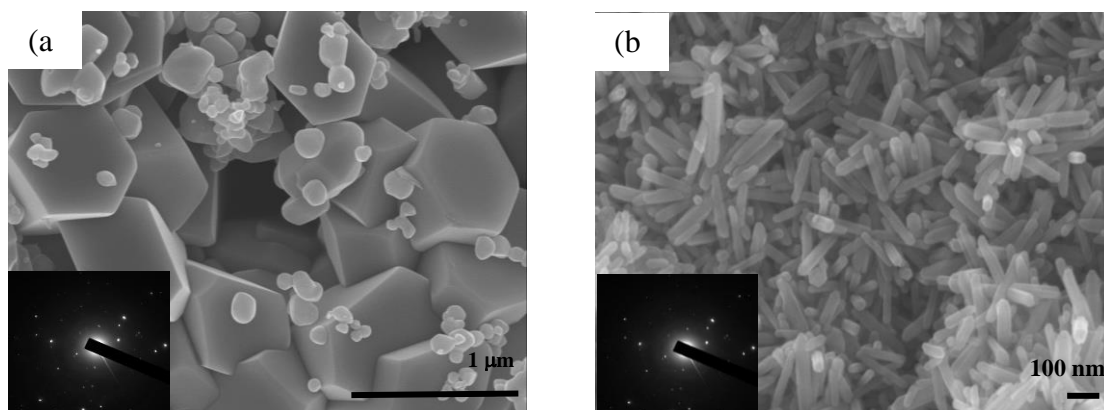


Figure 4.1 The FESEM images and selected area electron diffraction (inserted image) of sol-gel synthesized catalyst (a) and hydrothermal synthesized catalyst (b).

Powder and nanorods catalyst are then analyzed by X-ray diffraction to verify crystalline phase which confirm that both forms of catalyst are indeed ZnO in wurtzite phase as shown in Figure 4.2. No other peaks corresponded with other phase were detected. Although the peak height can indicate the crystallinity, the catalysts loading have to be controlled at the same quantities. Therefore, it cannot be compared the crystalline between ZnO powder and ZnO nanorods due to uncontrolled the amount of catalysts.

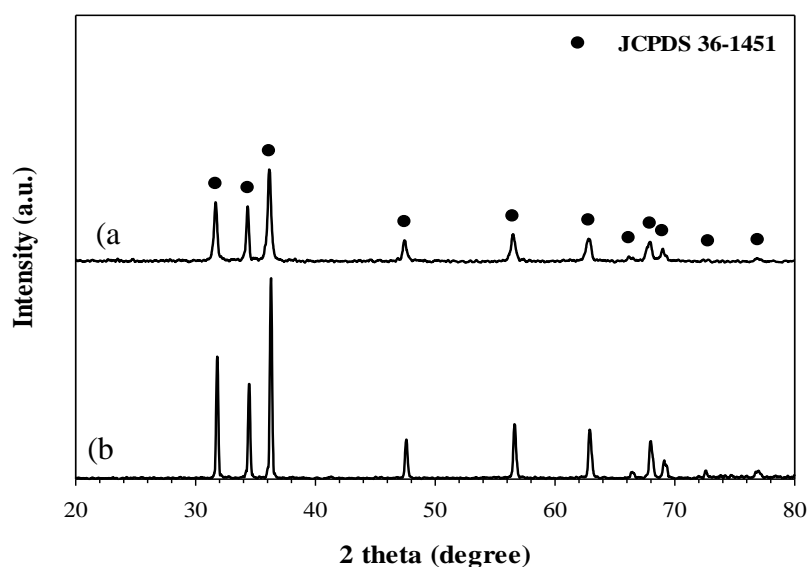


Figure 4.2 The X-ray diffraction of ZnO nanorods (a) and ZnO powder (b).

By their different nature of surfaces due to the polarity on surface, the isoelectric point as shown in Figure 4.3 are quite different i.e., 7.8 for ZnO powder versus 6.8 for ZnO nanorods. Both forms of ZnO are immersed in DI water of which pH are adjusted by 0.1M of HCl and 0.1M of NaOH. The charge on surface of ZnO at varied pH values are shown in Figure 4.3.

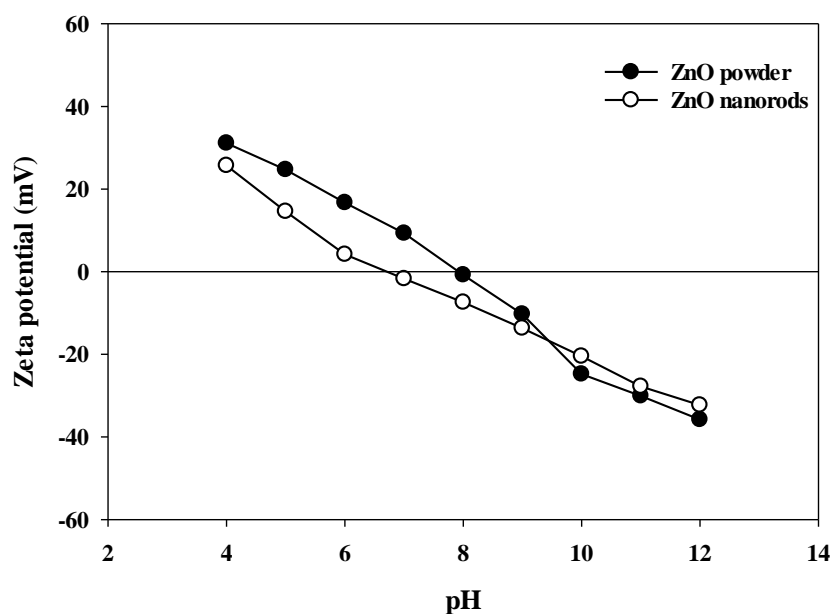


Figure 4.3 The Zeta potential plot of ZnO powder (black dots and line) and ZnO nanorods (white dots and black line).

In addition, the specific surface area measured by nitrogen adsorption via Brunauer-Emmett-Teller (BET) analyzer of ZnO powder and ZnO nanorods which are shown in Figure 4.4 are 1.4 and 17 m²/g, respectively. This is due to the small particle sizes of ZnO nanorods. The isotherm are identified in type II as non-porous materials [61, 62].

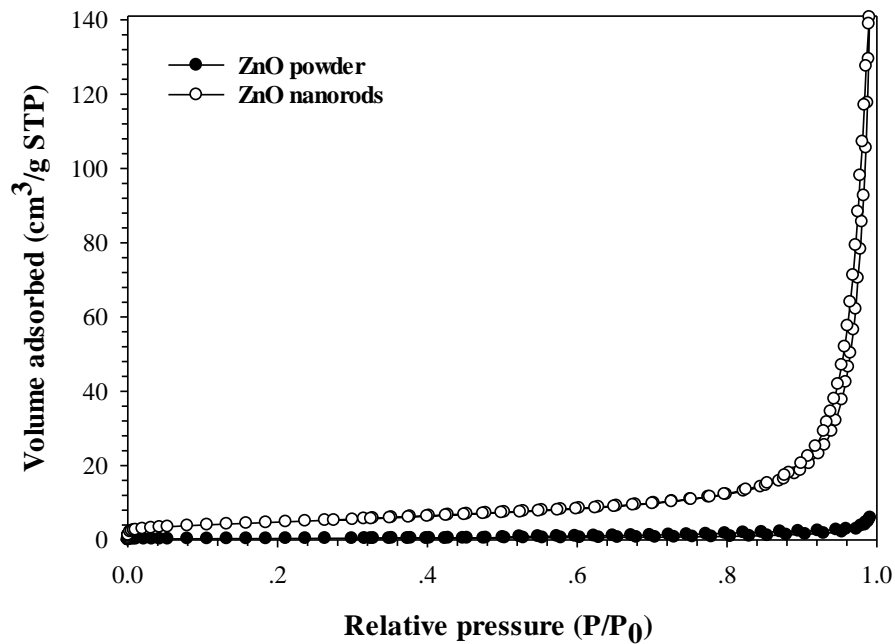


Figure 4.4 Nitrogen adsorption isotherm of ZnO powder (black dots and line) and ZnO nanorods (white dots and black line)

However, the band gap energy of both catalyst measured by Tauc plot are the same at 3.0 eV as shown in Figure 4.5. Tauc plot is widely applied for investigation of optical band gap energy of semiconductor which acquire the optical absorbance data in range between the below and above band gap transition. The plotting $(\alpha h\nu)^{1/2}$ versus $h\nu$ will obtain the energy that can activate electron from valence band to conduction band [63, 64].

where α = intensity absorbance
 h = Planck's constant
 ν = speed of light

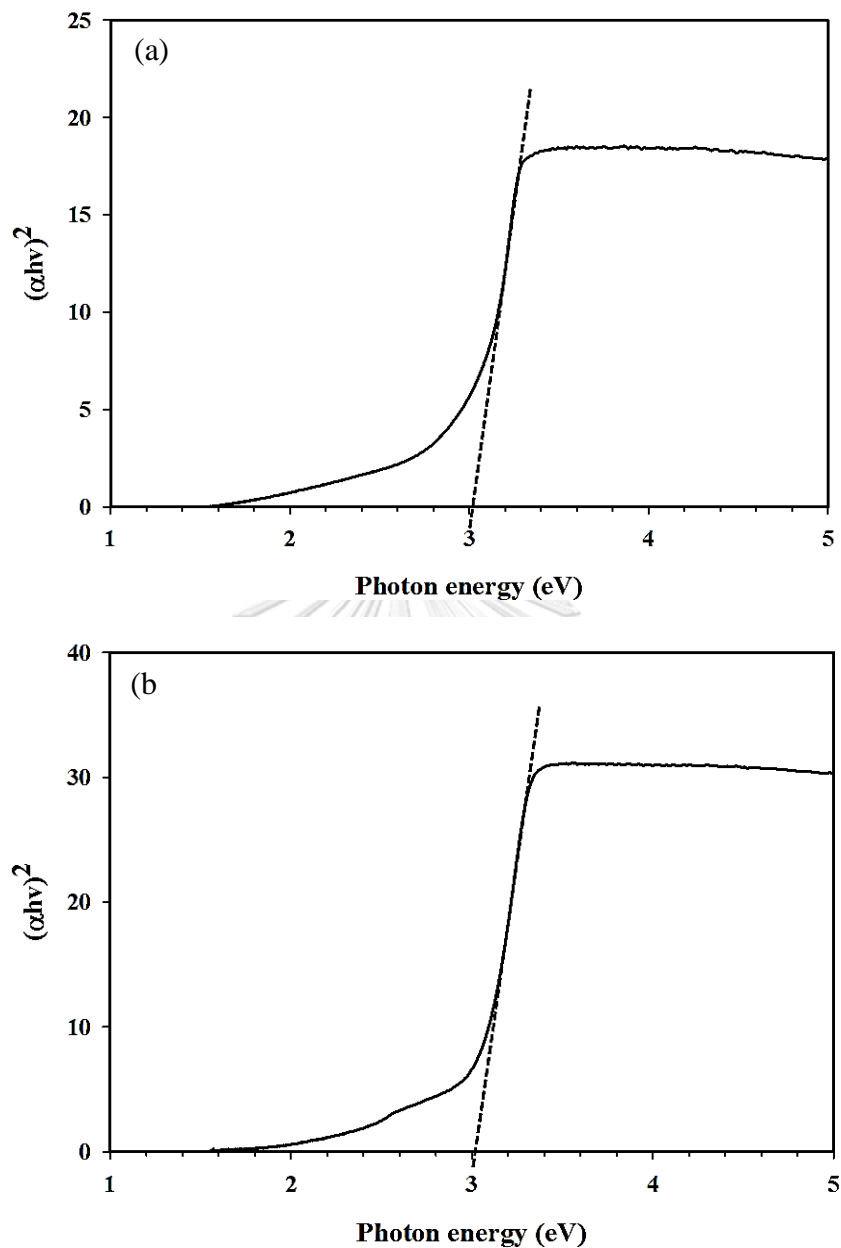


Figure 4.5 The absorbance spectra of ZnO powder (a) and ZnO nanorods (b).

It can be seen that the different morphologies of ZnO does not affect the band gap energy. The band gap energy is obtained by the orbital overlapping of large number of identical atoms which leads to solid state. When electrons in solid with different quantum number gather together as a macroscopic, the energy in each orbital is so close and then consider to continuous energy or energy band. Therefore, the energy level depends on the type of atom and atomic structure that is constituent of

lattice. The band gap energy is then the specific property of the substance with different atomic structure.

The surface chemistry of ZnO are characterized by X-ray photoelectron spectroscopy (XPS) and the results are shown in Figure 4.6. Three states in XPS spectra of O 1s located at 532.2, 531.0 and 530.0 of binding energy which refer to oxygen in hydroxyl group adsorbed on surface, oxygen vacancies and oxygen in lattice of ZnO, respectively [65-67]. In addition, the data of Zn 2p can be deconvoluted into two peaks at 1023.0 and 1021.8 of binding energy which are ascribed to Zn^{2+} of $Zn(OH)_2$ and Zn^{2+} in wurtzite ZnO, respectively [68-70]. Zn^{2+} bonded with hydroxide will occur at the oxygen vacancies due to the missing of oxygens on surface which leads to the incomplete bonding of ZnO lattice. Therefore, Zn^{2+} which is active species on surface can readily bond with adsorbed water or hydroxide anions. From XPS, The results show that the oxygen vacancies on surface of ZnO nanorods is about 6.3% higher than that of ZnO powder which are insignificantly different. Moreover, the amount of $Zn(OH)_2$ are much less than that of Zn in lattice of ZnO. Therefore, the effects of oxygen vacancies and zinc hydroxide can be neglected on experiment.

For the catalysts coated on glass for photocatalytic degradation in micro-reactor, the detached ZnO powder and ZnO nanorods in solution phase which were analyzed by inductively coupled plasma optical emission spectrometry (ICP-OES) are 0.46% and 0.23%, respectively. It may due to the difference in particles size of catalysts. The adhesion of small particles size should be better compared with the bigger particles size. However, it can be seen that the detached zinc in solution phase for both ZnO catalysts much less than 0.5%.

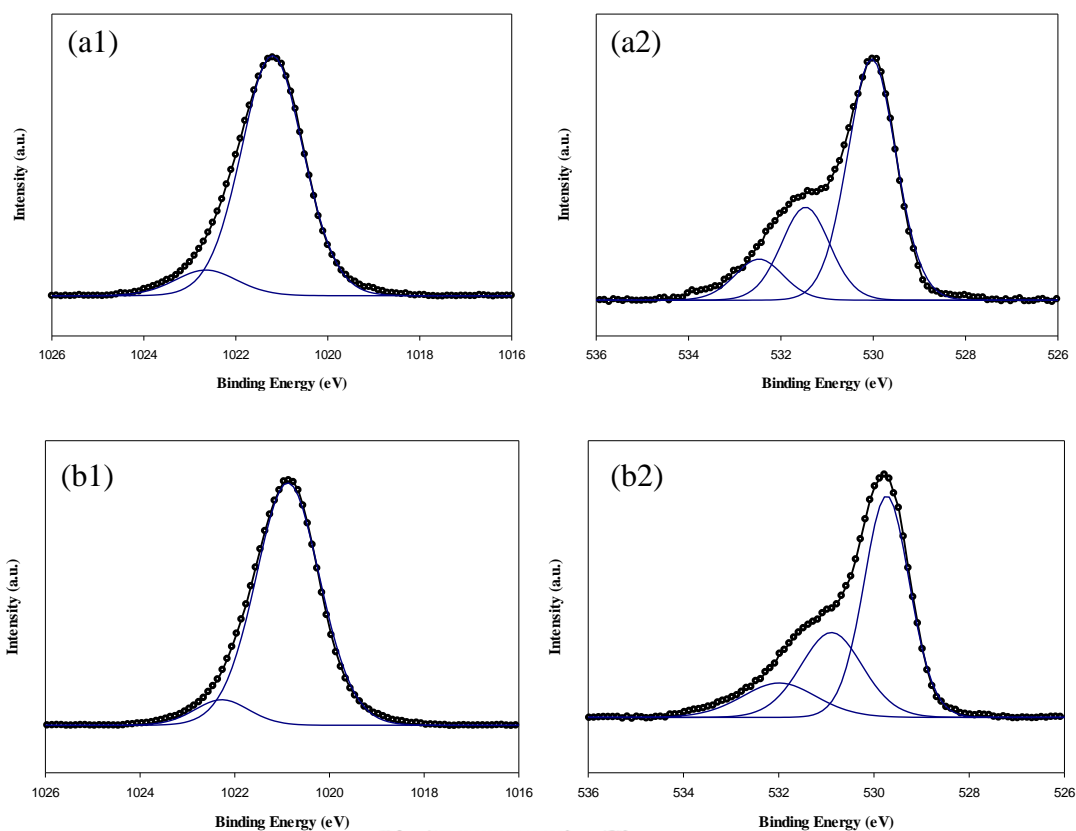


Figure 4.6 The high resolution XPS spectra of Zn 2p (1) and O 1s (2) of ZnO powder (a) and ZnO nanorods (b).

4.2 Adsorption studies

4.2.1. Effect of surfaces of ZnO.

At this part, the experiments were operated at pH 7. At this pH, the surfaces of ZnO are partially covered by the charges due to the different IEP of ZnO (6.8 for ZnO nanorods and 7.8 for ZnO powder). However, IEP of both types of ZnO are very close to the operated pH, so the small amount of covered charges on surface can be neglected. The adsorption of diuron, linuron and DCA are appropriately represented by the Freundlich isotherm model (Eq. 4.1). Normally, the Freundlich model is used to describe the adsorption of organic compounds on a solid surface or the heterogeneous adsorption process [42] which is consistent with our system as shown in Figure 4.7. All

parameters from fitting the model including R-squared are present in Table 4.1. The obtained Freundlich parameters $1/n$ which relates to the adsorption intensity [71, 72] are not more than 1 for all cases. They show that herbicides adsorb on both catalysts by physical adsorption. They are consistent with the Fourier transform infrared spectroscopy (FTIR) results. No signal peak which corresponds to chemical bonding after catalyst was used in adsorption.

$$q_e = K_f C_e^{1/n} \quad (4.1)$$



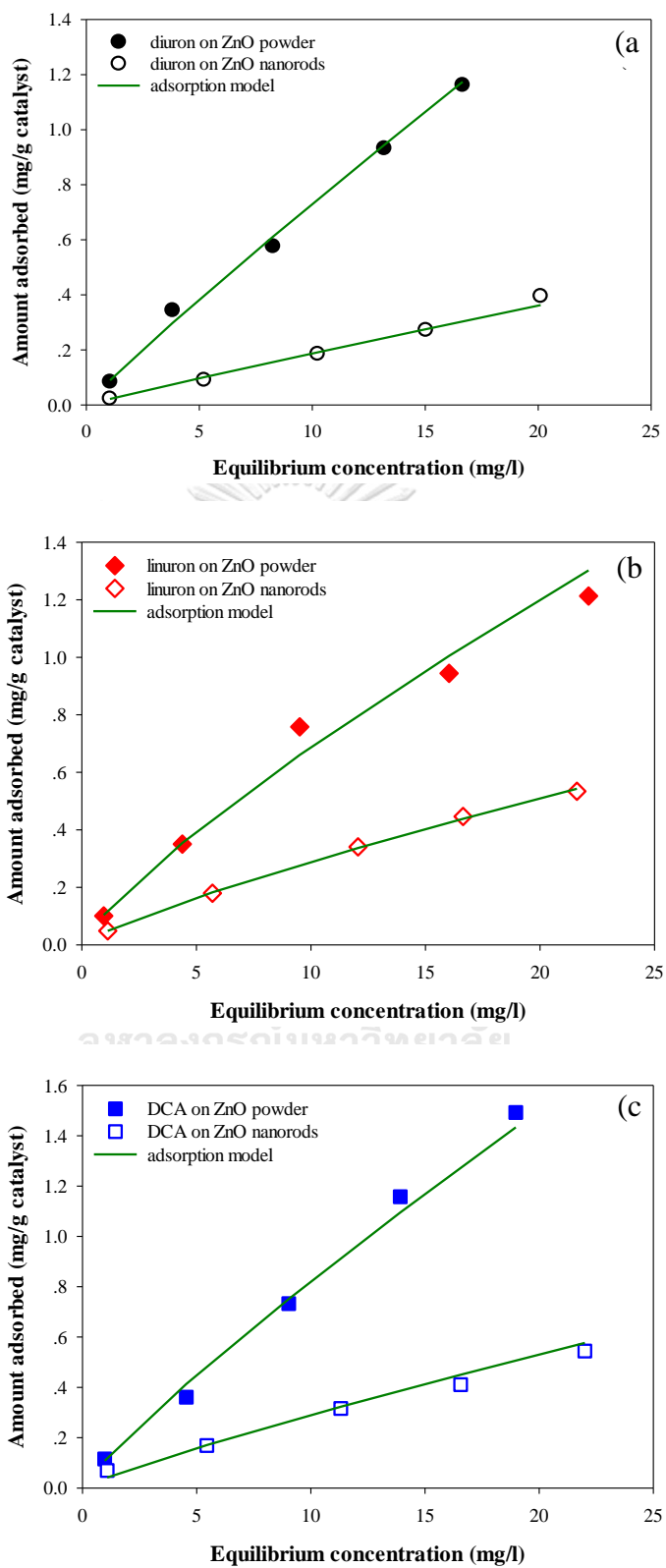


Figure 4.7 Freundlich isotherm fitting of diuron (a), linuron (b) and DCA (c).

In addition, the adsorption of molecular herbicides with polarity part on non-polar and polar surface results in different values of K_f . The parameters K_f which relate to the adsorption capacity [72] in case of ZnO powder are about twice higher than that of ZnO nanorods, even though the surface area of ZnO nanorods is one order of magnitude higher than that of ZnO powder. It means that the interaction between adsorbates and adsorbent greatly affect the ability in adsorption. It should be noted that other isotherm models such as Langmuir isotherm, *Temkin isotherm*, Dubinin–Radushkevich isotherm and Flory–Huggins *isotherm* are failed to fit with our adsorption data. In case of fitting the data with BET model, the R-squared are about 0.8 which is less than that of Freundlich model. These are the results of not enough data leading to plateau state. For better understanding of adsorption process, molecular simulation was conducted to explain these processes.

Table 4.1 The fitted parameters for Freundlich isotherm model.

ZnO	molecule	R^2	K_f	$1/n$
nanorods	3,4-dichloroaniline	0.976	0.049	0.772
	diuron	0.978	0.028	0.815
	linuron	0.999	0.036	0.901
powder	3,4-dichloroaniline	0.992	0.110	0.868
	diuron	0.983	0.082	0.959
	linuron	0.998	0.101	0.849

Figure 4.8 shows the adsorption configuration of herbicides on mixed-terminated surfaces of ZnO which are obtained by molecular simulation. The initial orientation of herbicides on several surfaces are varied to optimize the most stable configuration (see APPENDIX B). The adsorption energy from calculation are shown in Table 4.2. Generally, the properties of catalysts surfaces are changed by illumination such as oxygen vacancies. The oxygen vacancies is the phenomenon that oxygen atoms are left from the surface. Many studies report that oxygen vacancies

will increase the adsorption sites of adsorbates, so they make the adsorption is more efficient. From Table 4.1, it shows that the effect of oxygen vacancies is not dominant effect on the adsorption experiments due to the higher adsorption capacity of ZnO powder which has the lower amount of oxygen vacancies. Moreover, the XPS results of used ZnO powder and nanorods which show the insignificantly different quantities of oxygen vacancies, compared with new synthesized ZnO. Therefore, this effect is neglected on calculation.

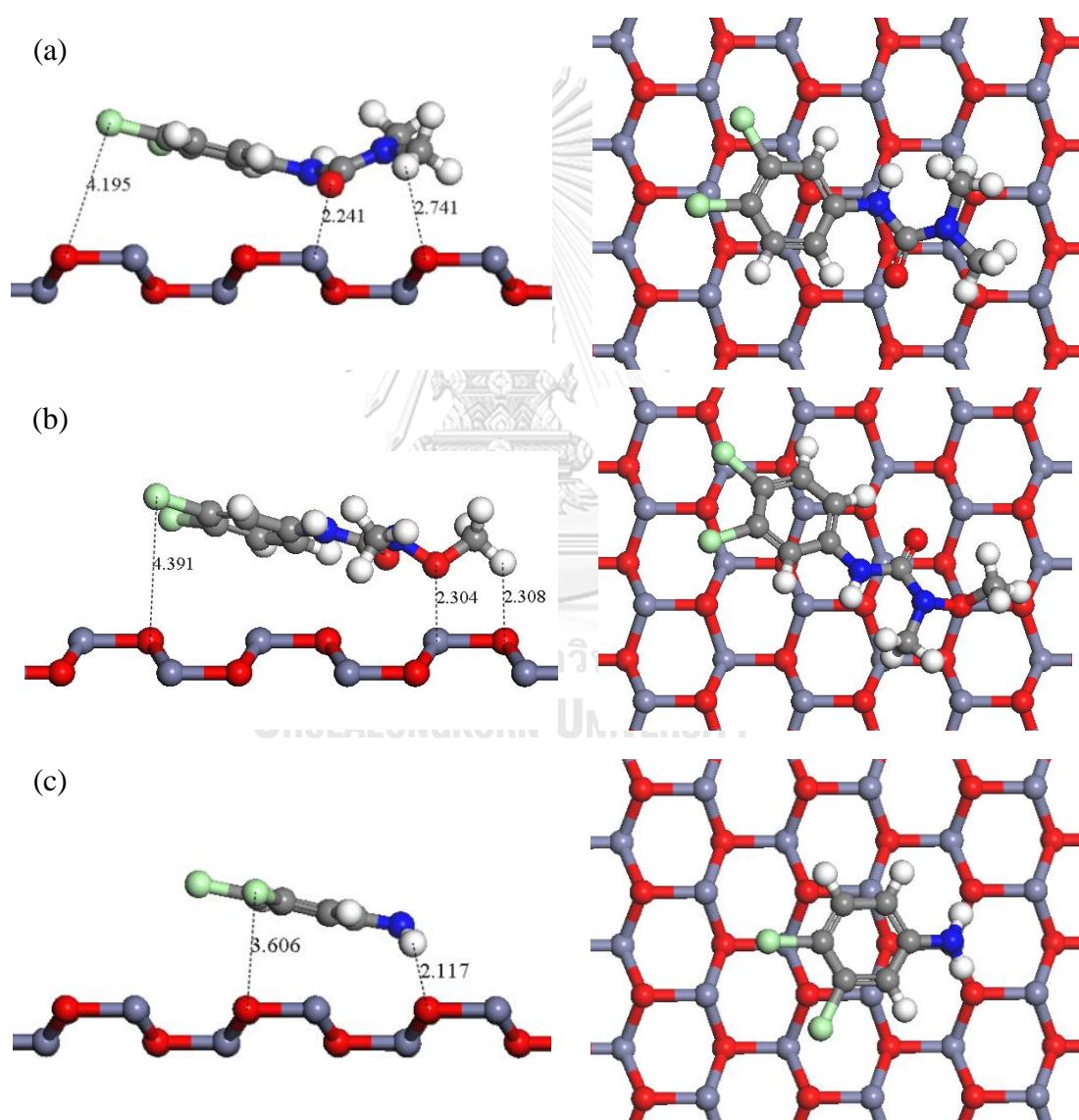


Figure 4.8 The adsorption models of diuron (a), linuron (b) and DCA (c) on mixed-terminated surface.

Table 4.2 The adsorption energy from calculation.

surfaces	Adsorption energy (kcal/mol)		
	3,4-dichloroaniline	diuron	linuron
Mixed-terminated	-23.13	-25.47	-22.60
Zinc-terminated	-29.40	-29.32	-37.01
Oxygen-terminated	-36.87	-36.91	-39.04

The less adsorption energy of mixed-terminated non-polar surface indicates the less favorable adsorption of herbicide on this surface compared with that of polar surfaces. The interaction between herbicide and ZnO surfaces are suggested to be electrostatic, as seen that herbicides strongly adsorb on surface with more polarity. Moreover, molecular herbicides also show the low polarity [73] due to their high electronegativity atoms. Therefore, the electron distribution on molecular herbicides are investigated as shown in Figure 4.9.

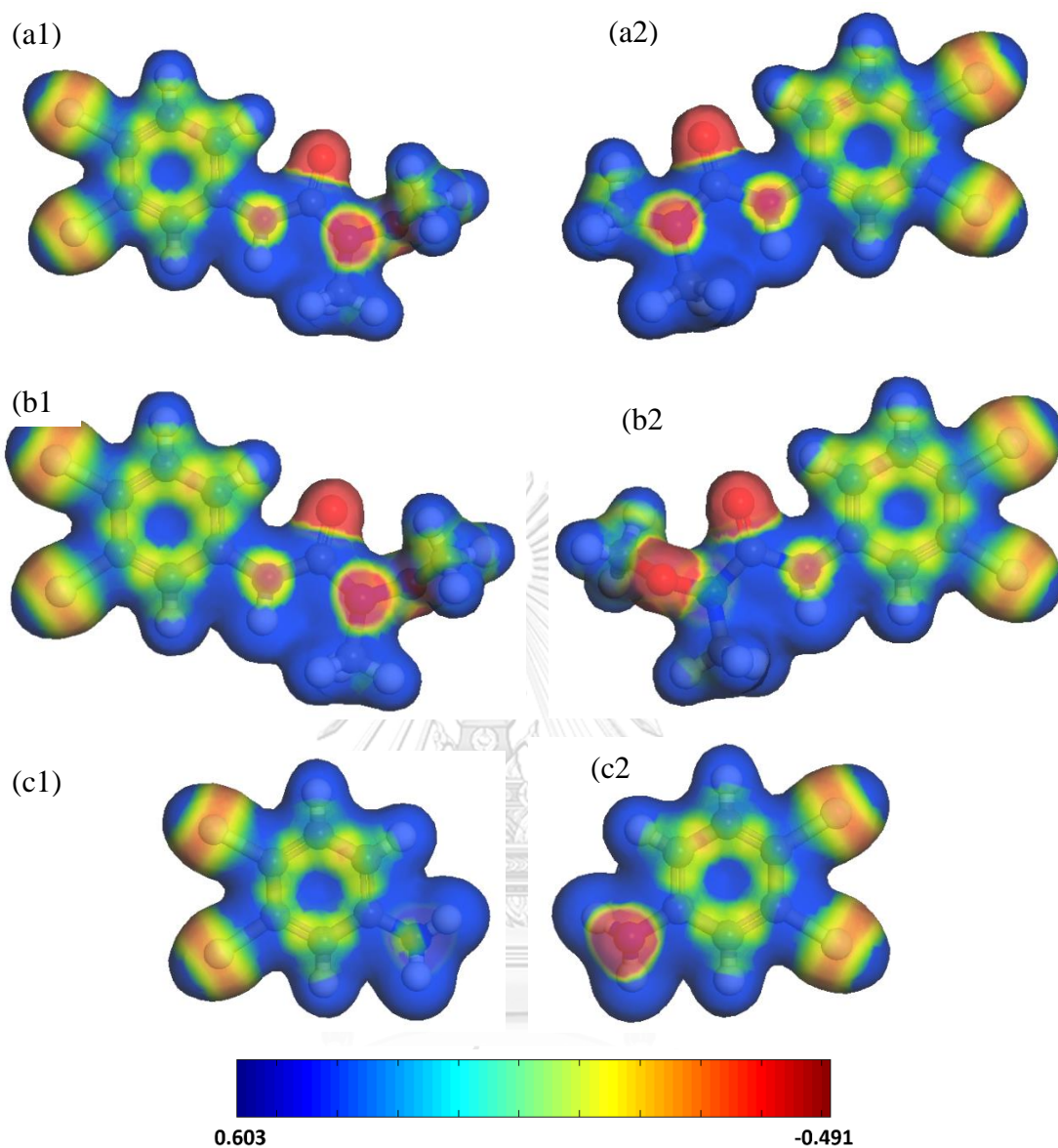


Figure 4.9 The electron distribution on diuron (a), linuron (b) and DCA (c) where the red and blue color indicate the most negative and positive part on molecule, respectively.

According to calculation, the bending of molecular structure occurs while diuron adsorbs on mixed-terminated surfaces which lead to the chance for the negative parts, i.e. oxygen of carbonyl group and nitrogen closed to aromatic approach to positive zinc atoms on surface at 2.2 and 2.6 Å of distance, respectively. At the same time, hydrogen of methyl group at the end of aliphatic located in position that is affected by the attraction of oxygen atom. The distance between hydrogen (of

diuron) and oxygen (of surface) is 2.7 Å which causes the formation of weak hydrogen bond. This interaction is classified into electrostatic force. By this position, two chlorine atoms attached to an aromatic ring are repelled by an oxygen atom which result in the wide distance from surface (4.2 Å). It should be noted that a negative nitrogen atom which attaches to two methyl groups cannot adsorb on surface due to the steric effect.

On the same surface, linuron adsorbs on surface in similarity way. Aromatic and substituted chlorine cause the wider gap than aliphatic side due to the repulsive of the similar polarity of oxygen on surface (4.4 Å). Because of oxygen of alkoxy group contained in linuron, it is more facile to adsorb on surface than carbonyl group. Without the steric effect, oxygen of alkoxide and hydrogen at the end of aliphatic easily approach to surface by the same distance at 2.3 Å.

Although diuron and linuron have similar structures and adsorption characteristics, the adsorption energies are slightly different. Linuron with the fewer adsorbed functions has the lower adsorption energy than diuron. Moreover, the polarity of oxygen from alkoxy group is less than that of oxygen from carbonyl group which results to unequal of interaction between herbicides and surface.

DCA adsorbs on surface by forming the weak hydrogen bond with oxygen atom on surface, while the repulsion between chlorine and oxygen on surface occur in the same time. Hydrogen bond can be classified by the characteristic of adsorption, i.e. the length between hydrogen and surface, bond angle, the length between electronegativity and hydrogen atom within molecule and the length of intermolecular bonding versus intramolecular bonding [74]. The distances between two hydrogen atoms and surface are equally at 2.1 Å and the wide distances at repelled position are 3.6 Å. Comparing DCA and linuron with equal adsorbed function, the adsorption energy of DCA is slightly higher than that of linuron. The shorter gap in case of DCA indicates the stronger interaction between DCA and surface. Diuron have exactly highest adsorption energy due to more adsorbed position but the results show the highest amount of DCA adsorbed on surface. With the small molecular size of DCA, it result to lower occupied surface (i.e. 79.8 Å² for DCA, 106.2 Å² for diuron and 116.9 Å² for linuron). It is observed that linuron has higher adsorption capacity than diuron even the occupied surface and the adsorption energy of diuron is higher than

that of linuron. As previously described, without the steric effect, linuron can easily adsorb on surface by its alkoxy group.

The occupied surface area of adsorbed herbicides on surfaces are calculated by projection adsorbed area of molecules from top view to surface. The adsorbed herbicides are in space-filling model which are useful to estimate the actual occupied surface because this model will show the realistic radii of atoms or molecules or the real distance between nuclei of two bonded atoms [75, 76]. Figure 4.10 shows the adsorbed herbicides on mixed-terminated surface in space-filling model.



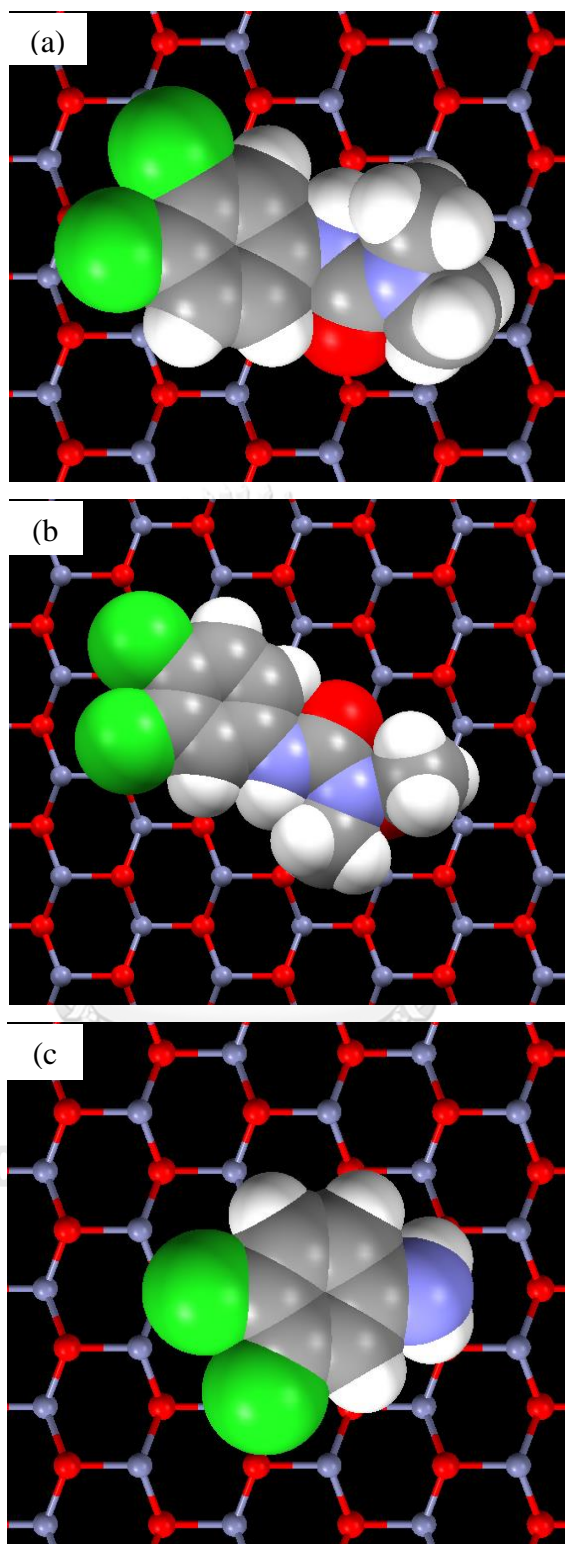


Figure 4.10 The space-filling model of diuron (a), linuron (b) and DCA (c) on mixed-terminated surface.

Adsorption on zinc-terminated surface are shown in Figure 4.11. Because only zinc atoms appeared on this surface which lead to uniformly positive-charge surface, it attracts all negative parts of herbicides lean toward on this surface. Two chlorine, aromatic and nitrogen of DCA which are negative and electron-rich parts simultaneously adsorb on zinc-surface. The shortest distance between DCA and surface is 2.3 Å which located on nitrogen of amine. It is noteworthy that hydrogen of amine group which is likely mild positive bent up to avoid unstable adsorption. In the same way, aromatic side of diuron adsorb in parallel orientation to the surface. Oxygen of carbonyl group at aliphatic side is also attracted to surface and cause the shortest distance equal to 2.1 Å. Meanwhile, hydrogen at the end of aliphatic lift up from the same plane of aromatic which result to the wider gap at 2.9 Å. For the adsorption of linuron, two oxygen of carbonyl and alkoxy group which are the most negative adsorb on positive surface by 2.2 and 2.5 Å of distance, respectively. Due to alkoxy group, two methyl groups flexibly twist up from surface to remain the stable configuration. In addition, it can be seen that the adsorption on positive-liked surface results to the higher adsorption energy than that on non-polar surface. Having more adsorbed functional group of linuron results to the highest adsorption energy while DCA and diuron with equal adsorbed position have the similar energy.

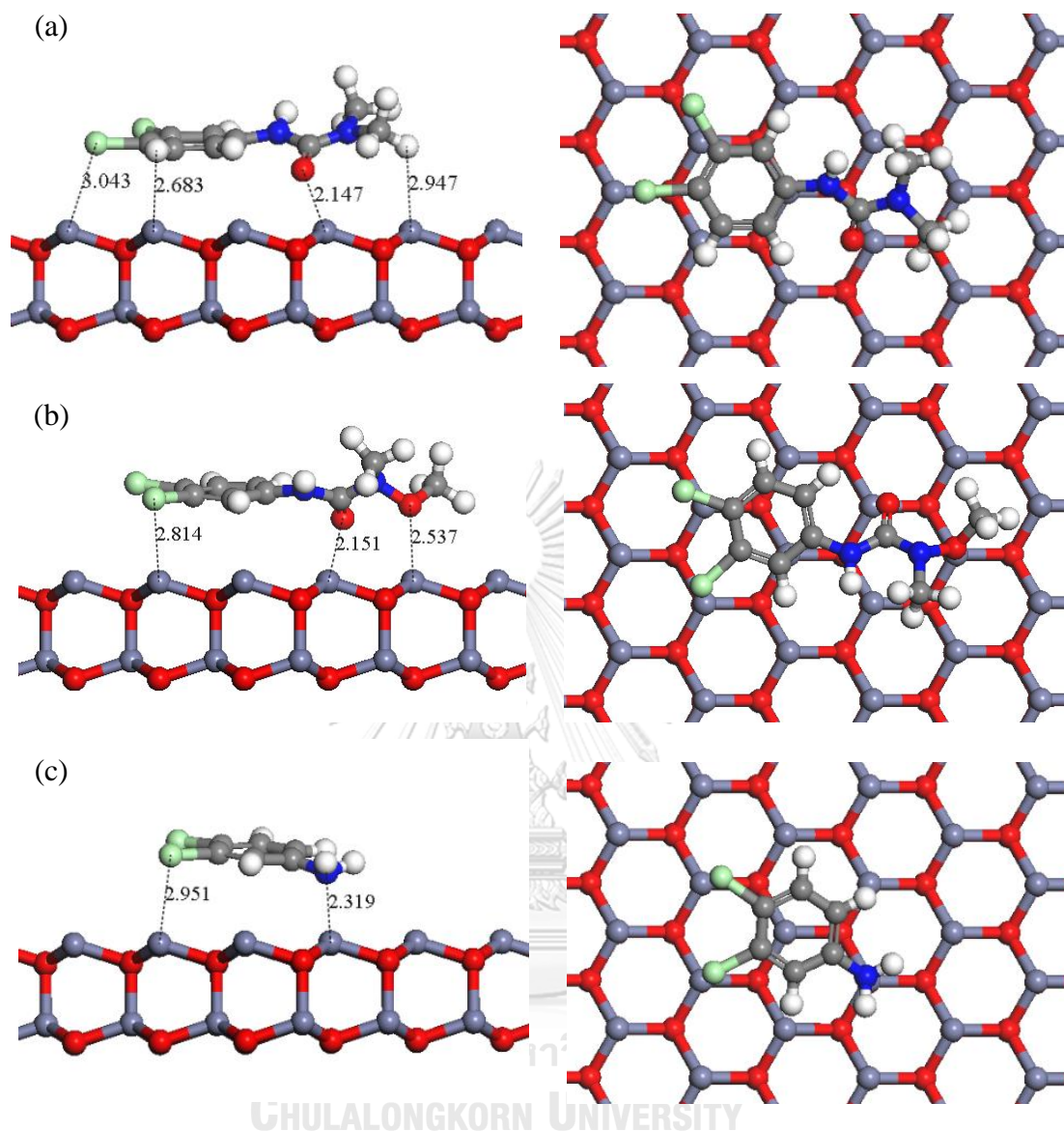


Figure 4.11 The adsorption models of diuron (a), linuron (b) and DCA (c) on zinc-terminated surface.

Opposite to zinc-surface, only oxygen atoms on the plane result to the negative-charged surface. The adsorption configuration on this surface are shown in Figure 4.12. DCA adsorbs on oxygen surface by two hydrogens of amine group with about 2.1 Å of distance which similar to the adsorption on mixed-terminated surface. In the same time, two chlorine and aromatic are repelled by the strongly negative surface result to the wider gap which is 4.3 Å. In addition, the adsorption of DCA on oxygen are significantly different higher than that of mixed-terminated surface. The

stronger attraction occurs on the higher negative surface. This is consistent with many reports that polar surface have the higher adsorption energy than non-polar surface [53, 77]. Adsorption on zinc and oxygen which are all polar surfaces are also result to different adsorption energy. On oxygen-terminated surface, hydrogen and highly electronegativity can form C–H···O interactions, which carbon behaves a hydrogen donor and oxygen of surface is the hydrogen acceptor. This bond type is stronger than the interaction between opposite charge [78]. It can be clearly seen that hydrogen of amine have the higher chance to adsorb, compared with hydrogen on aromatic, because the withdrawn-electron ability of nitrogen lead to more positively charged on adjacent hydrogen.



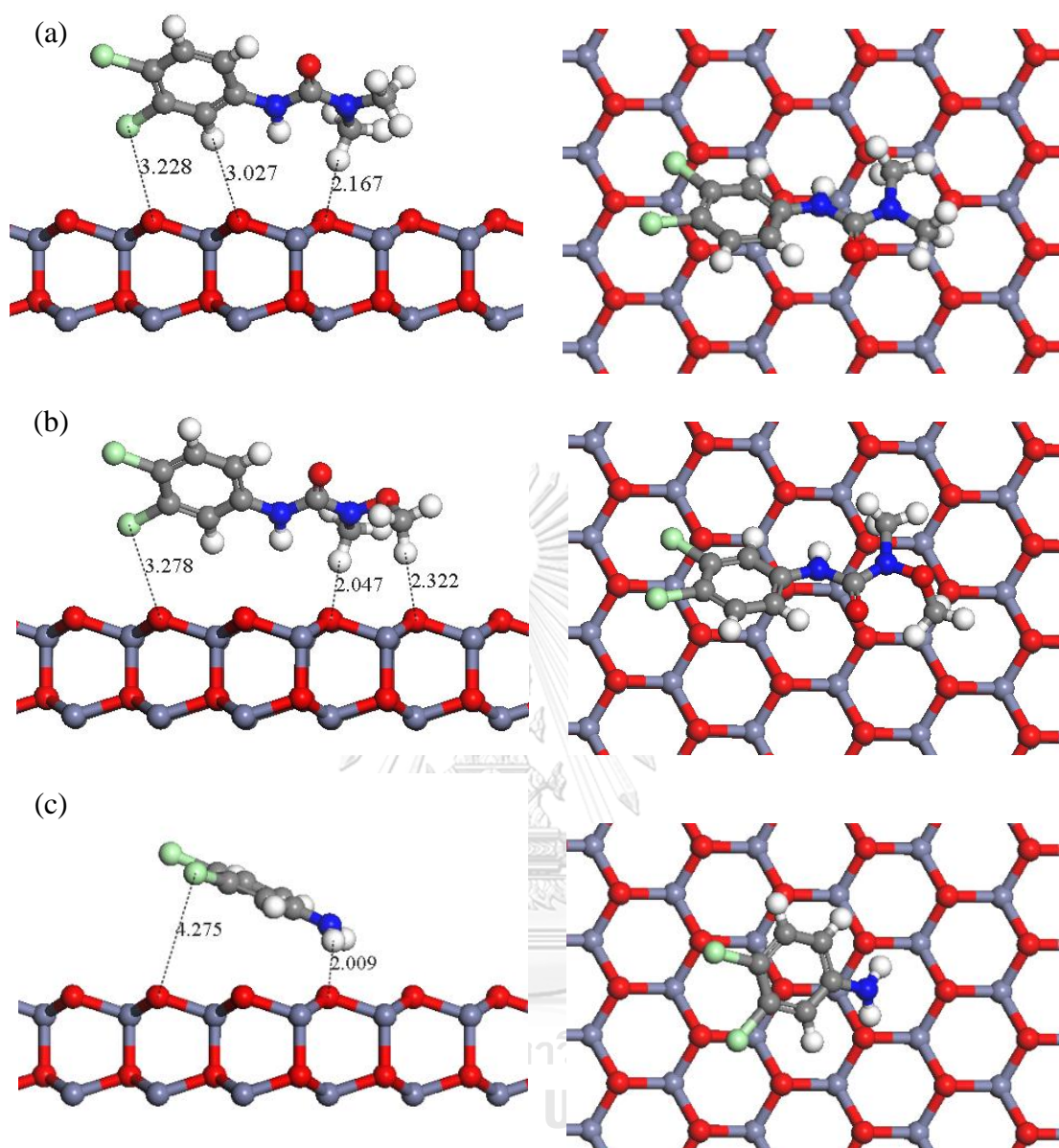


Figure 4.12 The adsorption models of diuron (a), linuron (b) and DCA (c) on oxygen-terminated surface.

Comparing between diuron and linuron, their molecular structure twists for the adsorption of hydrogen, while negative oxygen and nitrogen are away from surface to minimize the repulsive between the same negative polarities. These cause the shortest distance at this position which is 2.2 Å for diuron and 2.0 and 2.3 Å for linuron. Same as DCA, the formed energy of diuron and linuron on this surface are higher than that on zinc due to the formation of C–H···O interactions. Moreover, the two adsorbed

hydrogen of linuron lead to the slightly higher adsorption energy. However, hydrogen atoms of methyl group next to amide at aliphatic of linuron is more slightly positive-charged than hydrogen on amine of DCA because those hydrogens are double affected by the existence of two high electronegativity oxygen in molecular structure (i.e. carbonyl and alkoxy group). Therefore, the slightly stronger interaction between linuron and surface is results to the higher adsorption energy compared with DCA. Meanwhile, the adsorption energy of DCA and diuron are similar.

In term of adsorption capacity, DCA is also the highest K_f which relates to the highest adsorption capacity. Same as previously described, the occupied surface of DCA in adsorption is also lowest (not more than 80 \AA^2) due to the smallest molecular structure. Moreover, it can be seen that linuron has the higher adsorption capacity than diuron even the maximum occupied surface of linuron (about 120 \AA^2 on zinc-surface) is more than that of diuron (about 110 \AA^2 on zinc-surface). This is the result from higher adsorption energy which bring about to the favorable adsorption of linuron on polar surface.

The polar surface shows the higher ability to adsorb herbicide than non-polar surface. Firstly, herbicides are adsorb on either zinc or oxygen atom (i.e. oxygen for DCA and zinc for diuron and linuron) on mix-terminated surface so only half of atoms on surface are the adsorption sites. Furthermore, the adsorbed molecule on one site will provides the steric effect to the adsorption on nearby site. Inversely, due to identical atoms on surface, all atoms serve the adsorption sites for herbicides. Lastly, on polar surface with the high polarity greatly impact to the attracted herbicides while the balancing of zinc and oxygen on non-polar surface has the less attraction than polar surface.

4.2.2. Effect of pH.

The difference in adsorption behavior of herbicides is the result of the different nature of ZnO surface. Since the catalyst is in different environment such as in acid or base, surface of catalyst change, which will also affect the adsorption behavior. It should be note that DCA, linuron and diuron dissociate at pH 2.8, 12.9 and 13.8, respectively. Therefore, these herbicides do not show the charged characteristic of molecules in the range of operated pH. At pH7, most of ZnO surface

is not covered by any charges, so the adsorption behavior in normal condition is quite different from that in acidic or basic conditions. In this part, the pH is investigated for its effect on the adsorption. In the same time, diuron and DCA were conducted to compare the different behavior.

The experimental data can be fitted with Freundlich isotherm as well which are shown the best R-squared values. Parameters obtained from the fitted model are K_f and $1/n$ which represent the adsorption capacity of ZnO and the strength of interaction between ZnO and herbicides, respectively. All parameters and R-squared from model fitting are shown in Table 4.3.

The all values of $1/n$, as seen in table, are not more than 1, which also indicate the physisorption of herbicides in both acidic and basic condition. From the K_f value shown in Table 4.3, it is evident that the adsorption capacity of diuron in acidic conditions is better than that in base. Inversely, surface in base has the higher capacity to adsorbed DCA than surface in acid. Calculation of adsorption processes are conducted to explained the happened mechanism.

Table 4.3 The fitted parameters for Freundlich isotherm model at various pH.

ZnO	molecule	pH	R ²	K_f	$1/n$
nanorods	3,4-dichloroaniline	4	0.965	0.039	0.758
		10	0.987	0.062	0.805
	diuron	4	0.989	0.039	0.842
		10	0.890	0.021	0.789
powder	3,4-dichloroaniline	4	0.896	0.071	0.831
		10	0.989	0.150	0.896
	diuron	4	0.962	0.114	0.975
		10	0.984	0.073	0.881

At pH lower and higher than IEP, i.e. 7.8 for ZnO powder and 6.7 for ZnO nanorods, the net charge on surface is positive and negative, respectively. Due to the sharing aromatic part of diuron, adsorption of DCA is studied to predict the intermediates formed when the degradation of diuron is prolonged and intermediates formed is smaller molecular size. Figure 4.10 shows calculation of DCA adsorption on acidic and basic surfaces.

At low pH, negative oxygen of ZnO surfaces are captured by H^+ . Adsorption of DCA on both mixed and oxygen surface are similar as shown in Figure 4.13a and 4.13b, respectively. Due to the positive attraction, negative parts of DCA, i.e. chlorine and nitrogen, are approached to protons on surface in planar configuration. Two hydrogen of amine which likely to be positive part of DCA bent up to minimize the repulsive force. The average distances between DCA and surface are 2.6 Å for mixed-terminated and 2.5 Å for oxygen-terminated.

For the adsorption of diuron, the calculation is shown in Figure 4.13c and 4.13d. The similar configuration of diuron adsorbed on polar and non-polar occur at pH4. Oxygen and chlorine are attracted by H^+ on surface. Diuron tilts almost perpendicularly which is the result from the repulsive of surface to two methyl group and hydrogen substituted on aromatic. The shortest distance between surface and diuron is 2.1 Å located on oxygen of carbonyl group for non-polar surface and is 2.3 Å located on chlorine for polar surface. Due to more hydrogen at aliphatic end and the stronger repulsive of surface on polar surface, the wider gap between carbonyl group and surface form at 2.8 Å, while that on non-polar surface is equal at 2.6 Å at adsorbed chlorine atom.

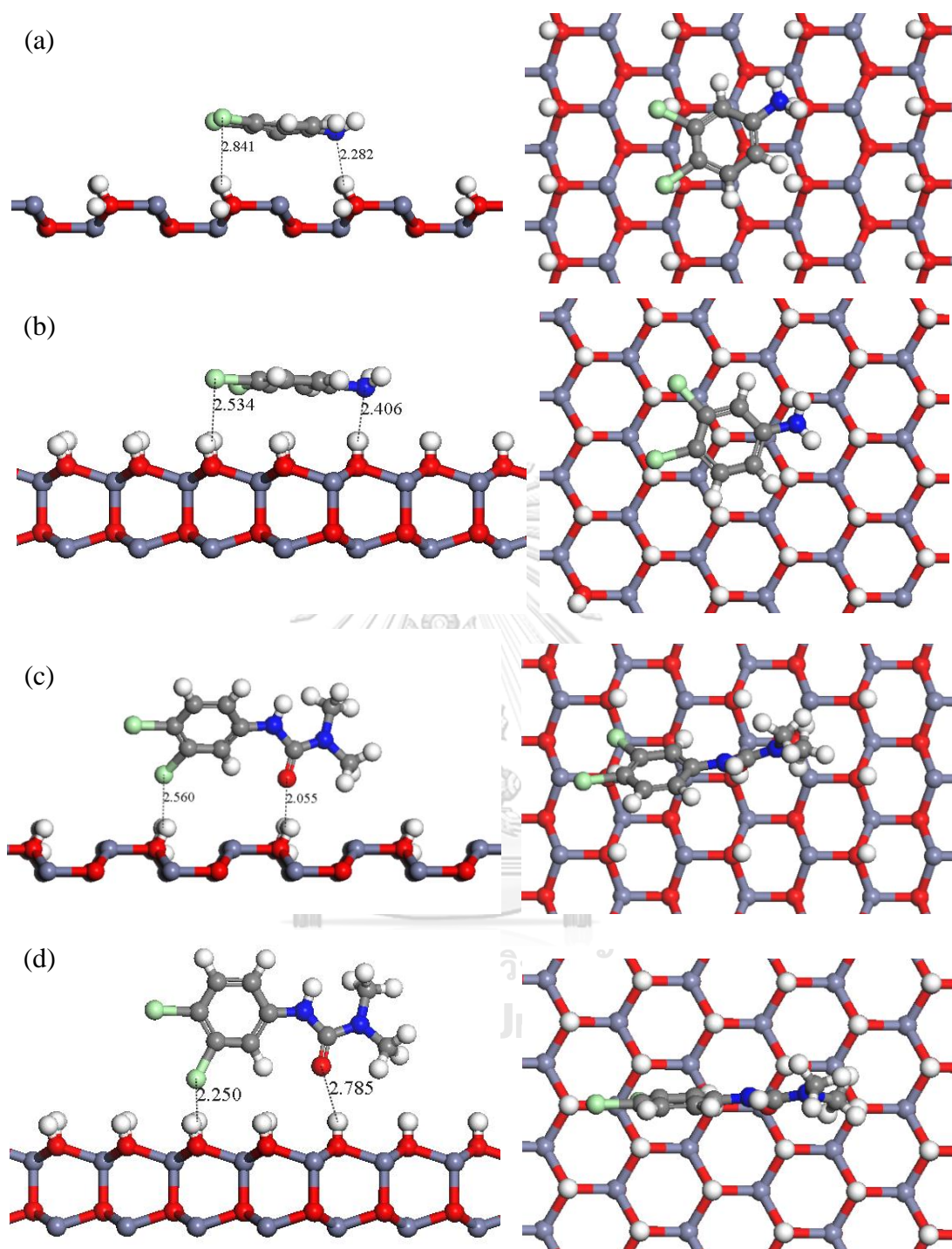


Figure 4.13 The adsorption models at pH4 of DCA on mixed-terminated surface (a), oxygen-terminated surface (b), diuron on mixed-terminated surface (c) and oxygen-terminated surface (c).

In basic condition, positive zinc will be covered by OH^- results to negatively charged surface. In this condition, DCA adsorbs on surfaces in similar manner. Two positive hydrogens adsorb on negative ions, while chlorines are repelled away from surfaces by the same polarity charge which result to the wider distance compared to distance between hydrogen and surfaces (see Figure 4.14a and 4.14b). The shortest distances between surface and adsorbed hydrogen are 2.4 Å and 2.1 Å for non-polar and polar surface, respectively. Although, the adsorption configurations of DCA on polar and non-polar surface are similar at the same pH, the adsorption energy as shown in Table 4.4 seem to be different. The amount of atoms on polar and non-polar surfaces covered by either positive or negative ions are unequal which results to the unequal interaction. Polar surface with identical atoms are covered by the higher amount of ions and can form the stronger interaction between DCA and surface compared with non-polar surface.

Diuron adsorbed on both surfaces at pH10 in similar trend. By the same polarity, chlorines are repelled away from surfaces, while hydrogen at aliphatic end adsorb on OH^- . It is noteworthy that there is only one adsorbed functional group on non-polar surface with 2.4 Å of distance but the atoms arrangement on polar surface causes two adsorbed positions with 2.3 and 2.6 Å of distance.

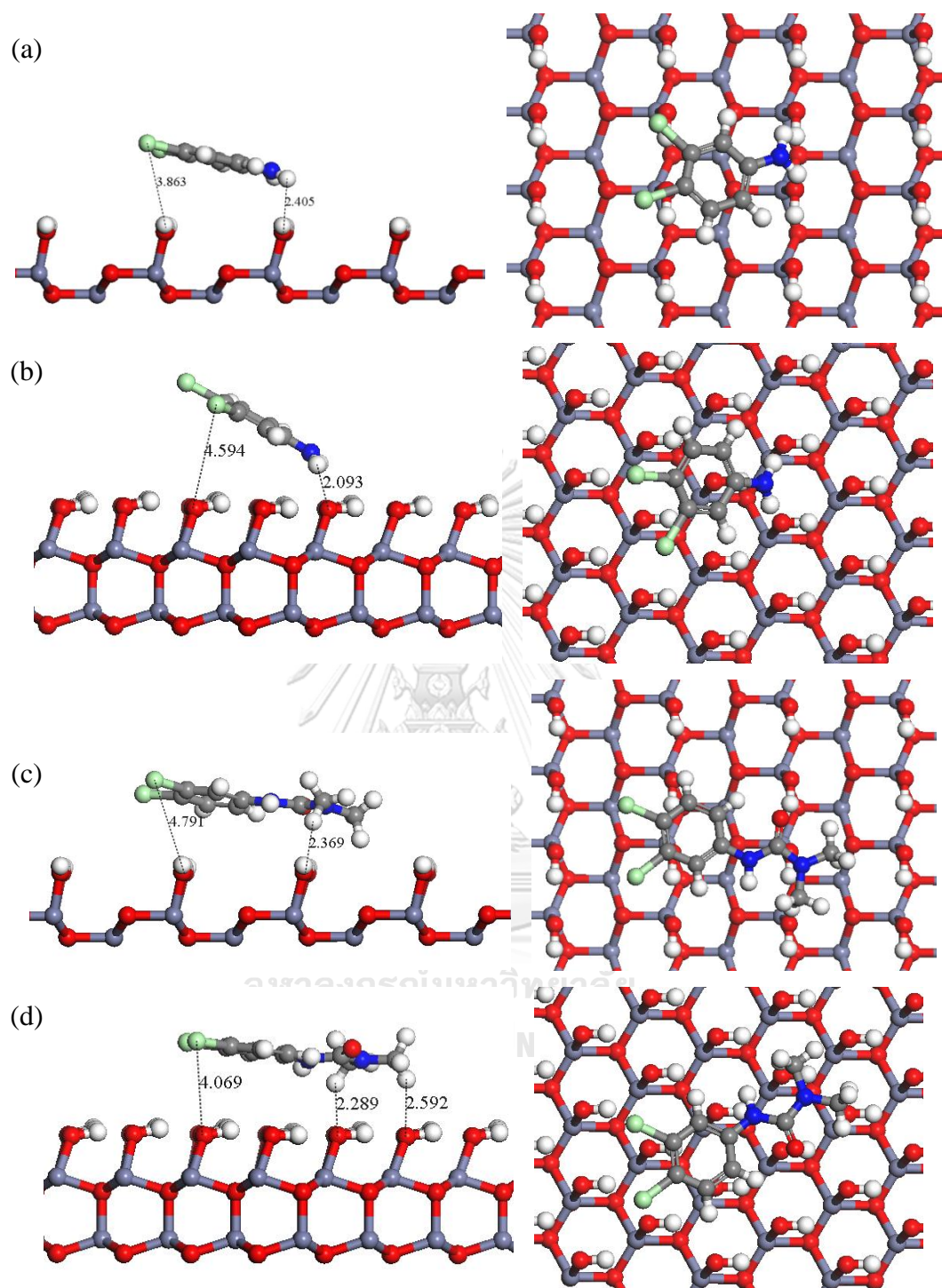


Figure 4.14 The adsorption models at pH10 of DCA on mixed-terminated surface (a), oxygen-terminated surface (b), diuron on mixed-terminated surface (c) and zinc-terminated surface (d).

Table 4.4 The adsorption energy from calculation at various pH.

conditions	surfaces	Adsorption energy (kcal/mol)	
		3,4-dichloroaniline	diuron
acid	polar surface	-27.90	-39.54
	non-polar surface	-20.56	-26.94
base	polar surface	-37.83	-27.95
	non-polar surface	-25.54	-21.05

Comparing at different pH, both ZnO nanorods and ZnO powder have the highest ability to adsorb DCA at pH10 and have the lowest adsorption capacity at pH4. The occupied area of DCA on surface are not significantly different in each condition. Therefore, they may be not the effective impact on adsorption in these cases. At pH10, two adsorbed hydrogen can form the weak hydrogen bond with oxygen of hydroxyl anions which are stronger than that with no-charged oxygen at pH7. Meanwhile, the interaction between DCA and surfaces at pH4 are only electrostatic of opposite charge which cause the lowest energy. The adsorption energy from calculation are consistent with the value of K_f from experiments. The higher adsorption energy indicates the favorable of adsorption process, so the preference of adsorption occur.

The adsorption energy, as shown in Table 4.4, of polar surface is higher than that of non-polar surface which deal to the stronger interaction. Inverse result from DCA adsorption, both surfaces have the highest adsorption capacity at pH4 and the lowest performance at pH10. At pH4, protons on surface attract two high electronegativity, i.e. chlorine and oxygen, and form strong interaction which correspond with the value of K_f . In addition, these adsorption configuration can cause the least occupied surface area in this condition which is 85.5 and 67.83 Å² for non-polar and polar surface, respectively and they allow more diuron adsorb on surfaces. On mixed-terminated, the less occupied surface and only dipole-dipole force formed in adsorption even there is the same number of adsorbed functional group, so the

adsorption capacity at pH7 is lower than that at pH4. Although the weak hydrogen bond also form, the large occupied surface area and low adsorption energy result to the lowest adsorption capacity at basic condition. These results are also applied for the adsorption on polar surface. The lowest adsorption energy and the largest of occupied surface area result to the lowest adsorption capacity at pH10. For pH7, the interaction formed is just the attraction between different polarities.

4.2.3 Adsorption in aqueous system

From previous discussion, the adsorption of herbicides on surfaces are considered in vacuum, so they will not be disturbed by other external factors. In real experiments, herbicides are dissolved in solvent (i.e. water), the characteristic of adsorption may be change. In this part, the effect of solvent on adsorption is considered. The COSMO model in Dmol3 program which is commonly used for determining the interaction between molecules and solvent is chosen to calculate the adsorption of herbicides in water-soluble system. Figure 4.15-4.19 show the adsorption of herbicides including DCA, diuron and linuron on ZnO surfaces.

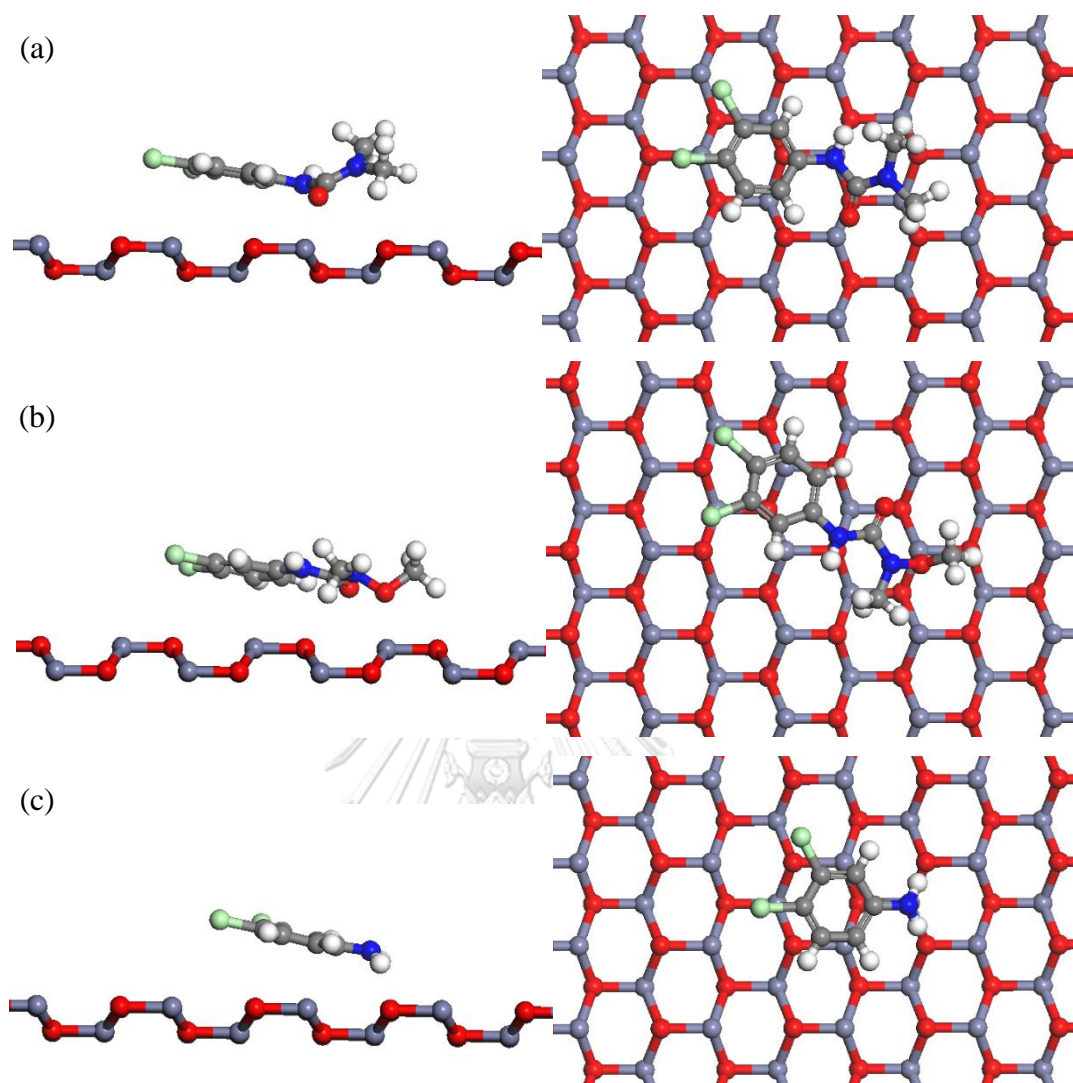


Figure 4.15 The adsorption models of diuron (a), linuron (b) and DCA (c) on mixed-terminated surface.

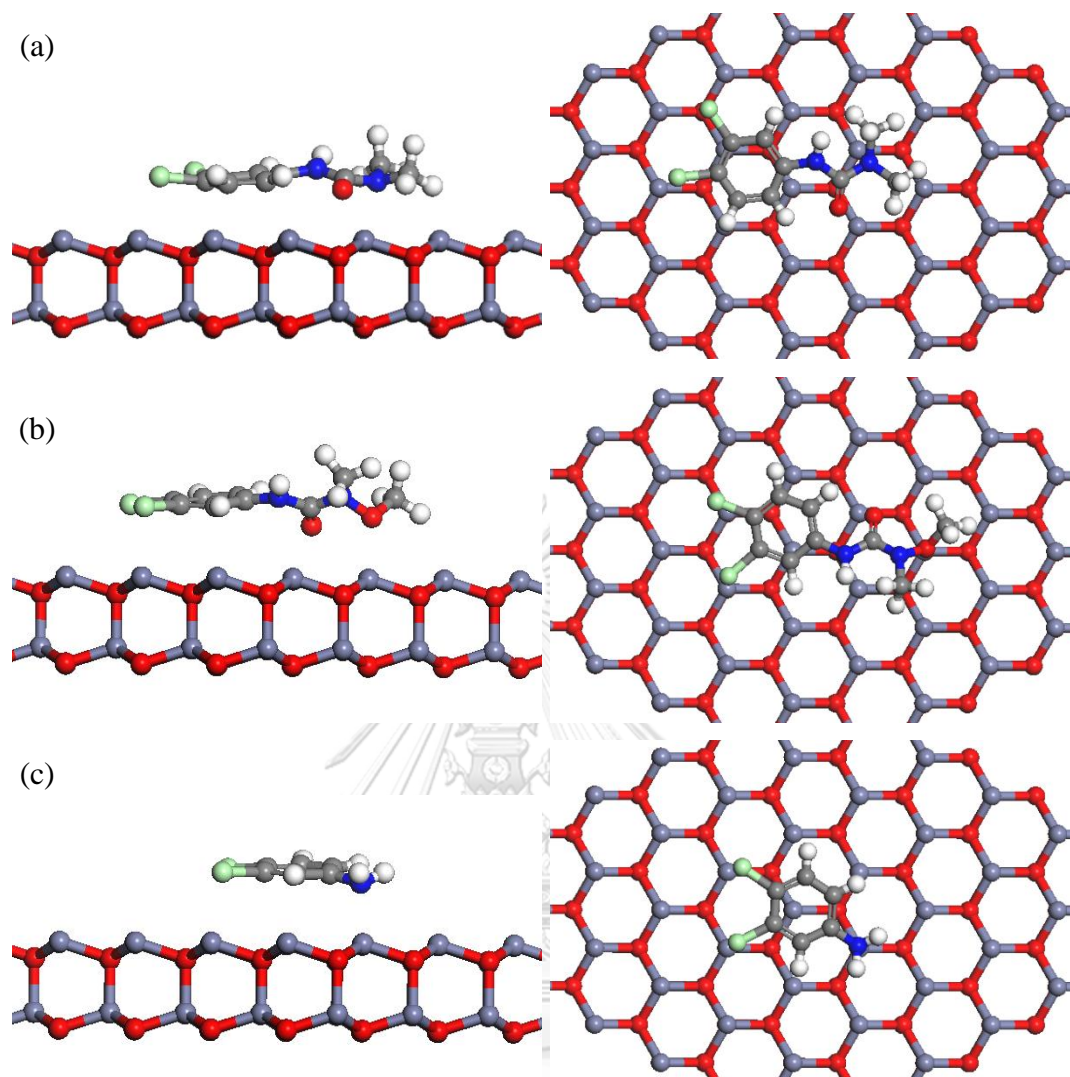


Figure 4.16 The adsorption models of diuron (a), linuron (b) and DCA (c) on zinc-terminated surface.

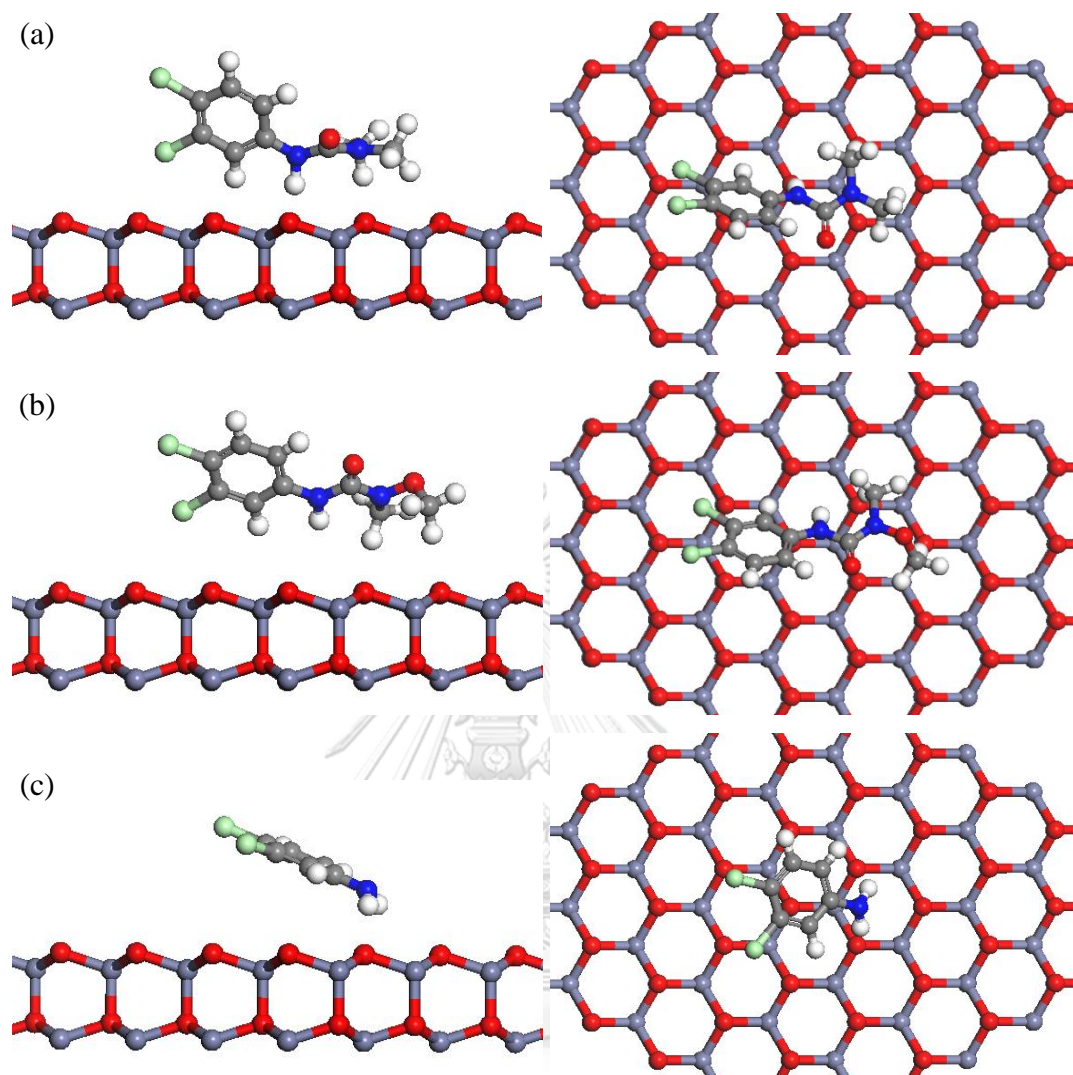


Figure 4.17 The adsorption models of diuron (a), linuron (b) and DCA (c) on oxygen-terminated surface.

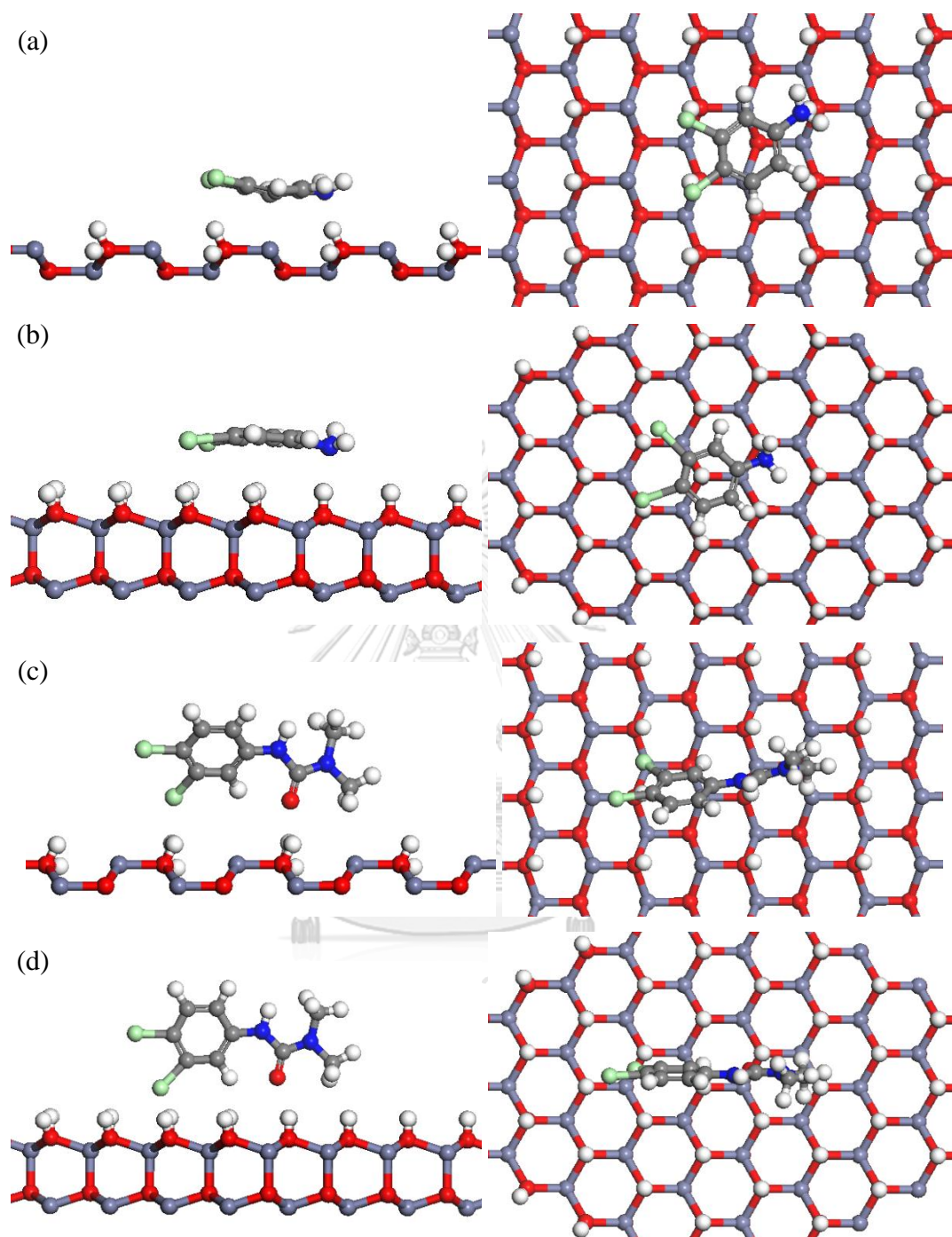


Figure 4.18 The adsorption models at pH4 of DCA on mixed-terminated surface (a), oxygen-terminated surface (b), diuron on mixed-terminated surface (c) and oxygen-terminated surface (c).

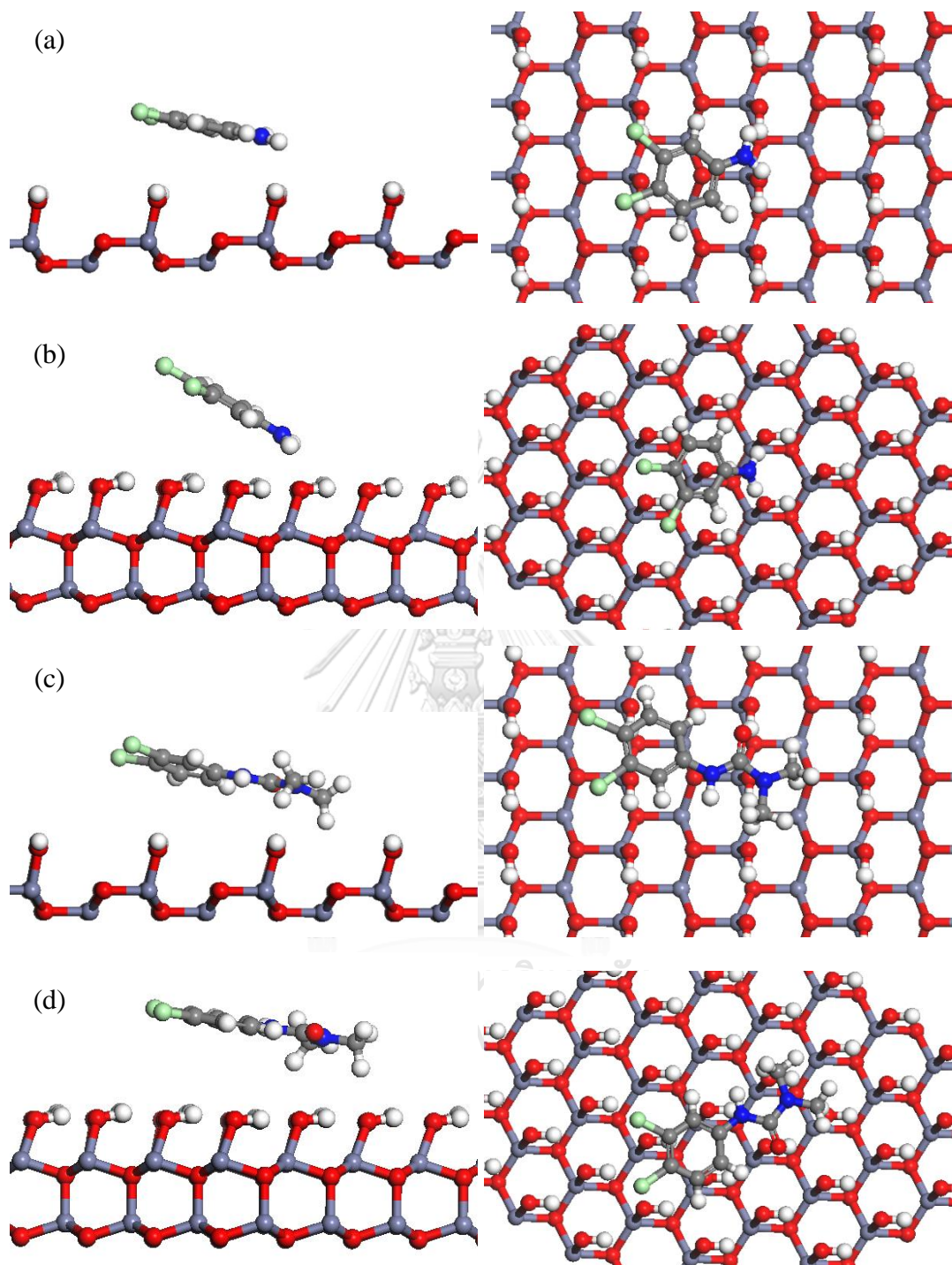


Figure 4.19 The adsorption models at pH10 of DCA on mixed-terminated surface (a), oxygen-terminated surface (b), diuron on mixed-terminated surface (c) and zinc-terminated surface (d).

As seen from the results, it can be clearly indicated that the adsorption configurations are similar to that in vacuum systems. The occupied surface area of herbicides are shown in Table 4.5.

Table 4.5 The occupied surface area of herbicides on ZnO surface in water-soluble system.

pH	molecule	surface	occupied surface area (\AA^2)
4	DCA	mixed-terminated	80.74
		oxygen-terminated	84.14
	diuron	mixed-terminated	84.63
		oxygen-terminated	72.36
7	DCA	mixed-terminated	80.54
		oxygen-terminated	73.48
		zinc-terminated	77.99
	diuron	mixed-terminated	112.88
		oxygen-terminated	95.20
		zinc-terminated	114.50
	linuron	mixed-terminated	124.87
		oxygen-terminated	105.24
		zinc-terminated	117.79
10	DCA	mixed-terminated	81.32
		zinc-terminated	75.61
	diuron	mixed-terminated	117.59
		zinc-terminated	118.80

Due to the similar adsorption configuration between in vacuum and in solvent, the occupied surface area of herbicides are also the same tendency. At pH10, the occupied surface area the largest while those are the smallest at pH4. However, the adsorption energy as shown in Table 4.6 is considered to slightly different.

Table 4.6 The adsorption energy of herbicides on ZnO surfaces in water-soluble system.

pH	surface	molecule	adsorption energy (kcal/mol)
4	oxygen-terminated	diuron	-48.58
		DCA	-30.97
	mixed-terminated	diuron	-35.39
		DCA	-27.06
7	oxygen-terminated	diuron	-42.86
		linuron	-46.51
		DCA	-39.91
	zinc-terminated	diuron	-38.17
		linuron	-40.89
		DCA	-34.48
	mixed-terminated	diuron	-31.89
		linuron	-27.89
		DCA	-28.93
10	zinc-terminated	diuron	-34.25
		DCA	-42.60
	mixed-terminated	diuron	-27.50
		DCA	-31.30

Although, the adsorption energy in water-soluble systems are higher than that in vacuum systems, these results are the same trend as the vacuum systems. This may be the interaction between herbicides and water lead to the stronger adsorption on surfaces.

In the system with the large amount of water, the adsorption sites of herbicides can be blocked by the adsorbed water. However, the adsorption energy of water on polar surfaces (i.e. -35.04 kcal/mol on zinc-terminated surface and -39.96 kcal/mol on oxygen-terminated surface) are less than that of herbicides. These cause herbicides can successfully take up the adsorption sites on polar surface which can be seen from the high adsorption capacities. In the same time, the adsorption energy of water is

slightly more than that of herbicides on non-polar surface which is -33.12 kcal/mol. This results to the lower coverages of herbicides on this surface which correspond with the low adsorption capacities.

4.3 Photocatalytic degradation

The catalysts are activated by equal or greater energy than the band gap's energy. The electrons are stimulated to conduction band and leave the holes on valence band in the same time. The photogenerated species transfer to react with the surrounding oxygen or water and hydroxyl ions on catalysts' surface which are resulted to reduction and oxidation reaction, respectively. The strongly oxidizing superoxide and hydroxyl radicals are formed. Due to the less amount of oxygen in system, so in this section will focus only on hydroxyl radicals. It is found that these radicals have the potential to degrade undesired organics compounds which are adsorbed on the surface of catalyst [79-83]. Although some of these radicals can diffuse to react with compound in bulk phase, the diffusion is limited by their lifetime. Therefore, the reaction can be neglected when compared with the reaction on surface [7, 84]. The photocatalytic oxidation can take place via either direct or indirect oxidation. Direct oxidation can take places when holes directly react with the adsorbed compounds while indirect oxidation occur when hydroxyl radicals which are generated from the reaction between holes and adsorbed hydroxide anions or water diffuse to oxidize the adsorbed compounds on surface. However, chemisorption is a prerequisite for direct oxidation [85], while physisorption is preferred for indirect oxidation. From previous discussion, herbicides adsorb on any surfaces of ZnO by electrostatic interaction, so degradation processes in this research are suggested to occur via indirect oxidation. Although, the adsorption characteristic during photocatalytic degradation which the catalysts are irradiated may be changed. Because the photocatalytic process is complex, the route of process (direct or indirect oxidation) are difficultly indication. Many researches propose that the physisorption in the dark adsorption can occur in the same way for irradiation. Moreover, the oxidation can proceed via indirect process in the system with large amount of water and high enough light intensity [86, 87]. Photocatalytic degradation was studies in

micro-reactor due to negligence of mass transfer resistance. ZnO powder and ZnO nanorods are coated on the glasses by spin-coating method. The catalysts are adhered on the glasses on the first layer and are adhered together on the next layers by van der Waals force. Both of ZnO films are assumed to have the similar thickness due to the catalyst loading control, the less volume of ZnO powder which has the larger particles size are coated on the glasses, compared with ZnO nanorods. However, the thickness of ZnO film does not affect the photocatalytic degradation because the exposed surface of ZnO which are only on the top layer are stimulated by illumination. The residence time within micro-reactor was easily controlled by adjusting the flowrate. It should be noted that the both catalyst contents coated on glass substrate were the same.

The experiments were also operated in batch for the preliminary studies. The reaction rate is clearly slow due to the effect of mass transfer. Although the light sources used in this experiment were the same, their number were not. Therefore, the batch operation cannot be compared with the continuous operation.

4.3.1 Effect of morphology of ZnO.

The photocatalytic degradation results of herbicides are shown in Figure 4.15. It should be noted that diuron, linuron and DCA are degraded to 2.11%, 4.10% and 2.96%, respectively by photolysis at the longest residence time.

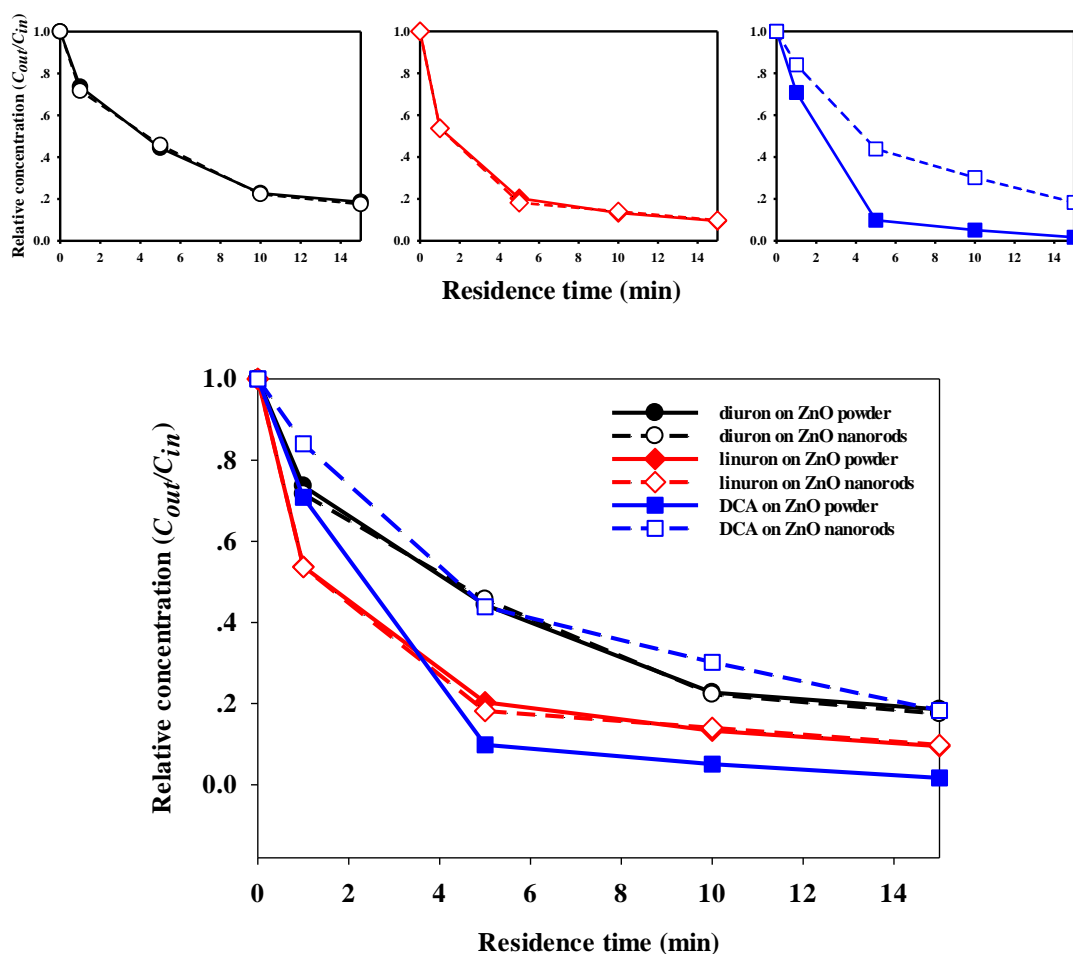


Figure 4.20 The photocatalytic degradation of diuron (black), linuron (red) and DCA (blue) on ZnO powder (solid) and ZnO nanorods (dash).

Although, ZnO powder has the highest adsorption capacity and is expected to mostly degrade herbicides, the results inversely show the equal ability for photocatalyst, except for the degradation of DCA. Therefore, the degradation rate on mixed-terminated of nanorods is suggested to be faster than the reaction on polar surface.

As explained above, the photogenerated holes transfer to react with water or hydroxyl groups adsorbed on surface to produce strong oxidize hydroxyl radicals ($\text{OH}\cdot$). Therefore, catalyst with smaller particle size have more exposed surface area to provide the reaction between photogenerated products and surrounding water [88]. The chemisorption of water or hydroxyl species, which are trap sites of electrons and

holes will decrease their recombination [89]. Therefore, the larger surface area will increase the surface for photogenerated electron and holes trapping. From catalysts characterization, the surface area of ZnO nanorods is one order of magnitude higher than that of ZnO powder. In addition, it has been reported that the degradation activity is decrease by the recombination of electrons and holes within the large volume of catalyst or large crystallized size [90]. Therefore, the transfer of electrons and holes to surface in large volume of ZnO powder have the higher opportunity for recombination. The rate limiting step of photocatalytic degradation is suggested to be the adsorption on surface due to the large time scale, compared with the generation of photogenerated electrons-holes or their transfer to surface.

However, the surface area is not one indicator for the activity of degradation of catalyst because it cannot explain the degraded behavior of DCA. It found that the ability of herbicides elimination is also relates to their adsorption configurations on surface. Degradation occurs from the attack of radicals on surface, so adsorbed area will increase degradation chance. Although ZnO powder has the high adsorption capacity, the adsorbed aromatic ring on polar surface is more difficult to break down. Aromatic is cyclic compound that consist of alternated single and double bond. Electron within aromatic can be delocalized around the ring, so it is more stable than other organic geometry. It is noteworthy that ring of degraded molecule will be opened in last step even it is attacked by radicals at the beginning of reaction [91-93]. The results show the faster degrading and higher amount of eliminated DCA on ZnO powder as seen in Figure 4.15. For DCA with no aliphatic side, the higher rate of DCA degradation on ZnO powder is the result of the higher amount of DCA adsorbed on surface, compared with the degradation rate on ZnO nanorods.

Comparing diuron and linuron, the degradation rate of linuron is higher than that of diuron which is due to the existence of alkoxy group on linuron's molecule. High electronegativity of oxygen in alkoxy group and nearby nitrogen of amide group is result to the longer bond length and less bond strength [94]. Moreover, it has been reported that linuron has more reactive sites for nucleophilic, electrophilic and free radicals attack [95]. These lead to instability in chemical reaction.

4.3.2 Effect of pH.

In natural environment, water source from used herbicides in agriculture shows different acidic-basic which depends on the type of herbicides. Generally, the pH values of water from agriculture are below 5.5 or above 9.5. However, there are many factors that affect the pH of natural water source such as ions and amount of residual herbicides. In this research, we focus on only the effect of pH on adsorption and photocatalytic degradation. The photocatalytic degradation of diuron at pH4 and 10 are shown in Figure 4.16. Under acidic and basic condition, ZnO nanorods show the ability in degradation same as ZnO powder even the adsorption capacity of ZnO powder is higher than that of ZnO nanorods. This is resulted from the large surface area of ZnO nanorods which provide for trapping the photogenerated products of adsorbed water as previous discussion. However, both ZnO powder and nanorods have the high adsorption capacity in acidic condition, the degradation rate of diuron on these catalysts are not significantly different. It is suggested that the removed diuron rate in basic condition is faster than that in acidic condition.

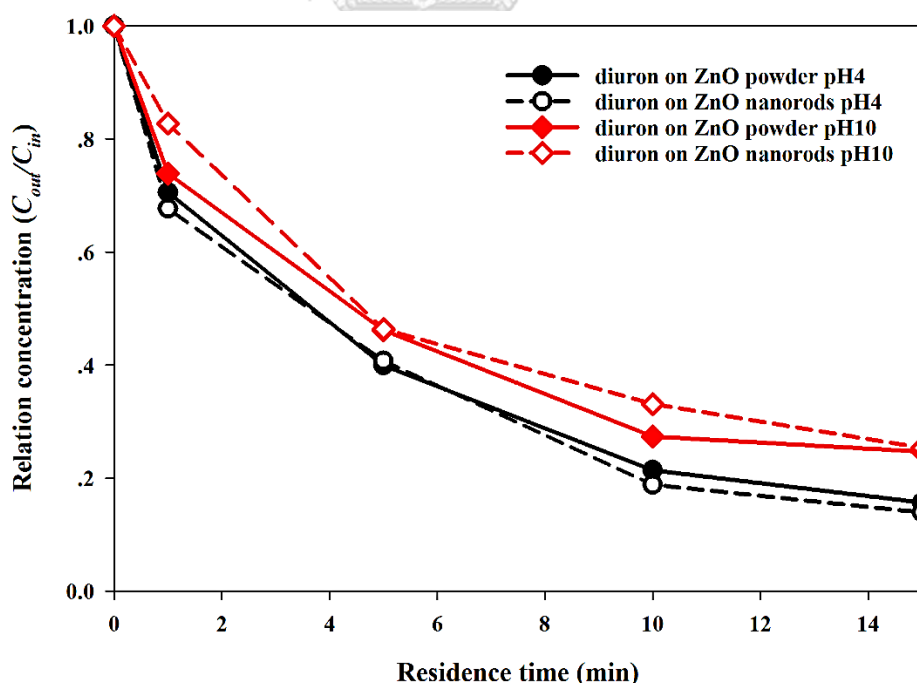


Figure 4.21 The photocatalytic degradation of diuron on ZnO powder (solid line) and ZnO nanorods (dash line) at pH4 (black) and pH10 (red).

In basic conditions, solution consists of large amount of hydroxyl anions which form strongly chemical adsorption on surface, and can react with positive holes to generate hydroxyls radical [96-100]. The generation of hydroxyl radicals on surface can be explained as in Equation 4.2 [8]. In addition, it has been reported that the ability in degradation of organic compound on ZnO is increase when pH is increase to optimum pH at pH10 and increasing pH higher than 10 the activity will be decreased.



4.4 Photodegraded intermediated

All intermediates are detected by LS-MS/MS in every residence time (the detection of intermediates are shown in APPENDIX E). It should be noted that the intermediates shown in this part are the major intermediates.

4.4.1 Effect of surface on photodegraded intermediates

Diuron and linuron solution were collected after the period of experiment at various residence time to arrange the pathway in degradation process. Figure 4.17 shows the intermediates formed from the degradation of linuron at the shortest residence time. They are assumed to directly derive from the adsorption of linuron on ZnO surfaces. Unfortunately, the degraded products from degradation of DCA cannot be identified by LC-MS/MS due to the limitation of small molecular size. It should be noted that no intermediates formed from photolysis process.

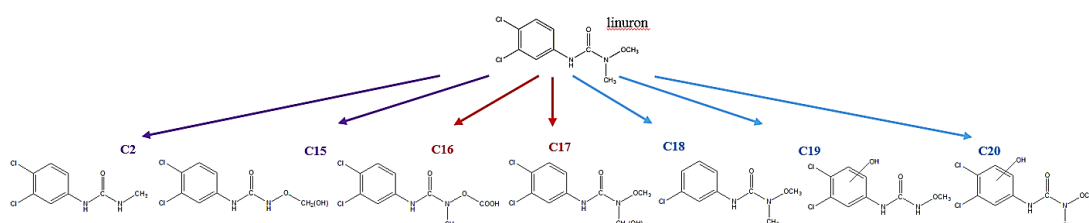


Figure 4.22 The detected intermediated from degradation of linuron at shortest residence time (1 min) on ZnO nanorods (red arrow) and ZnO powder (blue arrow). The common detected intermediates on both catalyst are presented on purple arrow.

It has been found that the molecular structure of intermediates formed at this residence time are suggested to directly relate to the adsorption configuration of linuron. From previous discussion, linuron adsorbs on mixed-terminated surface with its alkoxy group which leads to the shortest distance at this position while the longest distance between linuron and surface is located on substituent chlorine due to the repulsive of surface. Hydroxyl radicals formed on surface, as commonly background knowledge, are effortlessly attack at adsorbed part of linuron results to compound 2, 15, 16 and 17. By the attack at only aliphatic part, they are evidence to prove this hypothesis. Although, absorbed oxygen should has the high opportunity to be attack by radicals, other functional groups are also react with these radicals. In the same concept, the detected intermediates on ZnO powder, i.e. compound 2, 15, 18, 19 and 20, are attacked at both ends of molecule which correspond with the adsorption of linuron on polar surface.

Compound 2 and 15 are common intermediates that are found on both forms of ZnO. They are created from demethylation and hydroxylation at aliphatic sides. Generally, radicals will attack on weak bond so demethylation occur at adsorbed oxygen which bond with nitrogen of amide group. Two adjacent high electronegativity have long bond length and less bond energy which result to the high reactivity as previously explained. Therefore, elimination of alkoxy group easily occurs which results in compound 2. Two hydrogen of two methyl groups on aliphatic, which are found to adsorb on both polar and non-polar surface, are also attacked by radical lead to compound 15.

Compound 16 is suggested to form in higher amount than compound 17 because methyl of alkoxy group is closer to mixed-terminated surface than methyl group next to amide group.

Compound 18 and 20, which are formed on ZnO powder, are found to attack at aromatic side only. They can possibly occur on zinc-terminated surface. Although, oxygen of carbonyl group is the closet position to surface, the high bond energy and short bond length of this group will cause unstable radical form. In the same time, the bond of oxygen of alkoxy group is difficultly attacked by radicals due to the elevated two methyl group from the same plane of molecule. Compound 19 which is attacked

on both of molecule may be formed on oxygen-terminated. This is the result from the closest adsorbed methyl and aromatic are attacked simultaneously.

The detected intermediates from degradation of diuron at shortest residence time are shown in Figure 14.18. Compound 1 and 2 occur from the adsorbed methyl group at end of diuron on mixed-terminated of non-polar surface. It should be noted that oxygen of carbonyl group tolerate to the reaction of radicals. In addition, compound 2 is found to obtain on ZnO powder which is suggested to form on oxygen-terminated surface because this adsorbed methyl is closer to oxygen-terminated than zinc-terminated surface. Compound 11 is attacked at aromatic side only, while compound 9 and 11 are attacked at both sides of diuron. It is hard to confirm which compound occur on either zinc or oxygen-terminated surface due to the possibility of these intermediates formed on both surfaces.

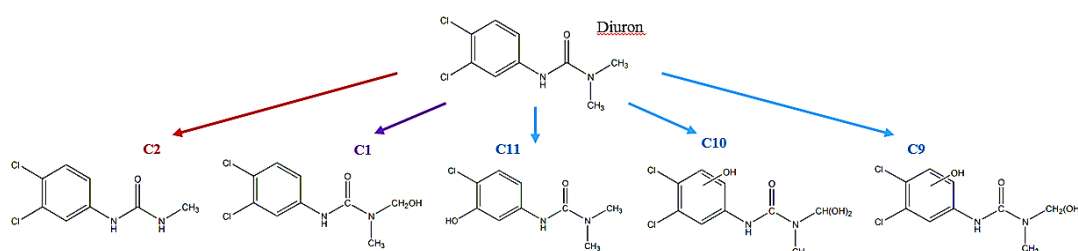


Figure 4.23 The detected intermediated from degradation of diuron at shortest residence time (1 min) on ZnO nanorods (red arrow) and ZnO powder (blue arrow).

The common detected intermediates on both catalyst are presented on purple arrow.

The intermediates are formed in degradation of diuron even in 1min of residence time, so these intermediates and diuron can compete to adsorb on surfaces. The comparison of adsorption between diuron and intermediates are difficult to predict because there are many factors that affect the adsorption. However, at this residence time, the large amount of diuron still remain in the system, so the adsorption sites which are covered by intermediates is much less than that covered by diuron.

In adsorption phenomenon with the large amount of diuron, it may be affected by the interaction between molecules of nearby adsorbed diuron. The calculation of interaction of diuron while they are adsorbing on surface are conducted to study. The

examples of these simulations are shown in Appendix C. It can be seen that the adsorption orientation of diuron on surface remains unchanged even though it has been influenced by the intermolecular interaction of diuron.

By the nature of physisorption, adsorbed molecules can adsorb and desorb throughout the process. The reaction is proceed, several intermediated will be formed. The intermediates formed at the first period affect the intermediates formed later on. The pathway of diuron and linuron arranged by residence time are shown in Figure 4.19 and 4.20, respectively.

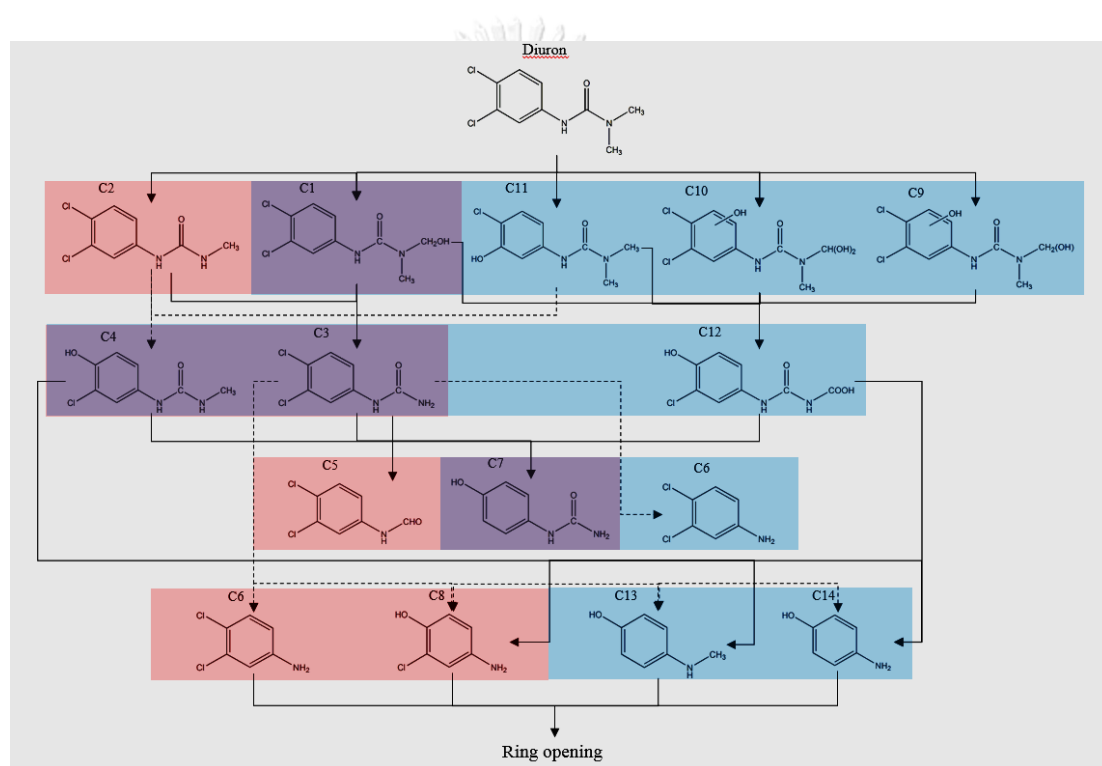


Figure 4.24 The intermediates formed arranged by residence time of diuron on ZnO nanorods (red box), ZnO powder (blue box) and both ZnO (purple box).

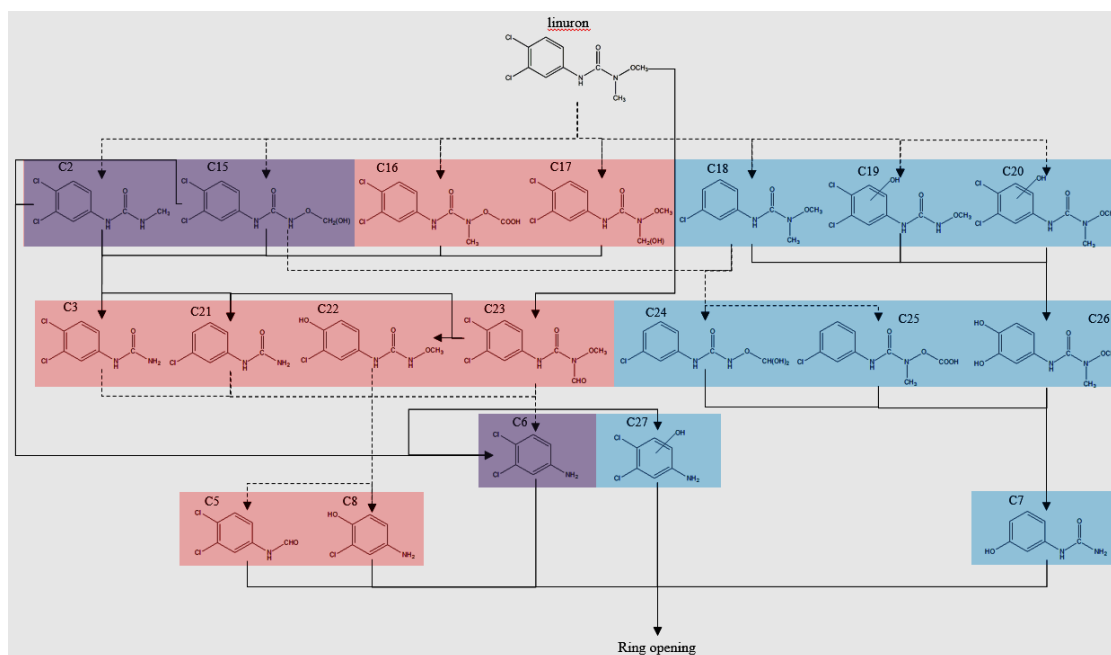


Figure 4.25 The intermediates formed arranged by residence time of linuron on ZnO nanorods (red box), ZnO powder (blue box) and both ZnO (purple box).

4.4.2 Effect of pH on Photodegraded intermediates

Figure 4.21 shows intermediates formed in acidic condition on ZnO powder and ZnO nanorods. Compound 2 and 3 are common intermediates formed on both ZnO powder and ZnO nanorods which is due to similar adsorption configuration of diuron on both surfaces. It should be noted that the attack of radicals at end methyl group to form secondary alkyl radicals is more stable than the attack at double bond of carbonyl group. Therefore, radical form will obtain in the most stable structure even double bond of carbonyl group is closer to surface than methyl group. Compound 1 are formed by the attack of radicals on both sides of molecules which different from that on the same surface at pH7. The sequences of intermediates on non-polar surface at this pH is different from that at pH7 due to the additional aromatic attacked intermediate. Compound 11 and 12 are formed on only ZnO powder. It has been clearly seen that one adsorbed methyl lead to hydroxylation reaction which is suggested from hydroxyl radicals, while no indication of reaction on another methyl which is more relaxing away from surface. While oxygen-terminated is formed bond with protons, zinc-terminated surface is slightly similar characteristic

as at pH7. This is confirmed by the result of zeta potential which net positive charged occur at the low pH. If any negative charges cover on zinc-surface, the balancing of opposite charges occur and the zeta potential result at this pH has not been shown the much higher positive than that at pH7. Compound 13 is the same intermediate found on polar surface at normal condition (compound 11 at pH7). By its molecular structure, the attack on aromatic, it can be assumed to occur from zinc-surface. Therefore, it can be detected at pH7 and pH4 which zinc-surface is not covered by any charges. It should be noted that the result from calculation show no cover of positive charge on zinc-surface due to the same polarity between charges and surface.

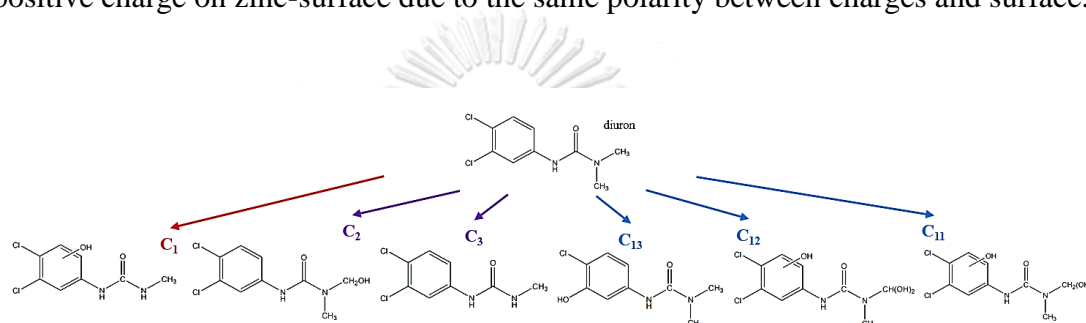


Figure 4.26 The detected intermediated from degradation of diuron at shortest residence time (1 min) pH4 on ZnO nanorods (red arrow) and ZnO powder (blue arrow). The common detected intermediates on both catalyst are presented on purple arrow.

Figure 4.22 shows the intermediates forms on both catalysts at pH10. The detected intermediates in this condition are formed on negative surface which is caused by the cover of hydroxide anions on zinc-terminated surface. Same as pH4, the negative charges does not cover on oxygen-surface due to the same polarity.

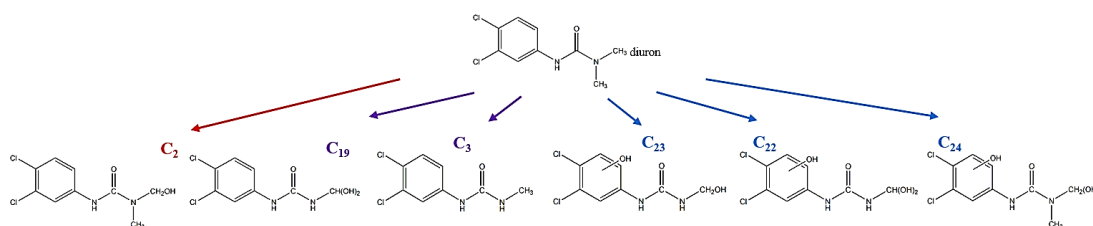


Figure 4.27 The detected intermediated from degradation of diuron at shortest residence time (1 min) pH10 on ZnO nanorods (red arrow) and ZnO powder (blue arrow). The common detected intermediates on both catalyst are presented on purple arrow.

Compound 19 and 3 are common intermediates that occur on both ZnO powder and ZnO nanorods. Two methyl groups are attack by hydroxyl radicals which is the results from the adsorption configuration of diuron. At this pH, diuron adsorb on both polar and non-polar surface in the similar orientation and lead to the attack of radicals in the similar way. The repulsive of surface to aromatic side cause the wide distance and it decrease opportunity of reaction at this side. Compound 2 is formed by hydroxylation on ZnO nanorods and no signal from the attack at aromatic side is detected. Compound 22 and 23 are formed on only polar surface of ZnO powder which are quite different from pH4 and 7. These intermediates are found to be attacked at both two methyl groups which are mostly approach to surface. Compound 24 is attacked at both sides of diuron and it also be found on oxygen-terminated at pH7 (compound 10). Therefore, it is suggested to formed on this surface without no cover of charges

Diuron and its intermediates adsorb and desorb on surface due to the nature of physical adsorption. The extend reaction cause smaller molecular size of degraded compounds which are various depend on the adsorption configuration of diuron at initial process and the way that radicals attack to form the most radical structure. The intermediates occur at each residence time are detected and shown in Figure 4.23 at pH4 and figure 4.24 for pH10.

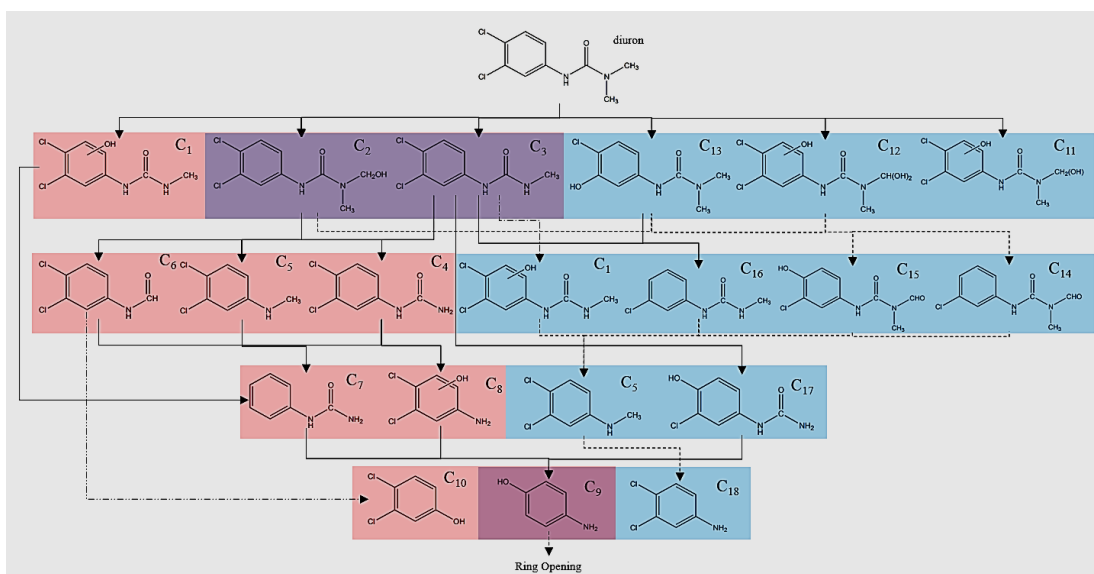


Figure 4.28 The intermediates formed arranged by residence time of diuron on ZnO nanorods (red box), ZnO powder (blue box) and both ZnO (purple box) at pH4.

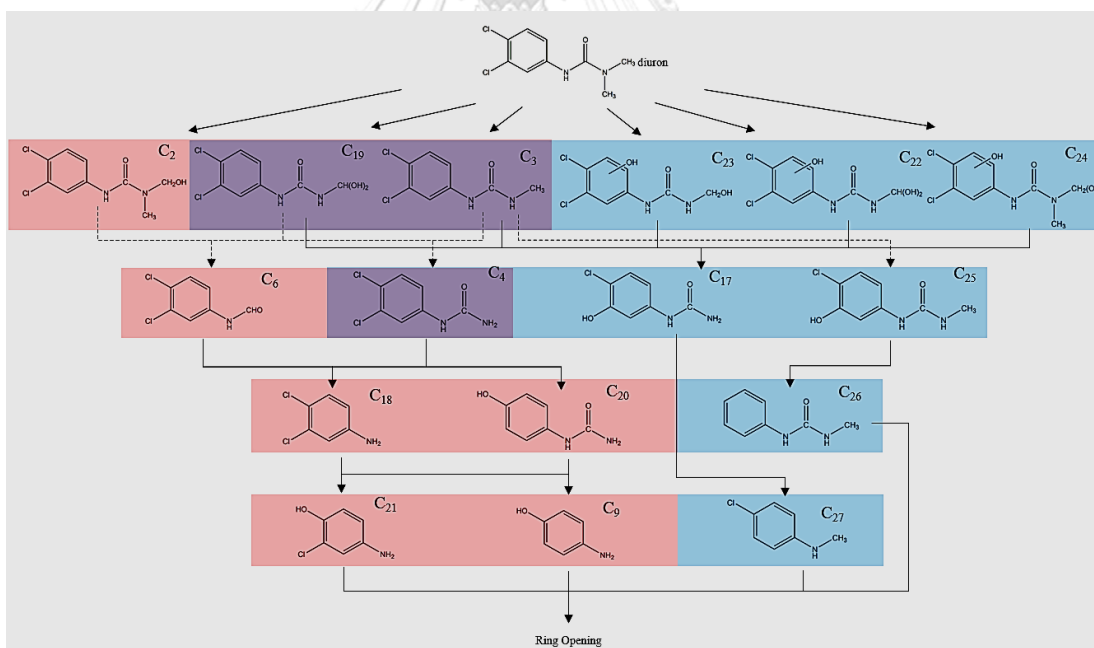


Figure 4.29 The intermediates formed arranged by residence time of diuron on ZnO nanorods (red box), ZnO powder (blue box) and both ZnO (purple box) at pH10.

4.5 Toxicity test

4.5.1. Effect of surface on toxicity

Diuron can affect toxicity of organism [101, 102] in many ways and its degradation which results to intermediates can cause more toxic than their parent. In degradation process, intermediate products formed during reaction were assessed the level of toxic to ensure the environmental safety. The mung bean seeds were used for toxicity measurement. Their sprouting length from herbicides solution were compared with those in DI water as seen in Figure 4.25.

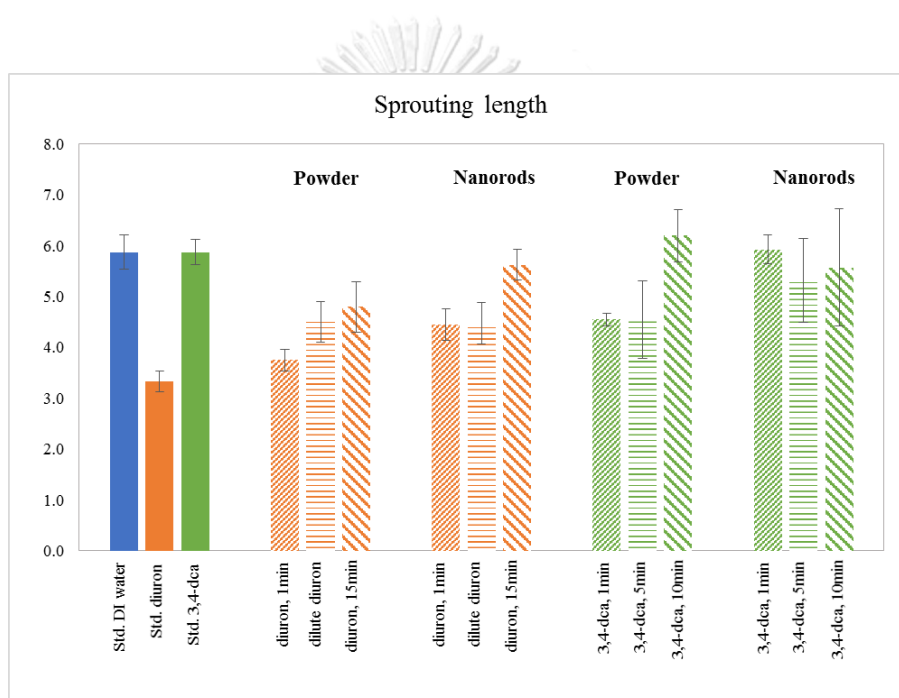


Figure 4.30 Phytotoxicity assessment of the degraded products from the photocatalytic degradation of diuron (striped orange bar) and DCA (striped green bar), compared with standard diuron (orange bar) and DCA (green bar).

Compares with control DI water, standard diuron is much more toxic while standard DCA seem not to be toxic as well. At 1 min of residence time, the degraded products on ZnO powder is more toxic than that on ZnO nanorods which indicates from the shorter sprouting length treated in degraded solution from ZnO powder system. Although intermediates have been already formed at shortest residence time, diuron is also incompletely degraded. Therefore, it cannot be clearly identified the

cause of toxicity. To prove that, diluted diuron to the equivalent concentration at outlet stream and the degraded solution were compared but there are not significantly different between these two solutions. However, the residence time is increased to longest residence time (15 min), the toxicity of degraded product is decreased in both ZnO powder and ZnO nanorods system.

In the same time, degraded DCA at 1 min and 5 min of residence time on ZnO powder are more toxic than standard DCA which may be due to some generated toxic intermediates. Inversely, the toxicity of degraded from DCA degradation on ZnO nanorods are seem to be not different at all residence time because some generated toxic intermediates may be formed slowly due to the slower rate of DCA degradation or differently toxic intermediates are formed. T-test was conducted to evaluate the different toxicity of two groups of samples. The results shows that the toxicity of these solutions are not different.

Cytogenotoxicity test is used for detailed assessment of intermediated in term of aberration and cell division. Table 4.5 shows the mitotic index which indicate the number of cell division from total observed cell. The higher amount of mitotic index refers to the less toxicity. The ratio of aberration cells and dividing cells are also presented. This ratio is calculated from cell in dividing step only. The abbreviations in the table have the following definition; CB: chromosome breaks, MC: metaphase cluster, ML: metaphase lagging chromosome, MA: metaphase aberration, AB: anaphase bridges, AL: anaphase lagging chromosome. Each value represents the mean \pm sd of four replicates per treatment and the total observed cells is 500 per replicates.

The indication of low level of toxicity is related to the high mitotic index (%MI) and low aberration index (%ARD). From the table, it can be seen that standard diuron is much more toxic than control DI water, while standard DCA is less toxic than diuron. At 1 min of residence time, degraded products on both ZnO catalysts are more toxic than diluted diuron solution which is the result from toxic intermediates formed in process. However, these intermediates cannot be compared the level of toxicity to diuron due to unknown concentration of intermediates. The values of %MI and %ARD indicate the higher toxicity of degraded products on ZnO powder, compared with that on ZnO nanorods. Therefore, intermediates formed on only ZnO

powder (i.e. Compound 9, 10 and 11) are toxicants. When the residence time is increased to 15min, the toxicity is decreased especially for degraded products on ZnO nanorods which the values of %MI and %ARD are close to that of control DI water. At longest residence time, degraded products on ZnO powder are still more toxic than that on ZnO nanoords. Only compound 13 and 14 formed on ZnO powder which assumed to be the cause of toxicity.



Table 4.7 The mitotic index, the number of chromosomal aberration and the aberration index of degraded products from diuron and DCA degradation.

Treatment	Number of dividing cells							Number of cells with chromosome aberrations				Mitotic index (%MI)	Aberration index (%ARD)
	CB	MC	ML	MA	AB	AL							
DI water pH7	4.25 ± 0.38	1.25 ± 0.15	2.00 ± 0.13	0.25 ± 0.08	0			19.70 ± 0.72	0.0787 ± 0.004				
diuron 10ppm pH7	1.50 ± 0.28	4.00 ± 0.31	3.50 ± 0.8	0.75 ± 0.20	0	0.50 ± 0.33		9.45 ± 0.27	0.2174 ± 0.033				
3,4-dichloroaniline 10ppm pH7	4.00 ± 0.80	4.50 ± 0.39	3.00 ± 0.42	1.25 ± 0.36	0	2.75 ± 0.58		16.20 ± 0.29	0.1917 ± 0.022				
degraded diuron on powder t: 1min	8.00 ± 0.78	1.50 ± 0.13	0.25 ± 0.05	0.25 ± 0.10	0	1.25 ± 0.80		10.30 ± 0.24	0.2188 ± 0.029				
dilute diuron in powder system	5.25 ± 0.23	2.00 ± 0.22	1.75 ± 0.70	0.50 ± 0.18	0	1.25 ± 0.63		13.50 ± 0.40	0.1598 ± 0.025				
degraded diuron on powder t: 15min	5.25 ± 0.27	2.25 ± 0.27	1.25 ± 0.32	0	0	0.75 ± 0.22		15.15 ± 0.22	0.1254 ± 0.007				
degraded diuron on nanorods t: 1min	7.75 ± 0.53	0.75 ± 0.13	1.50 ± 0.45	0	0	1.50 ± 0.58		11.45 ± 0.10	0.2008 ± 0.026				
dilute diuron in nanorods system	6.50 ± 0.36	3.00 ± 0.53	0.50 ± 0.13	0	0	1.00 ± 0.29		13.10 ± 0.13	0.1679 ± 0.014				
degraded diuron on nanorods t: 15min	6.25 ± 0.33	0.75 ± 0.27	0.25 ± 0.02	0.25 ± 0.03	0	1.00 ± 0.29		18.90 ± 0.38	0.0900 ± 0.004				
degraded 3,4-dca on powder t: 1min	9.00 ± 0.43	4.50 ± 0.40	0.50 ± 0.41	0.50 ± 0.12	0	13.90 ± 0.17		0.2086 ± 0.005					
degraded 3,4-dca on powder t: 5min	4.50 ± 0.14	8.00 ± 0.80	2.25 ± 0.25	0.50 ± 0.08	0	0.50 ± 0.06		15.00 ± 0.22	0.2102 ± 0.016				
degraded 3,4-dca on powder t: 10min	10.00 ± 0.49	1.75 ± 0.48	1.50 ± 0.09	0	0	1.50 ± 0.26		15.15 ± 0.38	0.1949 ± 0.009				
degraded 3,4-dca on nanorods t: 1min	6.50 ± 0.14	2.50 ± 0.61	2.50 ± 0.22	0.25 ± 0.03	0	1.75 ± 0.34		15.05 ± 0.22	0.1795 ± 0.010				
degraded 3,4-dca on nanorods t: 5min	9.50 ± 0.27	2.00 ± 0.40	0.75 ± 0.07	0	0.25 ± 0.10	0.75 ± 0.06		15.60 ± 0.24	0.1699 ± 0.002				
degraded 3,4-dca on nanorods t: 10min	10.50 ± 0.33	1.25 ± 0.13	0.50 ± 0.02	0	0	0.75 ± 0.04		15.25 ± 0.23	0.1705 ± 0.003				

There are many reports about the effects of these intermediates on mammals. Compound 13 which IUPAC name is 4-(methylamino)phenol can inhibit DNA of lung of hamster at 22mmol/L of dose (from NIOSH), while compound 14 or 4-aminophenol is toxic to liver in mice, renal proximal tubules and nephrotoxicity in rat [103, 104]. It should be noted that compound 1, 6 and 7 are common intermediates which formed in similar amount on both ZnO powder and ZnO nanorods. Therefore, the higher toxicity of degraded products on ZnO powder is not the result of different amount of formed intermediates.

For the toxic of DCA, although %ARD of DCA and diuron are similar, %MI of DCA shows less toxicity than diuron. It indicates that cells treated in DCA have the high dividing rate but its dividing cells are abnormal. The results show that intermediates formed on ZnO powder is more toxic than that on ZnO nanorods which is caused by some reasons. For example, some toxic intermediates specifically formed on ZnO powder or small acids have already generated due to the fast reaction rate in this condition which is supported by the slightly decrease pH from 7.1 to 6.4. Some acidic compounds can cause the toxic to environment [105, 106]. However, the residence time is increased to 5 and 10 min, %ARD is decreased which related to the less toxic. For DCA degradation on ZnO nanorods, the level of toxicity is decrease and stable at 5 min of residence time and the pH value is decreased from 7.0 to 6.6. It may be the result from less toxic intermediates or the less amount of generated acidic compounds. The results from phytotoxicity and cytogenotoxicity test seem to be the same direction. Figure 4.26 and 4.27 shows the examples of cells treated in degraded solution of diuron and DCA, respectively. Treated cells in controlled DI water is normal cells while other treated cells show abnormal cell in each dividing step. It should be noted that these examples can be the representative of population in each conditions.

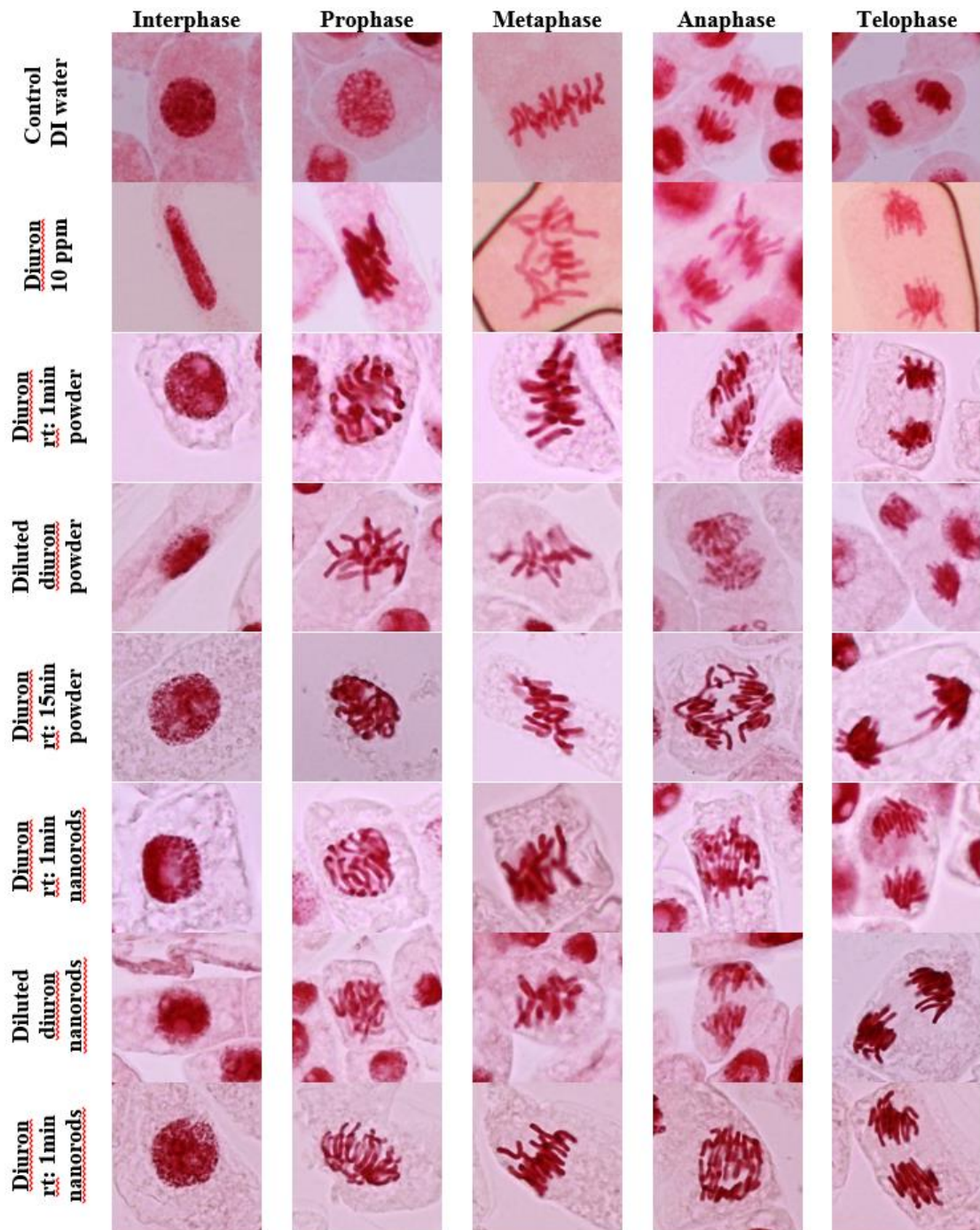


Figure 4.31 The abnormally population representative cells treated in different degraded solution of diuron in each dividing step. Treated cells in control DI water are normal cells.

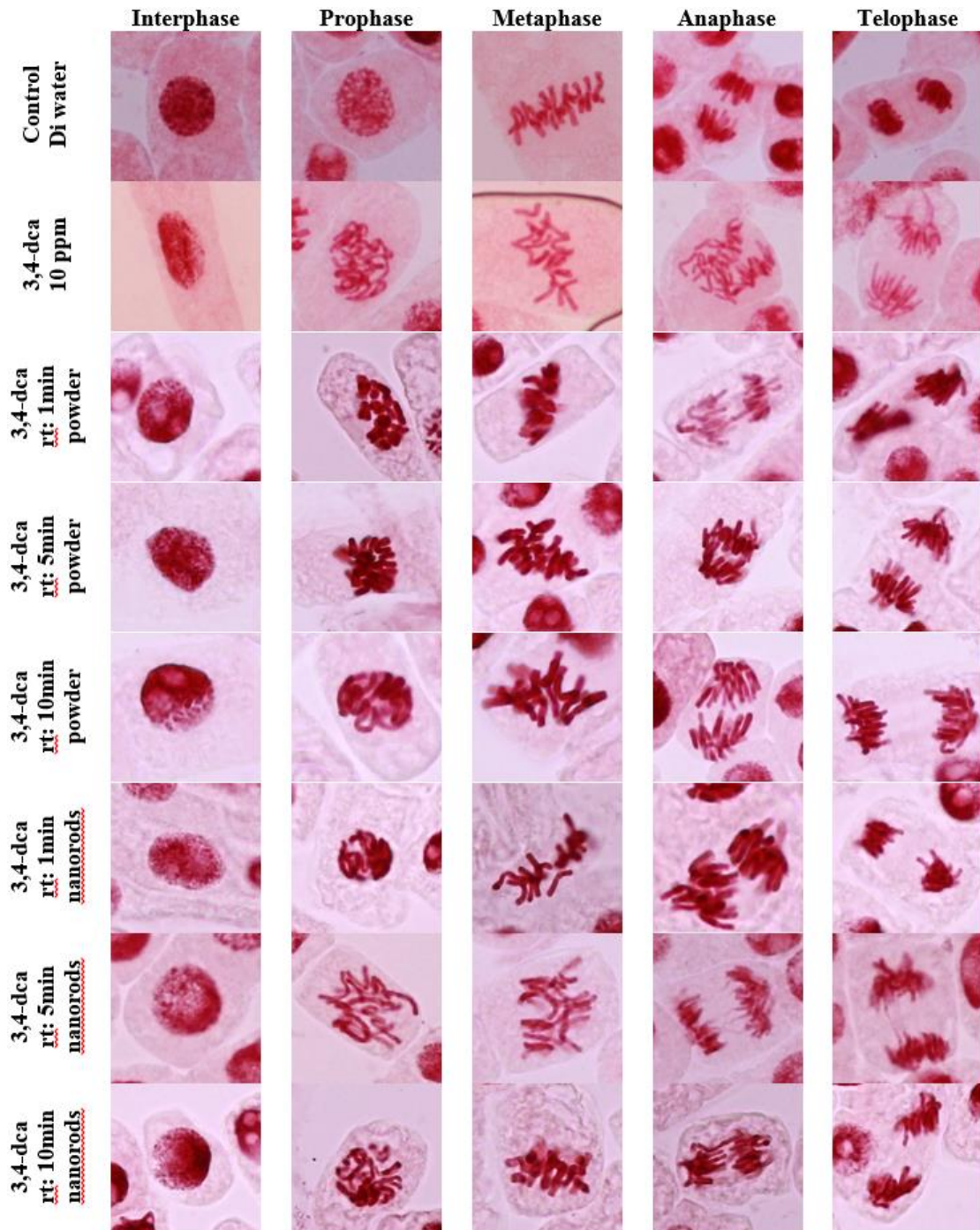


Figure 4.32 The abnormally population representative cells treated in different degraded solution of DCA in each dividing step. Treated cells in control DI water are normal cells.

4.5.2 Effect of pH on toxicity

The different environment may results in increasing the toxicity of diuron and its degradation in different conditions such as in acid or base environment can cause different toxicity. Plants used in toxic study of diuron and its intermediates in various conditions is mung bean which can be identified the level of toxic by the length of sprouting as shown in Figure 4.28.

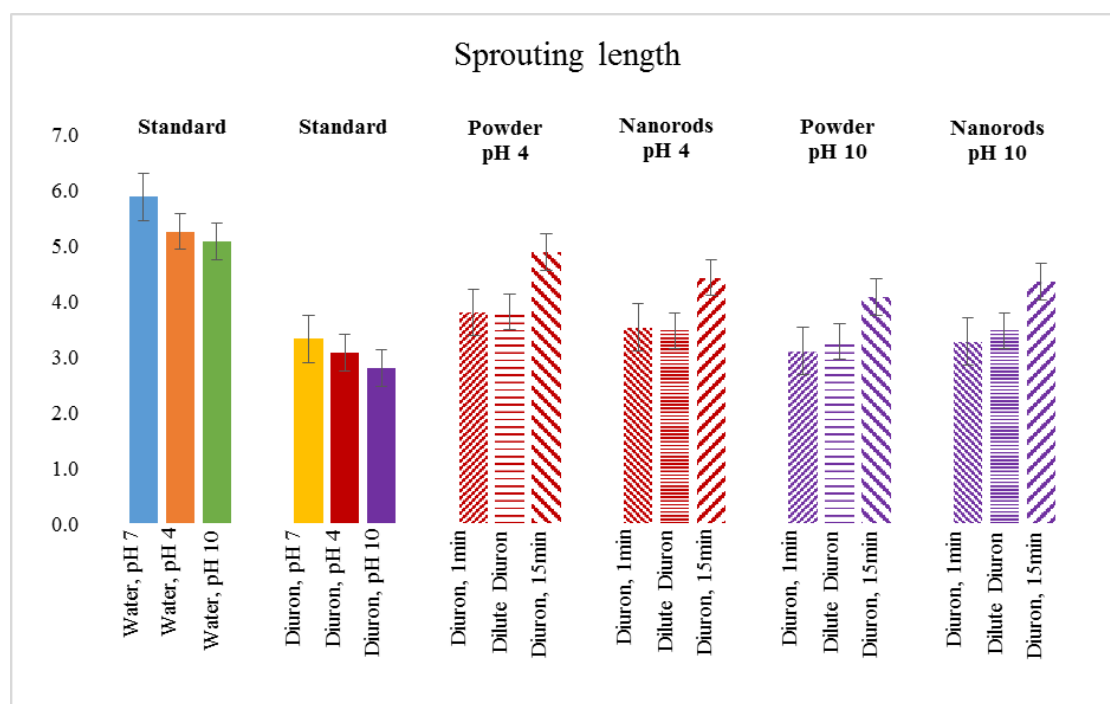


Figure 4.33 Phytotoxicity assessment of the degraded products from the photocatalytic degradation of diuron at pH 4 (striped red bar) and pH 10 (striped purple bar), compared with standard diuron at pH 4 (red bar) and pH 10 (purple bar).

From the figure, it can be seen that no significantly different toxicity of standard diuron in each pH. The toxic of degraded products on both ZnO powder and ZnO nanorods at 1 min of residence time are not different from dilute diuron solution (diluted standard diuron to equivalent concentration with outlet solution) at both pH4 and 10 which is consistent with the results of T-test. However, the decrease of toxicity can be observed when increasing of residence time at all conditions. This may be due to the significantly decrease of diuron and less toxic intermediates. The toxicity of

diuron and its intermediates cannot be exactly indicated in terms of the growth of plants so they are additionally studied in terms of deformation of cell in the dividing step.

The toxicity of diuron and its intermediates in different condition can be analyzed in terms of cell dividing. The plants used in this part is *Allium cepa*. The index used to determine toxicity is the mitotic index (%MI) and the aberration index (%ARD) which indicate the amount of dividing cells from total observed cells and abnormal cell in cell dividing, respectively. The mitotic index and the ratio of aberration cell are shown in Table 4.6. The abbreviations in the table have the following definition; CB: chromosome breaks, MC: metaphase cluster, ML: metaphase lagging chromosome, MA: metaphase aberration, AB: anaphase bridges, AL: anaphase lagging chromosome. Each value represents the mean \pm sd of four replicates per treatment and the total observed cells is 500 per replicates.

From the table, it can be seen that solution (i.e. DI water and degraded products) at both pH4 and 10 are more toxic than that at pH7. In addition, solutions at pH 10 exhibited a higher toxicity than that at pH4, although, their aberration index are similar. At pH4 and 1 min of residence time, degraded products on ZnO catalysts are more toxic than diluted diuron which are related to the formation of toxic intermediates. Moreover, degraded products on ZnO powder are more toxic than that on ZnO nanorods. It is indicated that compounds 11, 12 and 13 which are formed only on ZnO powder may be the cause of toxic. When the residence time is increased to 15 minutes, the degraded products on both catalysts are still toxic compared to DI water even their level of toxic dramatically decreased. The degraded products on ZnO powder are found to be more toxic than that on ZnO nanorods. It is the result from compound 18 which is intermediates occur on only ZnO powder system.

At pH 10 and 1 min of residence time, degraded products on both catalysts are more toxic than diluted diuron which indicates the toxic intermediates formed. When residence time is increased to 15 min, the toxicity of degraded products on ZnO powder is decrease, while that on ZnO nanorods show the opposite result. Degraded products at longest residence time are more toxic than intermediated formed at 1 min even the concentration of diuron is mostly disappeared. Compound 9 and 21 are considered to the toxicants. 4-aminophenol (compound 9) has been reported to be

toxic to renal proximal tubules and nephrotoxicity in rat [103, 104]. In addition, 4-amino2chlorophenol (compound 21) is also nephrotoxicity in the Fischer 344 rat [107].



Table 4.8 The mitotic index, the number of chromosomal aberration and the aberration index of degraded products from diuron at pH4 and pH10

Treatment	Number of dividing cells		Number of cells with chromosome aberrations							Mitotic index (%MI)	Aberration index (%ARD)
	CB		MC	ML	MA	AB	AL				
DI water pH7	98.50 ± 2.10	4.25 ± 0.38	1.25 ± 0.15	2.00 ± 0.13	0.25 ± 0.08	0	0	0	19.70 ± 0.72	0.0787 ± 0.004	
DI water pH4	72.25 ± 1.70	6.00 ± 0.20	1.50 ± 0.25	1.50 ± 0.12	0	0	1.25 ± 0.21	0	14.45 ± 0.78	0.1426 ± 0.014	
DI water pH10	62.75 ± 1.53	7.75 ± 0.60	1.00 ± 0.20	0.50 ± 0.17	0	0.25 ± 0.10	0.75 ± 0.19	0	12.55 ± 0.53	0.1605 ± 0.024	
diuron 10ppm pH7	47.25 ± 1.33	1.50 ± 0.28	4.00 ± 0.31	3.50 ± 0.8	0.75 ± 0.20	0	0.50 ± 0.33	0	9.45 ± 0.27	0.2174 ± 0.033	
diuron 10ppm pH4	37.25 ± 1.23	7.25 ± 0.70	2.50 ± 0.31	1.00 ± 0.19	0	0	0.25 ± 0.07	0	7.45 ± 0.23	0.2961 ± 0.025	
diuron 10ppm pH10	30.75 ± 1.12	6.75 ± 0.37	3.50 ± 0.41	1.50 ± 0.21	0.25 ± 0.18	0	0.75 ± 0.10	0	6.15 ± 0.12	0.4202 ± 0.017	
degraded diuron on powder pH4 at 1min	32.75 ± 1.57	7.25 ± 0.35	2.25 ± 0.28	1.75 ± 0.22	0.25 ± 0.16	0	1.00 ± 0.18	0	6.55 ± 0.57	0.3857 ± 0.012	
dilute diuron in powder system pH4	44.75 ± 1.69	4.00 ± 0.25	2.25 ± 0.21	2.75 ± 0.31	0.50 ± 0.23	0	1.75 ± 0.22	0	8.95 ± 0.69	0.2590 ± 0.023	
degraded diuron on powder pH4 at 15min	52.00 ± 1.27	6.25 ± 0.67	2.25 ± 0.23	1.25 ± 0.23	0	0	1.00 ± 0.18	0	10.40 ± 0.27	0.2065 ± 0.030	
degraded diuron on nanorods pH4 at 1min	38.00 ± 1.15	4.25 ± 0.51	2.50 ± 0.25	1.50 ± 0.24	0	0.25 ± 0.12	2.50 ± 0.36	0	7.60 ± 0.15	0.2900 ± 0.016	
dilute diuron in nanorods system pH4	45.00 ± 1.56	5.50 ± 0.48	1.25 ± 0.19	1.75 ± 0.29	0.25 ± 0.19	0	1.25 ± 0.21	0	9.00 ± 0.56	0.2237 ± 0.044	
degraded diuron on nanorods pH4 at 15min	55.25 ± 1.64	7.50 ± 0.59	0.75 ± 0.08	0.75 ± 0.10	0.25 ± 0.13	0	0	0	11.05 ± 0.34	0.1672 ± 0.008	
degraded diuron on powder pH10 at 1min	34.75 ± 1.43	8.25 ± 0.80	2.25 ± 0.31	0	0.25 ± 0.15	0.50 ± 0.13	2.00 ± 0.27	0	6.95 ± 0.43	0.3826 ± 0.040	
dilute diuron in powder system pH10	44.00 ± 1.36	7.50 ± 0.78	1.75 ± 0.18	1.25 ± 0.18	0	0	1.25 ± 0.16	0	8.80 ± 0.36	0.2741 ± 0.021	
degraded diuron on powder pH10 at 15min	56.50 ± 1.39	6.25 ± 0.44	2.25 ± 0.27	1.25 ± 0.17	0	0	1.00 ± 0.15	0	11.30 ± 0.39	0.1892 ± 0.003	
degraded diuron on nanorods pH10 at 1min	40.50 ± 1.61	7.75 ± 0.06	1.00 ± 0.09	0.75 ± 0.15	0	0	0.25 ± 0.23	0	8.10 ± 0.31	0.2425 ± 0.005	
dilute diuron in nanorods system pH10	45.00 ± 1.82	6.00 ± 0.47	1.50 ± 0.17	1.00 ± 0.19	0	0	0.50 ± 0.25	0	9.00 ± 0.42	0.2053 ± 0.016	
degraded diuron on nanorods pH10 at 15min	34.25 ± 1.78	7.00 ± 0.56	0.75 ± 0.21	0.75 ± 0.18	0.25 ± 0.17	0	0	0	6.85 ± 0.48	0.2590 ± 0.011	

Comparing the toxicity of standard DI water and standard diuron at pH 4 and 10 without the effect of intermediates formed, solutions at pH10 are more toxic than that at pH4. This may be due to the large amount of hydroxide anions which can be the cause of toxicity.

Considering the level of toxicity in diuron degradation process between acidic and basic conditions, at shortest residence time, the toxicity in both conditions are similar when using ZnO powder as a catalyst. In the same time on ZnO nanorods, the mitotic index are similar but the aberration index at pH4 is more than that at pH 10. It can be concluded that the number of dividing cells in both conditions are equal but the higher amount of aberration cells occur at pH4. The residence time is increased to 15 min, on ZnO powder, the mitotic index at pH 4 is higher than that at pH 10 while the aberration index between these conditions are similar. Figure 4.29 shows the aberration cells in dividing step compared with treated cells in DI water at pH7. Another interested point from table, it should be noteworthy that aberration cells can be found in metaphase more than that in anaphase. It is possible to be found the aberration in early stage of cell division rather than that in last step.

However, the toxicity of each intermediated compound cannot be specifically identified due to the lack of their standards. It can only be predicted the toxicity of intermediates from the difference in sequence of intermediates formed between on ZnO powder and ZnO nanorods. It can be suggested that the intermediates which occur from hydroxylation at more positions will increase the toxicity than intermediates which occur from the attack of hydroxyl radicals at less positions. For example, at 1 min of residence time at pH10, intermediates formed on ZnO powder which are caused by hydroxylation reaction at both sides of molecules are more toxic than that on nanorods which are formed by hydroxylation at only one position. It has been shown that the different adsorption configuration of herbicides affect the level of toxicity of intermediates.

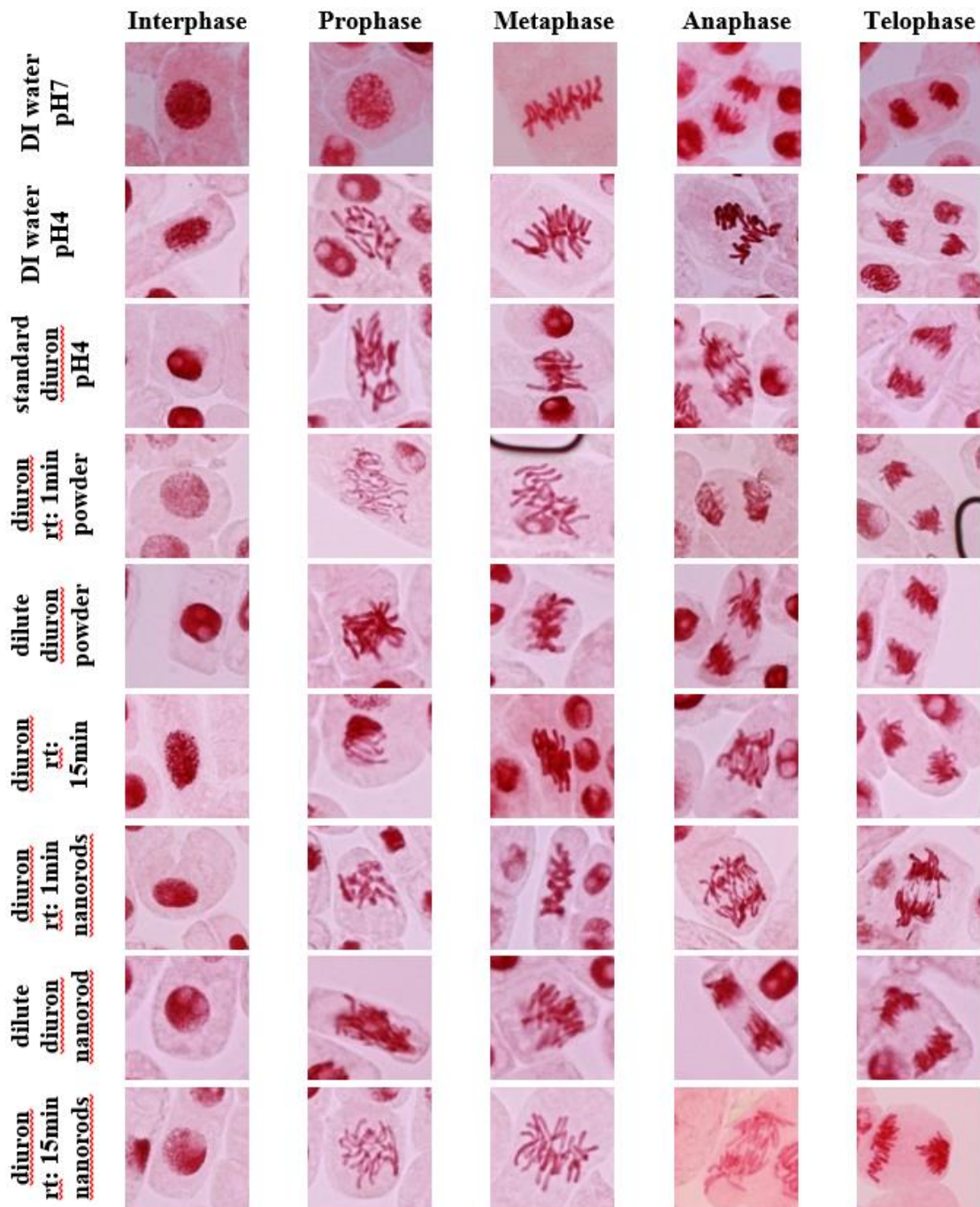


Figure 4.34 The abnormally population representative cells treated in different degraded solution of diuron in each dividing step. Treated cells in control DI water are normal cells

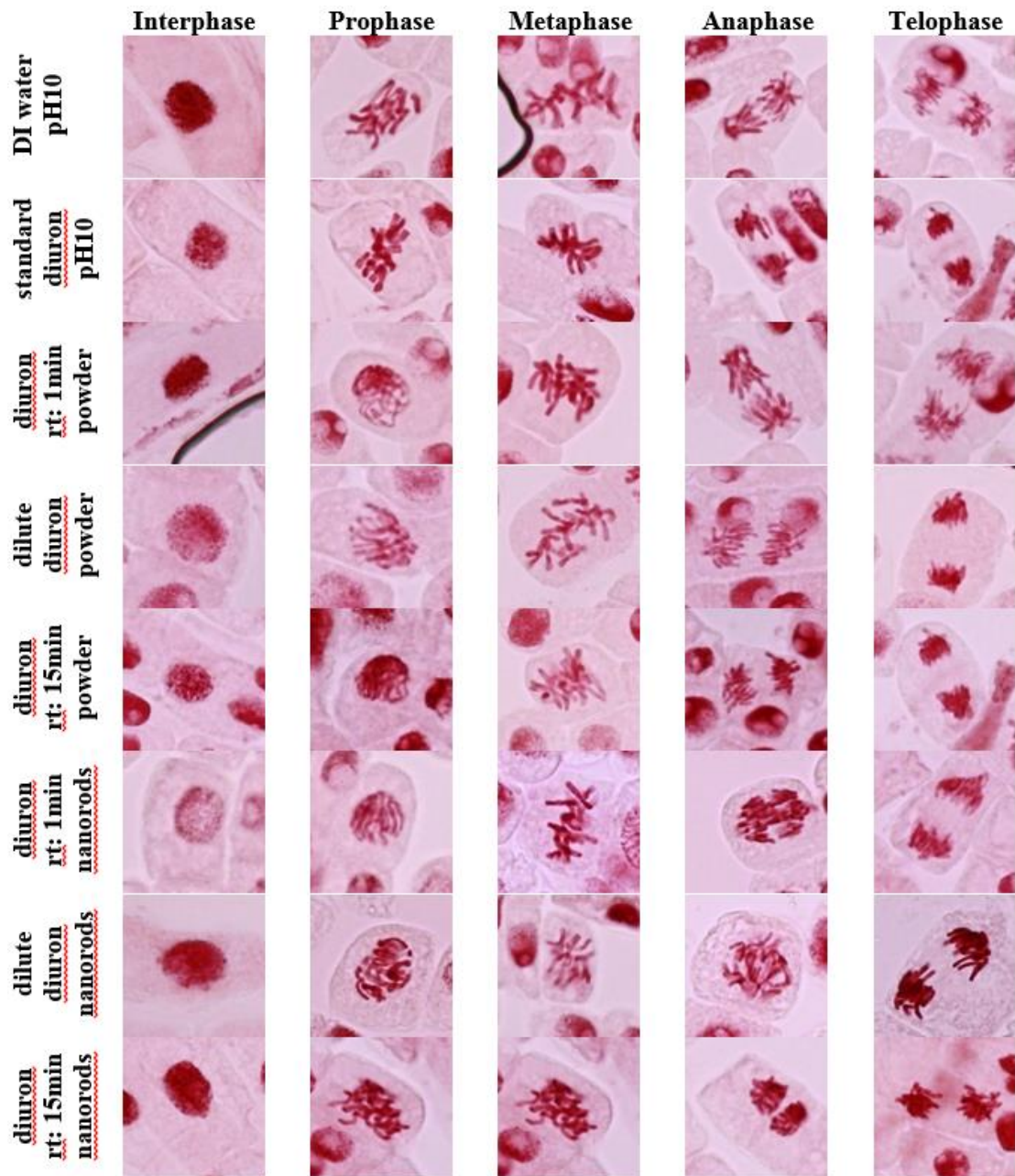


Figure 4.34 (continue). The abnormally population representative cells treated in different degraded solution of diuron in each dividing step. Treated cells in control DI water are normal cells.

Chapter 5

CONCLUSIONS

5.1 Summary of findings

1. ZnO are synthesized by different techniques for different morphology of ZnO powder and ZnO nanorods.
2. The molecular structure and the nature of surfaces affects the adsorption behavior of herbicides.
3. The characteristic of surface is changed by pH and results to the change of adsorption behavior of herbicides.
4. The adsorption configuration and the morphology of ZnO catalysts affects the degradation rate of herbicides
5. Hydroxyl radicals are generated in higher amount at pH10, compared with that at pH4.
6. The intermediate products are formed in different structure depending on the adsorption configuration.
7. The intermediates products on ZnO powder are more toxic than that on ZnO nanorods.

5.2 Conclusions

ZnO was successfully synthesized by sol-gel and hydrothermal techniques to provide ZnO powder with large fraction of polar-surface (i.e. zinc-terminated surface and oxygen-terminated surface) at both ends of hexagonal column and ZnO nanorods with non-polar surface (mixed-terminated surface) appeared on side of column. The results show the surface area of ZnO nanorods is about one order of magnitude larger than that of ZnO powder but the ZnO nanorods has less adsorption capacity than ZnO powder. This due to the large amount of adsorption sites and the affinity of polar surface. Calculations were applied to study the adsorption behavior of herbicides on

surfaces of ZnO and were conducted to explain the experimental results. The high adsorption capacity of nanorods is expected to show the high performance for photocatalytic degradation process but it give the opposite results. The degradation rate of herbicides on ZnO powder and ZnO nanorods are insignificantly different which is suggest that ZnO nanorods has the faster degradation rate than ZnO powder. This is due to the morphologies of ZnO and the adsorption configurations of herbicides on surfaces. The adsorption of herbicides with their aliphatic sides which is less stability than aromatic structure will increase the degradation rate. The large surface area of ZnO nanrods leads to the high reaction area between photogenerated and adsorbed species to produce the higher strongly oxidizing radicals. The higher ability in degradation is found in basic condition due to the high amount of hydroxyl anions related to higher amount of hydroxyl radicals. It found that the attack of radicals are selectively occur on the reactivity adsorbed position which are result to various intermediated products. Phytotoxicity and cytogenotoxicity indicated the toxicity of degraded products on ZnO nanrods is less than that on ZnO powder.

5.3 Recommendations

1. This research is suitable for the minimization the toxicity of intermediates from the removal of toxic organic compounds using photocatalytic degradation.
2. Dynamic simulation should be applied to study the adsorption of herbicides surrounded by molecules of solvent.
3. The effect of imperfectly arranged atoms on surface should be detailed studied.
4. The ratio between polar and non-polar surface should be varied to study the effect of surface on adsorption, photocatalytic degradation and intermediates formed.

REFERENCES

1. Dabrowski, J.M., J.M. Shadung, and V. Wepener, *Prioritizing agricultural pesticides used in South Africa based on their environmental mobility and potential human health effects*. Environ Int, 2014. **62**: p. 31-40.
2. Hall, L.W., Jr. and R.D. Anderson, *Temporal trends analysis of 2004 to 2012 toxicity and pesticide data for California's Central Valley water quality coalitions*. J Environ Sci Health A Tox Hazard Subst Environ Eng, 2014. **49**(3): p. 313-26.
3. King, J., F. Alexander, and J. Brodie, *Regulation of pesticides in Australia: The Great Barrier Reef as a case study for evaluating effectiveness*. Agriculture, Ecosystems & Environment, 2013. **180**: p. 54-67.
4. Hasenbein, S., S.P. Lawler, and R.E. Connon, *An assessment of direct and indirect effects of two herbicides on aquatic communities*. Environ Toxicol Chem, 2017. **36**(8): p. 2234-2244.
5. Céline, T., et al., *Fungal biodegradation of a phenylurea herbicide, diuron: structure and toxicity of metabolites*. Pest Management Science, 2000. **56**(5): p. 455-462.
6. Sun, K., et al., *Adsorption of diuron, fluridone and norflurazon on single-walled and multi-walled carbon nanotubes*. Sci Total Environ, 2012. **439**: p. 1-7.
7. Lawless, D., N. Serpone, and D. Meisel, *Role of hydroxyl radicals and trapped holes in photocatalysis. A pulse radiolysis study*. The Journal of Physical Chemistry, 1991. **95**(13): p. 5166-5170.
8. Wang, J.L. and L.J. Xu, *Advanced Oxidation Processes for Wastewater Treatment: Formation of Hydroxyl Radical and Application*. Critical Reviews in Environmental Science and Technology, 2012. **42**(3): p. 251-325.
9. Carrier, M., et al., *Photocatalytic Degradation of Diuron: Experimental Analyses and Simulation of HO[•] Radical Attacks by Density Functional Theory Calculations*. The Journal of Physical Chemistry A, 2009. **113**(22): p. 6365-6374.

10. Hana, K., et al., *Photocatalytic degradation of diuron [3-(3,4-dichlorophenyl)-1,1-dimethylurea] on the layer of TiO₂ particles in the batch mode plate film reactor*. Journal of Chemical Technology & Biotechnology, 1998. **72**(2): p. 169-175.
11. Malato, S., et al., *Photocatalytic Treatment of Diuron by Solar Photocatalysis: Evaluation of Main Intermediates and Toxicity*. Environmental Science & Technology, 2003. **37**(11): p. 2516-2524.
12. Evgenidou, E., et al., *Study of the removal of dichlorvos and dimethoate in a titanium dioxide mediated photocatalytic process through the examination of intermediates and the reaction mechanism*. J Hazard Mater, 2006. **137**(2): p. 1056-64.
13. Woo, O.T., et al., *Photocatalytic oxidation of polycyclic aromatic hydrocarbons: intermediates identification and toxicity testing*. J Hazard Mater, 2009. **168**(2-3): p. 1192-9.
14. Wöll, C., *The chemistry and physics of zinc oxide surfaces*. Progress in Surface Science, 2007. **82**(2): p. 55-120.
15. Schweizer, E.E. and M.J. May, *Weeds and weed control*, in *The Sugar Beet Crop*, D.A. Cooke and R.K. Scott, Editors. 1993, Springer Netherlands: Dordrecht. p. 485-519.
16. Moncada, A., *Environmental fate of diuron*. Environmental Monitoring Branch, Department of Pesticide Regulation, Sacramento, California, 2004.
17. Twining, J., *Environmental Fate of Linuron Risk Characterization*.
18. Agency, E.P., *Linuron: Reregistration Eligibility Decision*. Prevention, Pesticides And Toxic Substances. 1995.
19. Commission, E., *Plant health, animal health and welfare*, in *Food Safety*. 2002.
20. Protection, I.f.H.a.C., *3,4-Dichloroaniline (3,4-DCA)*. 2006: Italy.
21. Morkoç, H. and Ü. Özgür, *Zinc oxide: fundamentals, materials and device technology*. 2008: John Wiley & Sons.
22. Apichatsanee, K., *Investigation of kinetics and intermediates of photodegradation of phenylurea herbicides on nanosized ZnO*, in *Chemical Engineering*. 2008, Chulalongkorn University.

23. Fan, Z. and J.G. Lu, *Zinc Oxide Nanostructures: Synthesis and Properties*. Journal of Nanoscience and Nanotechnology, 2005. **5**(10): p. 1561-1573.
24. Takahashi, K., A. Yoshikawa, and A. Sandhu, *Wide bandgap semiconductors*. Springer-Verlag Berlin Heidelberg., 2007: p. 239.
25. Ntep, J.M., et al., *ZnO growth by chemical vapour transport*. Journal of Crystal Growth, 1999. **207**(1): p. 30-34.
26. Yu, W., X. Li, and X. Gao, *Catalytic Synthesis and Structural Characteristics of High-Quality Tetrapod-Like ZnO Nanocrystals by a Modified Vapor Transport Process*. Crystal Growth & Design, 2005. **5**(1): p. 151-155.
27. Chu, S.-Y., T.-M. Yan, and S.-L. Chen, *Characteristics of sol-gel synthesis of ZnO-based powders*. Journal of materials science letters, 2000. **19**(4): p. 349-352.
28. Hasnidawani, J.N., et al., *Synthesis of ZnO Nanostructures Using Sol-Gel Method*. Procedia Chemistry, 2016. **19**: p. 211-216.
29. Kolekar, T., et al., *Synthesis by sol-gel method and characterization of ZnO nanoparticles*. Indian streams research journal, 2011. **1**(1).
30. Rani, S., et al., *Synthesis of nanocrystalline ZnO powder via sol-gel route for dye-sensitized solar cells*. Solar Energy Materials and Solar Cells, 2008. **92**(12): p. 1639-1645.
31. Spanhel, L. and M.A. Anderson, *Semiconductor clusters in the sol-gel process: quantized aggregation, gelation, and crystal growth in concentrated zinc oxide colloids*. Journal of the American Chemical Society, 1991. **113**(8): p. 2826-2833.
32. Vafaei, M. and M.S. Ghamsari, *Preparation and characterization of ZnO nanoparticles by a novel sol-gel route*. Materials Letters, 2007. **61**(14): p. 3265-3268.
33. Hench, L.L. and J.K. West, *The sol-gel process*. Chemical reviews, 1990. **90**(1): p. 33-72.
34. Zak, A.K., et al., *Effects of annealing temperature on some structural and optical properties of ZnO nanoparticles prepared by a modified sol-gel combustion method*. Ceramics International, 2011. **37**(1): p. 393-398.

35. Lin, K.-F., et al., *Band gap variation of size-controlled ZnO quantum dots synthesized by sol-gel method*. Chemical Physics Letters, 2005. **409**(4): p. 208-211.
36. Feng, S.H. and G.H. Li, *Hydrothermal and Solvothermal Syntheses*. 2017: p. 73-104.
37. Rao, B.G., D. Mukherjee, and B.M. Reddy, *Novel approaches for preparation of nanoparticles*. 2017: p. 1-36.
38. Chen, Y., et al., *Size-controlled synthesis and optical properties of small-sized ZnO nanorods*. The Journal of Physical Chemistry C, 2009. **113**(18): p. 7497-7502.
39. Lepot, N., et al., *Synthesis of ZnO nanorods from aqueous solution*. Materials Letters, 2007. **61**(13): p. 2624-2627.
40. Králik, M., *Adsorption, chemisorption, and catalysis*. Vol. 68. 2014.
41. Limousin, G., et al., *Sorption isotherms: A review on physical bases, modeling and measurement*. Applied Geochemistry, 2007. **22**(2): p. 249-275.
42. Foo, K.Y. and B.H. Hameed, *Insights into the modeling of adsorption isotherm systems*. Chemical Engineering Journal, 2010. **156**(1): p. 2-10.
43. Sime, R.J., *The Langmuir Adsorption Isotherm*. Physical Chemistry: Methods, Techniques, Experiments, 1990.
44. Houas, A., et al., *Photocatalytic degradation pathway of methylene blue in water*. Applied Catalysis B: Environmental, 2001. **31**(2): p. 145-157.
45. Daneshvar, N., et al., *Removal of C.I. Acid Orange 7 from aqueous solution by UV irradiation in the presence of ZnO nanopowder*. Journal of Hazardous Materials, 2007. **143**(1): p. 95-101.
46. Behnajady, M.A., N. Modirshahla, and R. Hamzavi, *Kinetic study on photocatalytic degradation of C.I. Acid Yellow 23 by ZnO photocatalyst*. Journal of Hazardous Materials, 2006. **133**(1): p. 226-232.
47. Daneshvar, N., D. Salari, and A.R. Khataee, *Photocatalytic degradation of azo dye acid red 14 in water on ZnO as an alternative catalyst to TiO₂*. Journal of Photochemistry and Photobiology A: Chemistry, 2004. **162**(2): p. 317-322.
48. Konstantinou, I.K. and T.A. Albanis, *Photocatalytic transformation of pesticides in aqueous titanium dioxide suspensions using artificial and solar*

- light: intermediates and degradation pathways*. Applied Catalysis B: Environmental, 2003. **42**(4): p. 319-335.
49. Mestankova, H., et al., *Evolution of algal toxicity during (photo)oxidative degradation of diuron*. Aquatic Toxicology, 2011. **101**(2): p. 466-473.
50. *Mechanisms of Direct and TiO₂-Photocatalysed UV Degradation of Phenylurea Herbicides*. ChemPhysChem, 2005. **6**(10): p. 2064-2074.
51. Rao, Y.F. and W. Chu, *Reaction Mechanism of Linuron Degradation in TiO₂ Suspension under Visible Light Irradiation with the Assistance of H₂O₂*. Environmental Science & Technology, 2009. **43**(16): p. 6183-6189.
52. Sittichoktum, S., *Photodegradation of linuron on titania and zinc oxide*, in *Chemical Engineering*. 2011, Chulalongkorn University.
53. Kornherr, A., et al., *Interaction of adsorbed organosilanes with polar zinc oxide surfaces: a molecular dynamics study comparing two models for the metal oxide surface*. Chemical Physics Letters, 2004. **393**(1-3): p. 107-111.
54. Gao, Y., et al., *Ab initio DFT study of urea adsorption and decomposition on the ZnO surface*. Computational and Theoretical Chemistry, 2012. **992**: p. 1-8.
55. Parasuraman, S., *Toxicological screening*. J Pharmacol Pharmacother, 2011. **2**(2): p. 74-9.
56. Sojic Merkulov, D.V., et al., *Photocatalytic decomposition of selected biologically active compounds in environmental waters using TiO₂/polyaniline nanocomposites: Kinetics, toxicity and intermediates assessment*. Environ Pollut, 2018. **239**: p. 457-465.
57. Armakovic, S.J., et al., *Photocatalytic degradation of 4-amino-6-chlorobenzene-1,3-disulfonamide stable hydrolysis product of hydrochlorothiazide: Detection of intermediates and their toxicity*. Environ Pollut, 2018. **233**: p. 916-924.
58. Hong, S.J., et al., *Heterojunction BiVO₄/WO₃ electrodes for enhanced photoactivity of water oxidation*. Energy & Environmental Science, 2011. **4**(5): p. 1781-1787.
59. Khongthon, W., et al., *Degradation of diuron via an electrochemical advanced oxidation process in a microscale-based reactor*. Chemical Engineering Journal, 2016. **292**: p. 298-307.

60. Silambarasan, S. and A.S. Vangnai, *Biodegradation of 4-nitroaniline by plant-growth promoting Acinetobacter sp. AVLB2 and toxicological analysis of its biodegradation metabolites*. Journal of Hazardous Materials, 2016. **302**: p. 426-436.
61. Kapoor, A. and R.T. Yang, *Correlation of equilibrium adsorption data of condensable vapours on porous adsorbents*. Gas Separation & Purification, 1989. **3**(4): p. 187-192.
62. Lowell, S. and J.E. Shields, *Powder surface area and porosity*. Vol. 2. 2013: Springer Science & Business Media.
63. D., V.B., et al., *Evaluation of the Tauc method for optical absorption edge determination: ZnO thin films as a model system*. physica status solidi (b), 2015. **252**(8): p. 1700-1710.
64. Liu, H., et al., *Sunlight-sensitive anti-fouling nanostructured TiO₂ coated Cu meshes for ultrafast oily water treatment*. Scientific reports, 2016. **6**: p. 25414.
65. Fan, F., et al., *Facile synthesis and gas sensing properties of tubular hierarchical ZnO self-assembled by porous nanosheets*. Sensors and Actuators B: Chemical, 2015. **215**: p. 231-240.
66. Khokhra, R., et al., *Visible and UV photo-detection in ZnO nanostructured thin films via simple tuning of solution method*. Scientific reports, 2017. **7**(1): p. 15032.
67. Lee, J., J. Chung, and S. Lim, *Improvement of optical properties of post-annealed ZnO nanorods*. Physica E: Low-dimensional Systems and Nanostructures, 2010. **42**(8): p. 2143-2146.
68. Hsu, J.-C., et al., *Spectroscopic ellipsometry studies on various zinc oxide films deposited by ion beam sputtering at room temperature*. Applied optics, 2012. **51**(9): p. 1209-1215.
69. Wang, M., et al., *Electronic structure and optical properties of Zn (OH)₂: LDA+ U calculations and intense yellow luminescence*. RSC Advances, 2015. **5**(106): p. 87496-87503.
70. Yan, X., et al., *Pathway of zinc oxide formation by seed-assisted and controlled double-jet precipitation*. CrystEngComm, 2016. **18**(6): p. 924-929.

71. Hameed, B., A. Ahmad, and K. Latiff, *Adsorption of basic dye (methylene blue) onto activated carbon prepared from rattan sawdust*. *Dyes and Pigments*, 2007. **75**(1): p. 143-149.
72. Sivakumar, P. and P. Palanisamy, *Adsorption studies of basic Red 29 by a non-conventional activated carbon prepared from Euphorbia antiquorum L*. *Int. J. Chem. Tech. Res*, 2009. **1**(3): p. 502-510.
73. Zhang, F., et al., *Substructure-activity relationship studies on antibody recognition for phenylurea compounds using competitive immunoassay and computational chemistry*. *Sci Rep*, 2018. **8**(1): p. 3131.
74. Steiner, T., *The Hydrogen Bond in the Solid State*. Vol. 41. 2002. 49-76.
75. Goodsell, D.S., *Visual Methods from Atoms to Cells*. *Structure*, 2005. **13**(3): p. 347-354.
76. Warme, P.K., *Space-filling molecular models constructed by a computer*. *Computers and Biomedical Research*, 1977. **10**(1): p. 75-82.
77. Kornherr, A., et al., *Adsorption of organosilanes at a Zn-terminated ZnO (0001) surface: Molecular dynamics study*. *Langmuir*, 2006. **22**(19): p. 8036-8042.
78. Steiner, T., *Unrolling the hydrogen bond properties of C-H...O interactions*. *Chemical Communications*, 1997(8): p. 727-734.
79. Daneshvar, N., D. Salari, and A.R. Khataee, *Photocatalytic degradation of azo dye acid red 14 in water: investigation of the effect of operational parameters*. *Journal of Photochemistry and Photobiology A: Chemistry*, 2003. **157**(1): p. 111-116.
80. Machado, A.E., et al., *Photocatalytic degradation of lignin and lignin models, using titanium dioxide: the role of the hydroxyl radical*. *Chemosphere*, 2000. **40**(1): p. 115-124.
81. Palmisano, G., et al., *Selectivity of hydroxyl radical in the partial oxidation of aromatic compounds in heterogeneous photocatalysis*. *Catalysis Today*, 2007. **122**(1): p. 118-127.

82. Xiang, Q., J. Yu, and P.K. Wong, *Quantitative characterization of hydroxyl radicals produced by various photocatalysts*. Journal of Colloid and Interface Science, 2011. **357**(1): p. 163-167.
83. Xiao, Q., et al., *Photoinduced hydroxyl radical and photocatalytic activity of samarium-doped TiO₂ nanocrystalline*. Journal of Hazardous Materials, 2008. **150**(1): p. 62-67.
84. Turchi, C.S. and D.F. Ollis, *Photocatalytic degradation of organic water contaminants: Mechanisms involving hydroxyl radical attack*. Journal of Catalysis, 1990. **122**(1): p. 178-192.
85. Montoya, J.F., et al., *Comprehensive kinetic and mechanistic analysis of TiO₂ photocatalytic reactions according to the direct–indirect model:(ii) experimental validation*. The Journal of Physical Chemistry C, 2014. **118**(26): p. 14276-14290.
86. Martinez-Huitle, C.A. and S. Ferro, *Electrochemical oxidation of organic pollutants for the wastewater treatment: direct and indirect processes*. Chemical Society Reviews, 2006. **35**(12): p. 1324-1340.
87. Montoya, J.F., J. Peral, and P. Salvador, *Comprehensive Kinetic and Mechanistic Analysis of TiO₂ Photocatalytic Reactions According to the Direct–Indirect Model: (I) Theoretical Approach*. The Journal of Physical Chemistry C, 2014. **118**(26): p. 14266-14275.
88. Tsai, S.-J. and S. Cheng, *Effect of TiO₂ crystalline structure in photocatalytic degradation of phenolic contaminants*. Catalysis Today, 1997. **33**(1): p. 227-237.
89. Lee, K.M., et al., *Recent developments of zinc oxide based photocatalyst in water treatment technology: a review*. Water research, 2016. **88**: p. 428-448.
90. Zhang, Z., et al., *Role of particle size in nanocrystalline TiO₂-based photocatalysts*. The Journal of Physical Chemistry B, 1998. **102**(52): p. 10871-10878.
91. Chusaksri, S., et al., *Photocatalytic degradation of 3,4-dichlorophenylurea in aqueous gold nanoparticles-modified titanium dioxide suspension under simulated solar light*. Journal of Hazardous Materials, 2011. **190**(1): p. 930-937.

92. Farré, M.J., et al., *Evaluation of the intermediates generated during the degradation of Diuron and Linuron herbicides by the photo-Fenton reaction*. Journal of Photochemistry and Photobiology A: Chemistry, 2007. **189**(2): p. 364-373.
93. Katsumata, H., et al., *Photocatalytic degradation of diuron in aqueous solution by platinized TiO₂*. Journal of Hazardous Materials, 2009. **171**(1): p. 1081-1087.
94. Mendoza-Huizar, L.H., *Chemical Reactivity of Isoproturon, Diuron, Linuron, and Chlorotoluron Herbicides in Aqueous Phase: A Theoretical Quantum Study Employing Global and Local Reactivity Descriptors*. Journal of Chemistry, 2015. **2015**: p. 1-9.
95. Pearson, R.G., *Chemical hardness and bond dissociation energies*. Journal of the American Chemical Society, 1988. **110**(23): p. 7684-7690.
96. Akpan, U.G. and B.H. Hameed, *Parameters affecting the photocatalytic degradation of dyes using TiO₂-based photocatalysts: A review*. Journal of Hazardous Materials, 2009. **170**(2): p. 520-529.
97. Akyol, A., H.C. Yatmaz, and M. Bayramoglu, *Photocatalytic decolorization of Remazol Red RR in aqueous ZnO suspensions*. Applied Catalysis B: Environmental, 2004. **54**(1): p. 19-24.
98. Huang, S., et al., *Photocatalytic degradation of thiobencarb by a visible light-driven MoS₂ photocatalyst*. Separation and Purification Technology, 2018. **197**: p. 147-155.
99. Sakthivel, S., et al., *Solar photocatalytic degradation of azo dye: comparison of photocatalytic efficiency of ZnO and TiO₂*. Solar Energy Materials and Solar Cells, 2003. **77**(1): p. 65-82.
100. Tung, C.-H., et al., *Comparison of hydroxyl radical yields between photo- and electro-catalyzed water treatments*. Journal of the Taiwan Institute of Chemical Engineers, 2014. **45**(4): p. 1649-1654.
101. Oturan, N., et al., *Study of the toxicity of diuron and its metabolites formed in aqueous medium during application of the electrochemical advanced oxidation process "electro-Fenton"*. Chemosphere, 2008. **73**(9): p. 1550-1556.

102. Schuytema, G.S. and A. Nebeker, *Comparative toxicity of diuron on survival and growth of Pacific treefrog, bullfrog, red-legged frog, and African clawed frog embryos and tadpoles*. Archives of Environmental Contamination and Toxicology, 1998. **34**(4): p. 370-376.
103. Fan, Y., et al., *Graphene–polyaniline composite film modified electrode for voltammetric determination of 4-aminophenol*. Sensors and Actuators B: Chemical, 2011. **157**(2): p. 669-674.
104. Song, H. and T.S. Chen, *p-Aminophenol-induced liver toxicity: Tentative evidence of a role for acetaminophen*. Journal of biochemical and molecular toxicology, 2001. **15**(1): p. 34-40.
105. Bian, M., et al., *Molecular approaches unravel the mechanism of acid soil tolerance in plants*. The Crop Journal, 2013. **1**(2): p. 91-104.
106. Liesivuori, J., Savolainen, and Heikki, *Methanol and formic acid toxicity: biochemical mechanisms*. Pharmacology & toxicology, 1991. **69**(3): p. 157-163.
107. Hong, S.K., et al., *Nephrotoxicity of 4-amino-2-chlorophenol and 2-amino-4-chlorophenol in the Fischer 344 rat*. Toxicology, 1996. **110**(1-3): p. 47-58.

APPENDIX



จุฬาลงกรณ์มหาวิทยาลัย
CHULALONGKORN UNIVERSITY

APPENDIX A
CALIBRATION CURVE

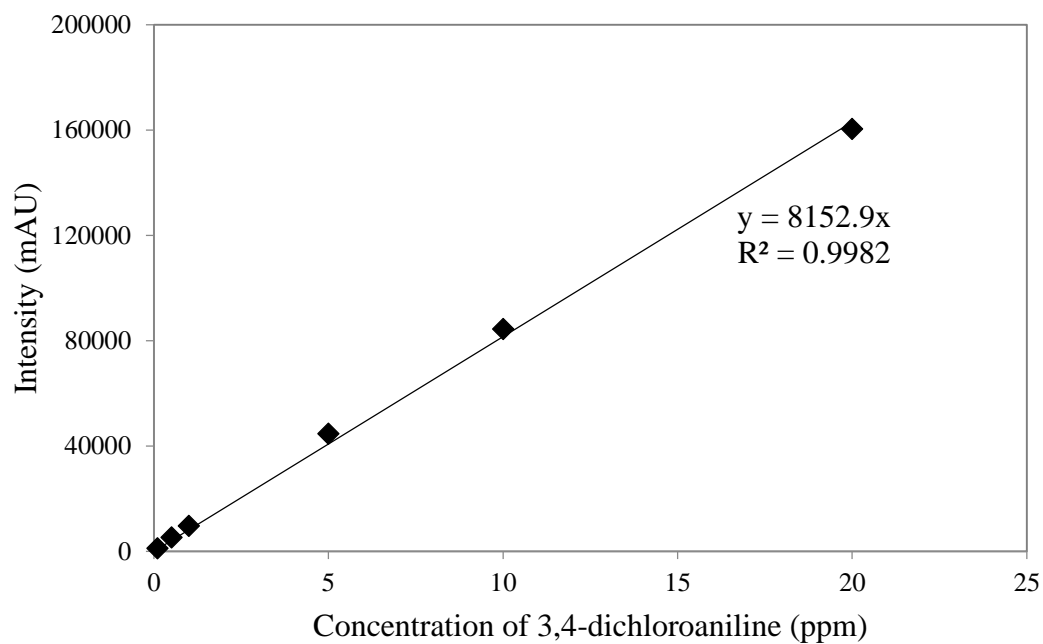


Figure A1 The calibration curve of 3,4-dichloroaniline.

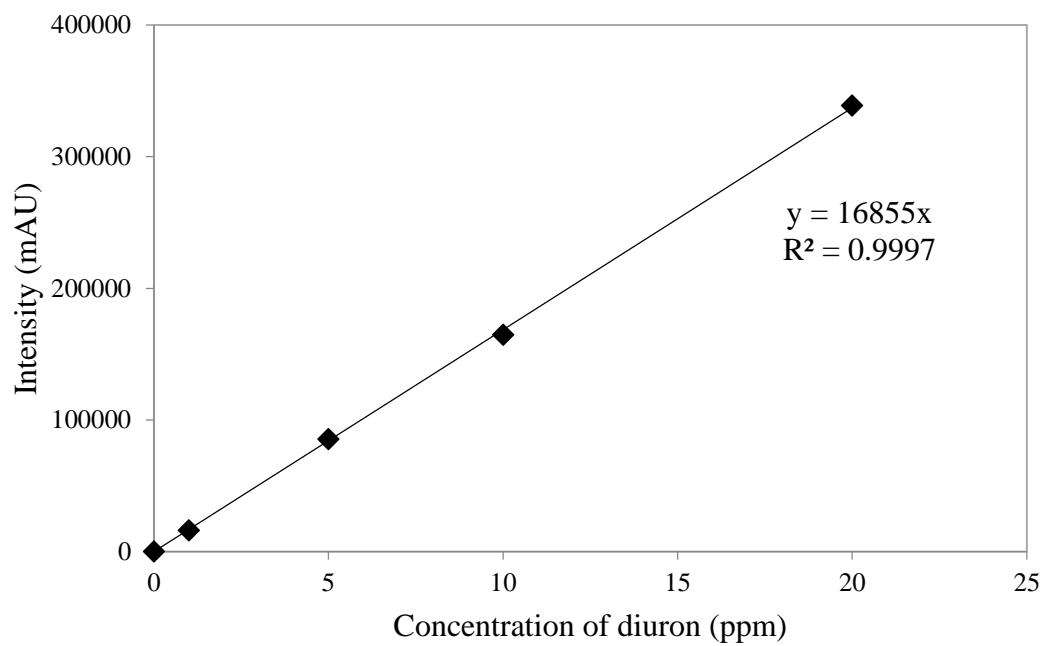


Figure A2 The calibration curve of diuron.

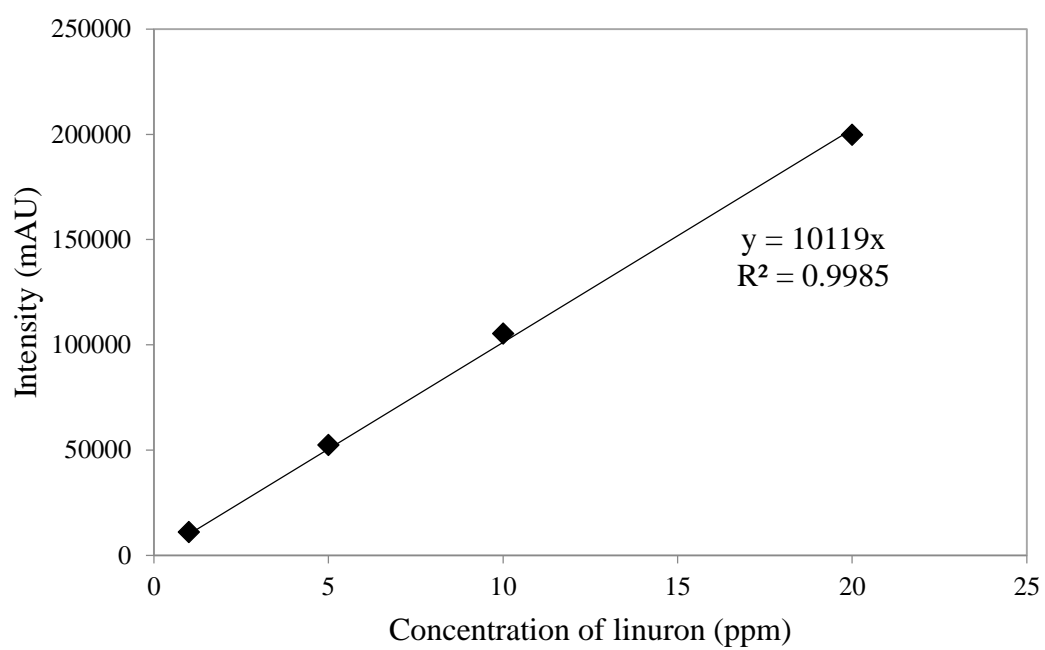
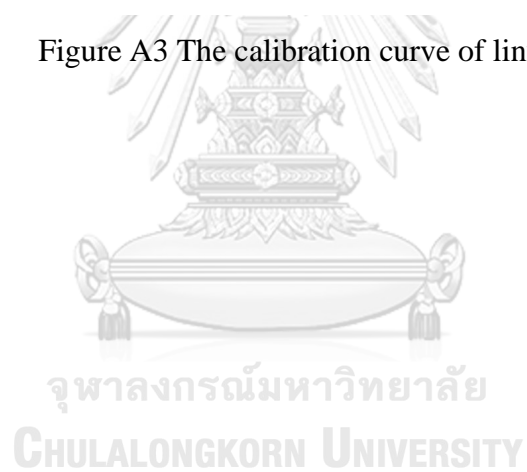


Figure A3 The calibration curve of linuron.



APPENDIX B

THE INITIAL ORIENTATION OF HERBICIDES OF SURFACES

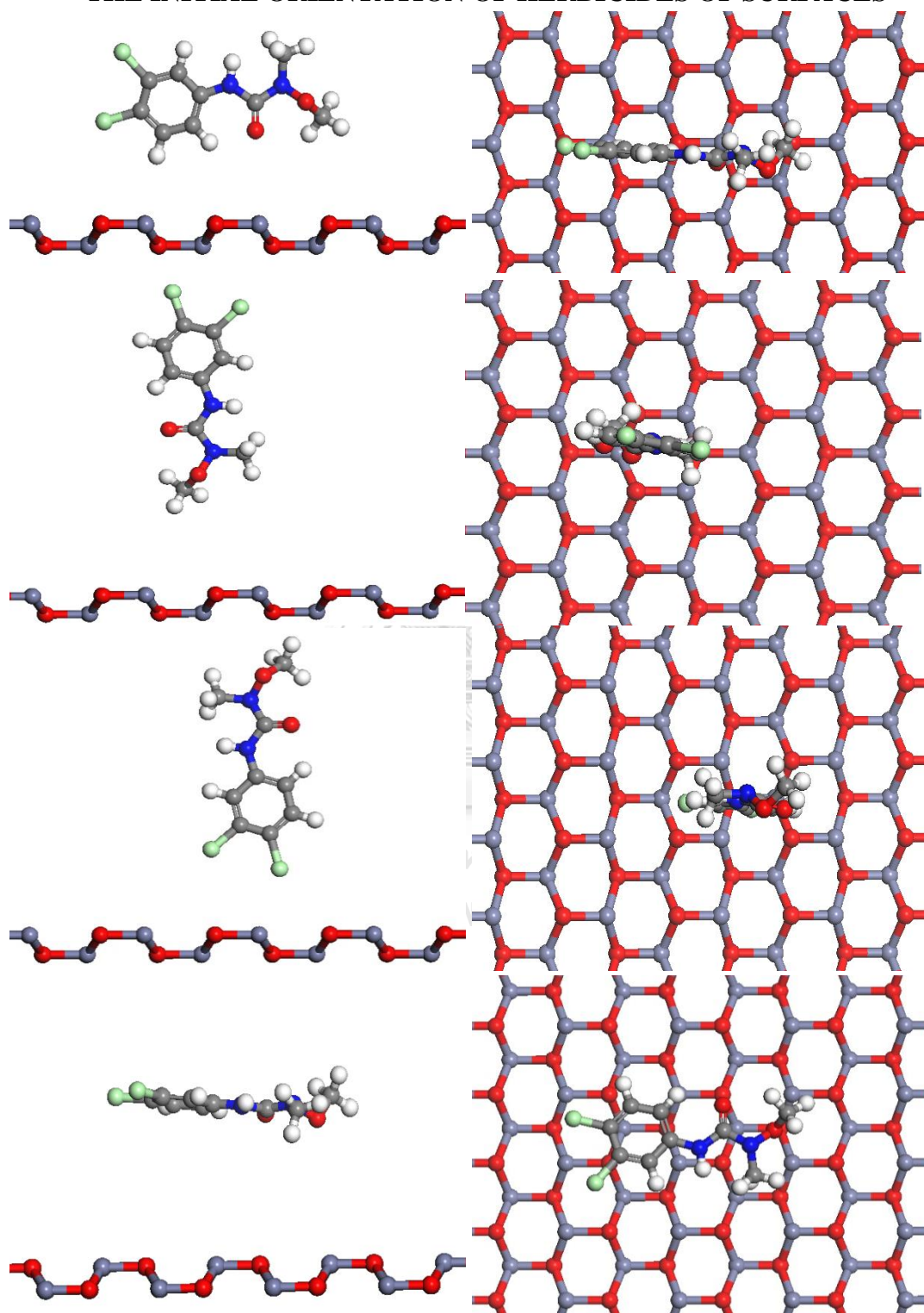


Figure B1 The variation of initial orientation of linuron on mixed-terminated surface.

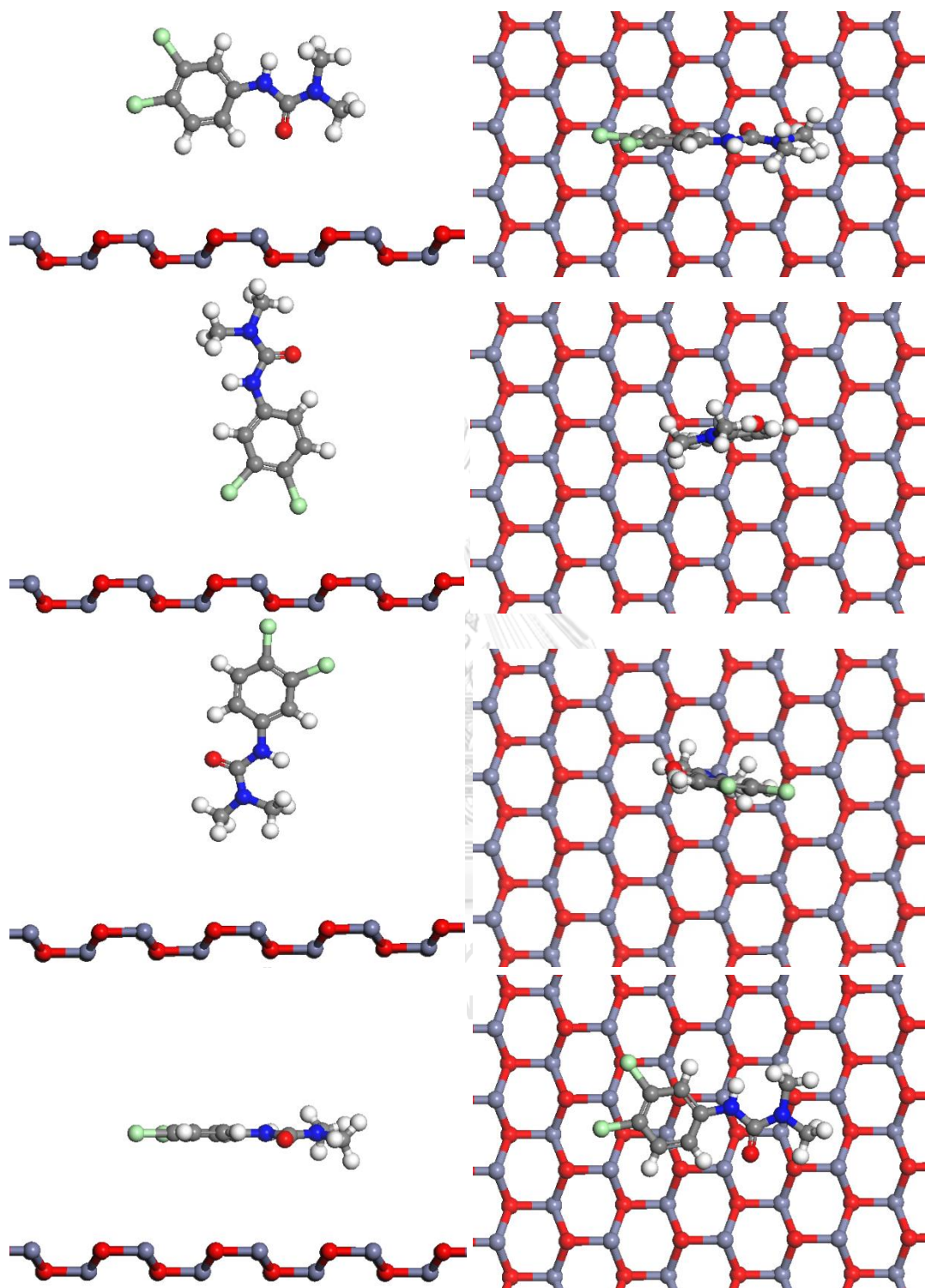


Figure B2 The variation of initial orientation of diuron on mixed-terminated surface.

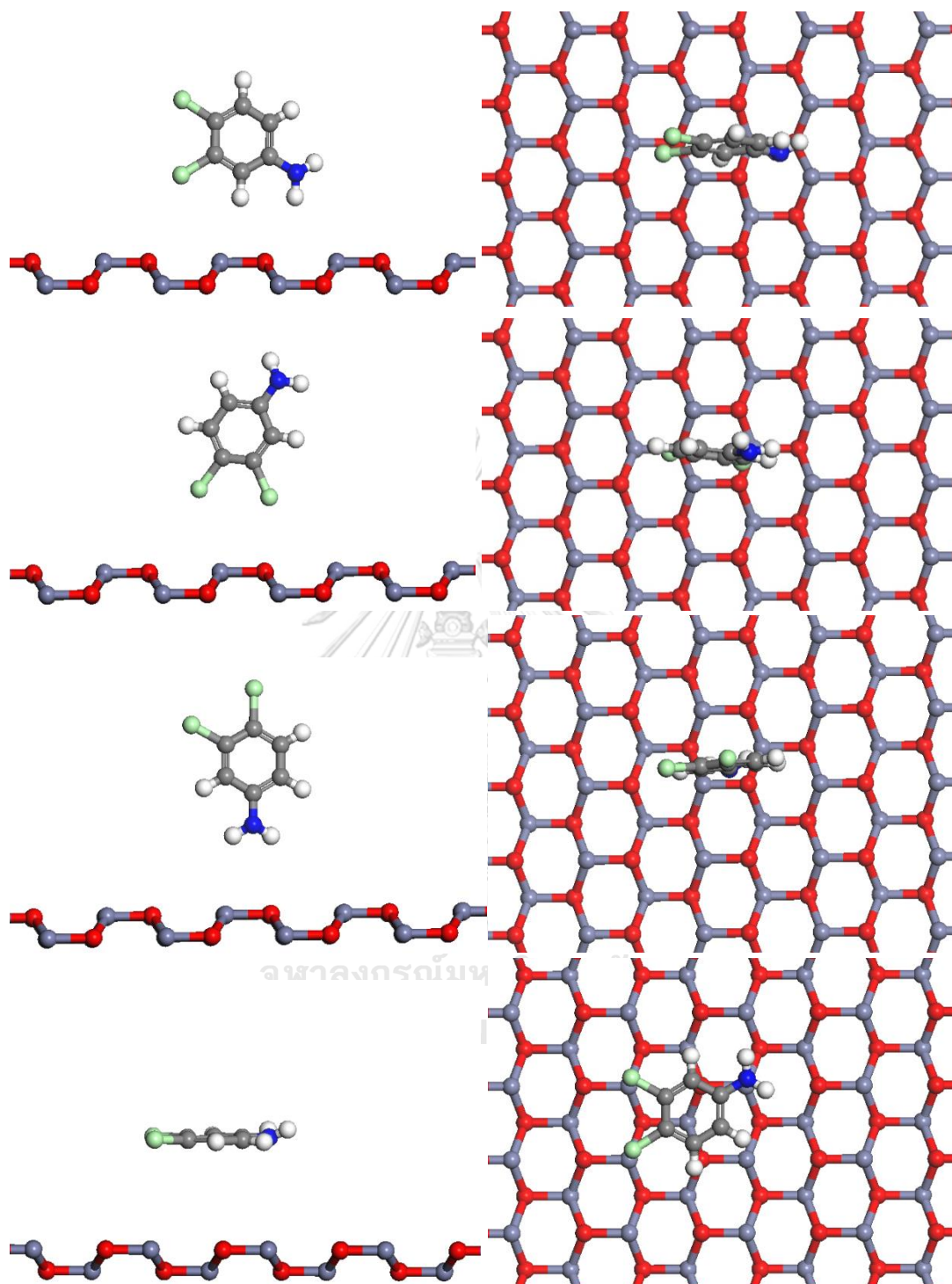


Figure B3 The variation of initial orientation of 3,4-dichloroaniline.

APPENDIX C

THE INTERACTION OF DIURON ON SURFACES

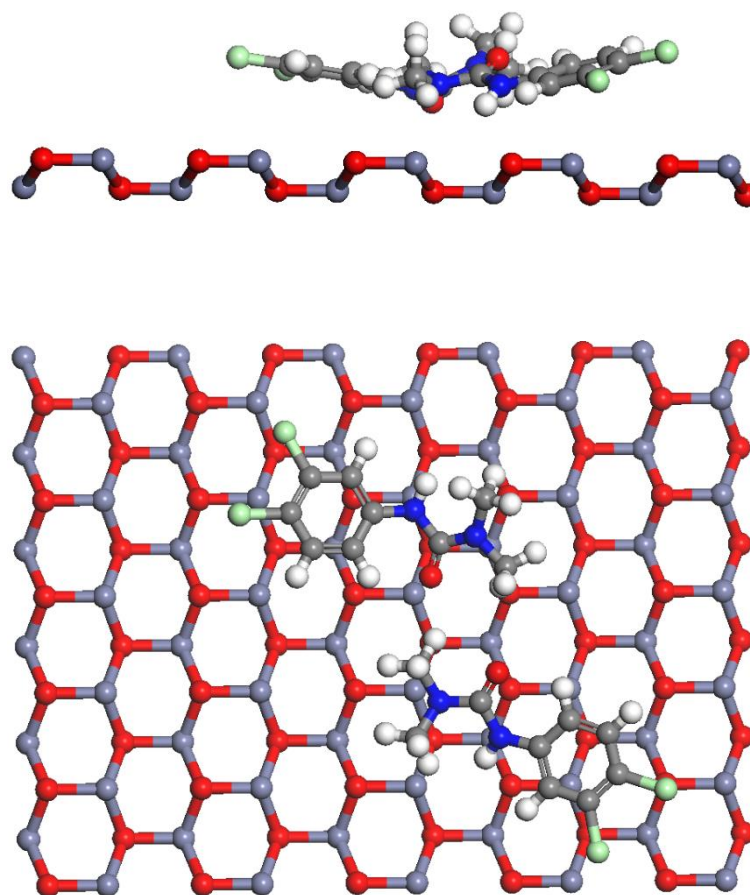


Figure C1 The interaction of diuron on mixed-terminated surface.

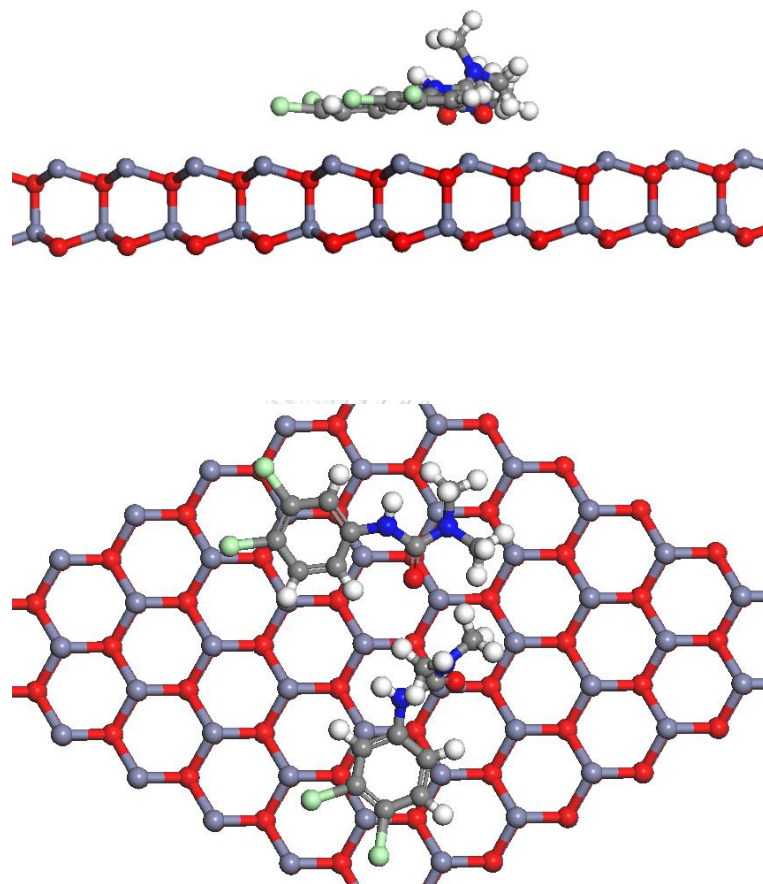


Figure C2 The interaction of diuron on zinc-terminated surface.

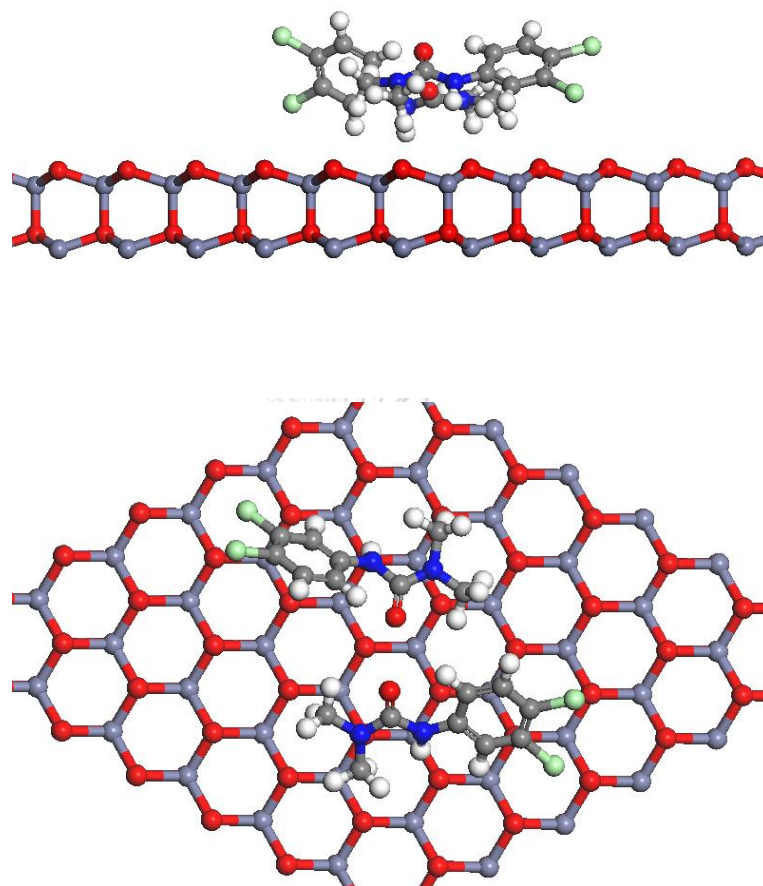


Figure C3 The interaction of diuron on oxygen-terminated surface.

APPENDIX D

THE ADSORPTION OF WATER ON SURFACES

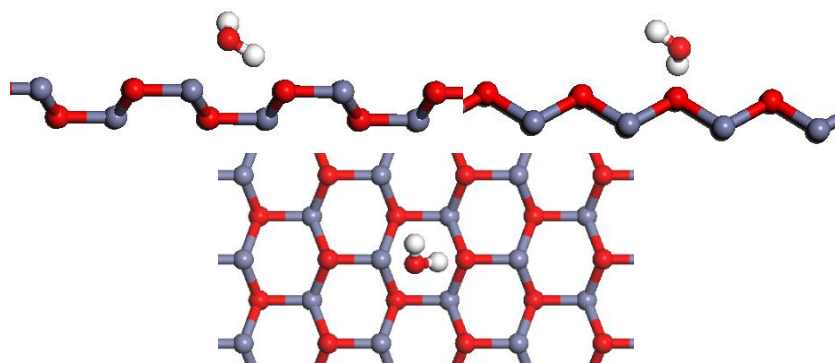


Figure D1 The adsorption of water on mixed-terminated surface.

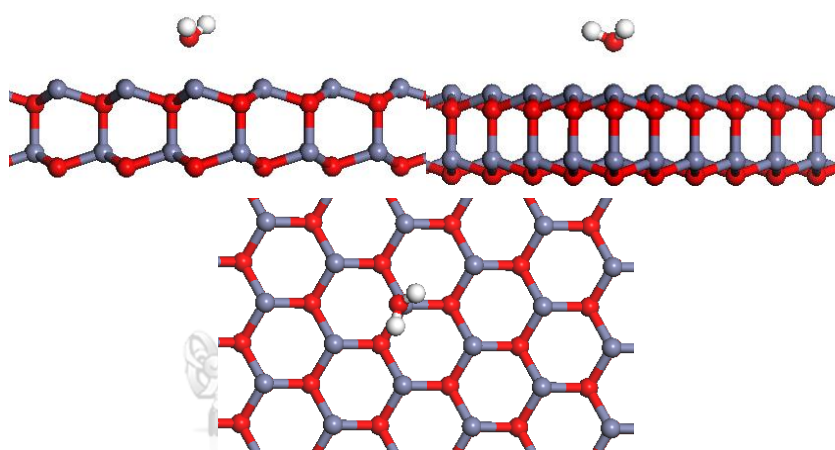


Figure D2 The adsorption of water on zinc-terminated surface.

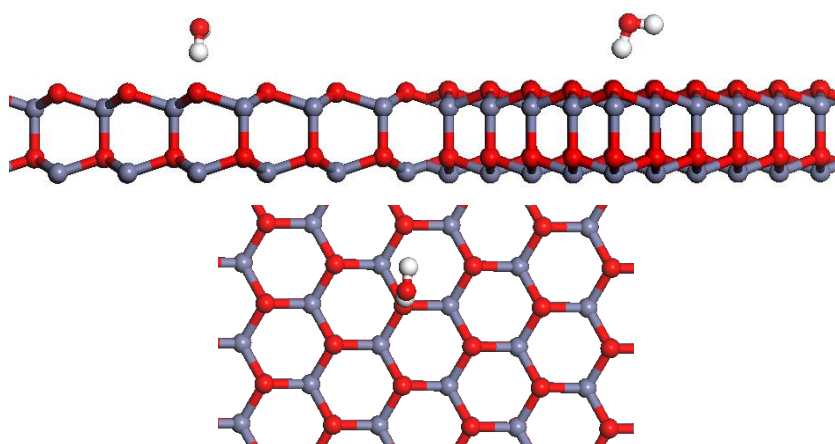


Figure D3 The adsorption of water on oxygen-terminated surface.

APPENDIX E

MOLECULAR STRUCTURE OF INTERMEDIATES (FRAGMENT IONS)

Table E1 Mass fraction of intermediates from degradation of linuron.

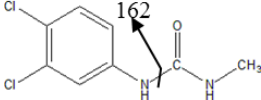
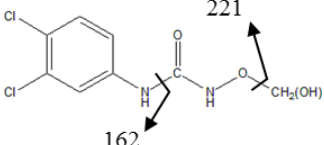
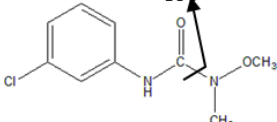
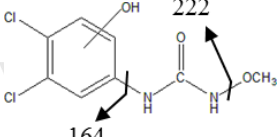
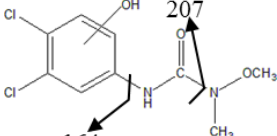
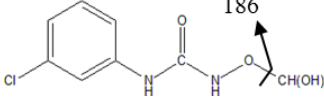
compound	retention time (min)	molecular weight (m/z)	molecular ion and fragmentations	photoproduct
1	2.15	220	221(100), 162 (19)	
2	7.35	252	253 (15), 221 (100), 162 (35)	
3	6.25	215	216(100), 155 (22)	
4	5.08	253	254(20), 222 (70), 164 (100)	
5	8.20	267	268(22), 207 (100), 164 (40)	
6	6.40	236	237(17), 186 (100)	

Table E.1 (continue).

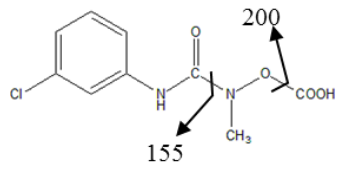
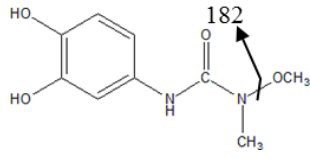
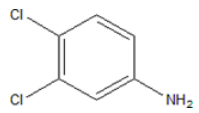
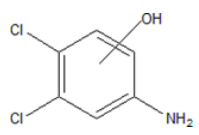
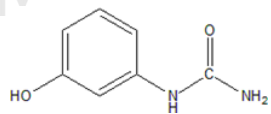
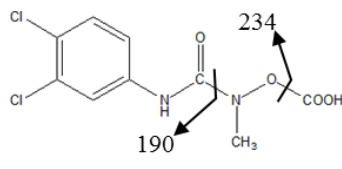
compound	retention time (min)	molecular weight (m/z)	molecular ion and fragmentations	photoproduct
7	7.11	246	247(10), 200 (100), 155 (55)	
8	6.30	213	214(100), 182 (25)	
9	2.53	163		
10	1.20	180		
11	1.00	153		
12	9.00	280	281(15), 234 (30), 190 (100)	

Table E.1 (continue).

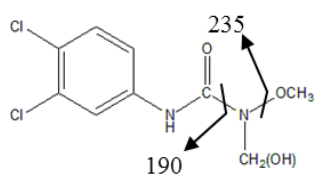
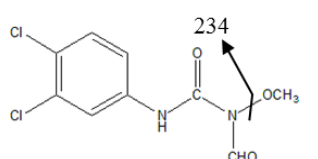
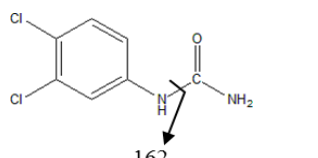
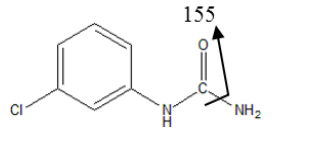
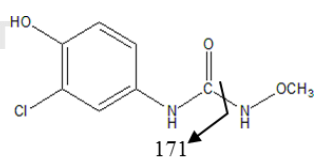
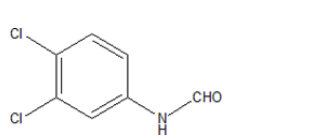
compound	retention time (min)	molecular weight (m/z)	molecular ion and fragmentations	photoproduct
13	1.90	266	267(8), 235 (40), 190 (100)	
14	1.80	264	265(30), 234 (100)	
15	1.31	206	207(100), 162 (15)	
16	6.26	172	173(100), 155 (20)	
17	2.71	216	217(100), 171 (10)	
18	3.63	191		

Table E.1 (continue).

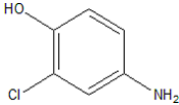
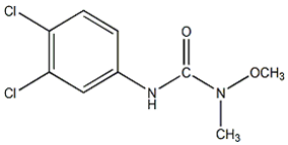
compound	retention time (min)	molecular weight (m/z)	molecular ion and fragmentations	photoproduct
19	1.04	145		
20 (linuron)	3.15	250	249	

Table E2 Mass fraction of intermediates from degradation of diuron at pH7.

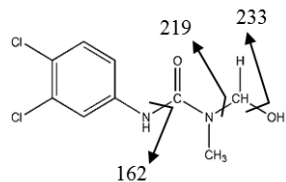
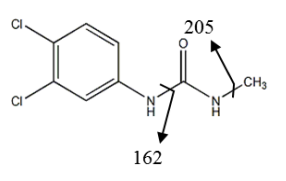
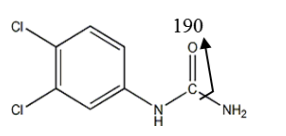
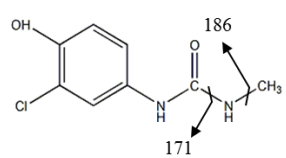
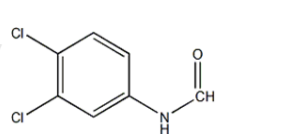
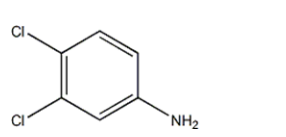
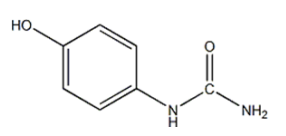
compound	retention time (min)	molecular weight (m/z)	molecular ion and fragmentations	photoproduct
1	3.00	249	250 (5), 233 (100), 219 (65), 162 (25)	
2	2.65	219	220 (100), 205 (68), 162 (27)	
3	2.70	205	206 (100), 190 (27)	
4	2.05	200	201 (100), 186 (40), 171 (12)	
5	2.00	190		
6	2.50	162		
7	1.00	152		

Table E.3 (continue).

compound	Retention time (min)	molecular weight (m/z)	molecular ion and fragmentations	photoproduct
8	1.04	143		
9	2.65	265	266 (12), 235 (100), 206 (68), 163 (21)	
10	2.15	281	282 (15), 235 (100), 178 (65), 163 (27)	
11	2.6	214	215 (100), 171 (18)	
12	3.03	230	231 (100), 171 (15)	
13	1.50	123		
14	1.65	109		

Table E.3 (continue).

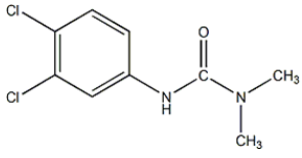
compound	retention time (min)	molecular weight (m/z)	molecular ion and fragmentations	photoproduct
15 (diuron)	3.51	233	234	



Table E 3 Mass fraction of intermediates from degradation of diuron at pH4 and pH10.

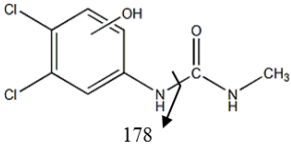
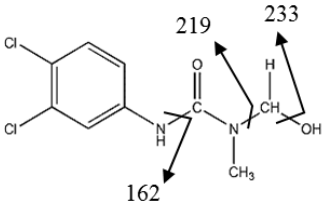
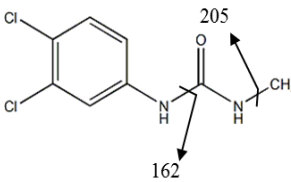
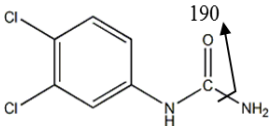
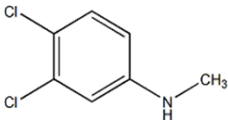
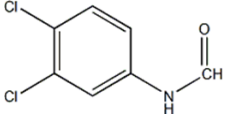
compound	Retention time (min)	molecular weight (m/z)	molecular ion and fragmentations	photoproduct
1	12.5	235	236 (100), 178 (14)	
2	3.00	249	250 (5), 233 (100), 219 (65), 162 (25)	
3	2.65	219	220 (100), 205 (68), 162 (27)	
4	2.70	205	206 (100), 190 (27)	
5	1.09	176		
6	2.00	190		

Table E.3 (continue).

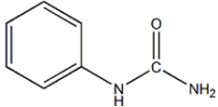
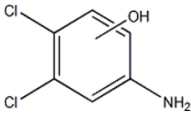
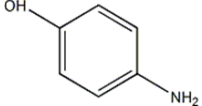
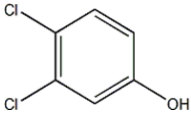
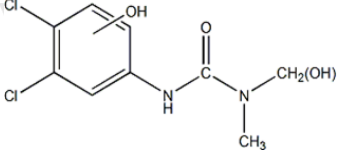
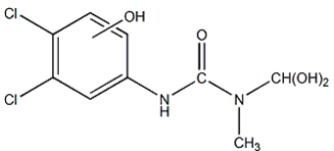
compound	Retention time (min)	molecular weight (m/z)	molecular ion and fragmentations	Photoproduct
7	3.05	136		
8	2.50	178		
9	1.65	109		
10	1.80	163		
11	2.65	265	266 (12), 236 (100), 207 (68), 163 (21)	
12	2.15	281	282 (15), 235 (100), 178 (65), 163 (27)	

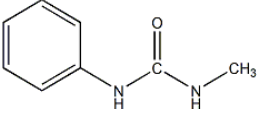
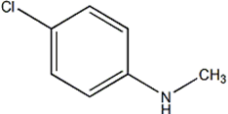
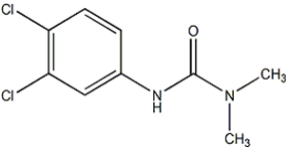
Table E.3 (continue).

compound	Retention time (min)	molecular weight (m/z)	molecular ion and fragmentations	photoproduct
13	2.60	214	215 (100), 171 (18)	
14	7.80	212	213 (100), 184 (18)	
15	7.95	228	229 (100), 171 (12)	
16	10.2	183	184 (100), 170 (40)	
17	7.65	186	187 (100), 171 (32)	
18	2.50	162		

Table E.3 (continue).

compound	Retention time (min)	molecular weight (m/z)	molecular ion and fragmentations	photoproduct
19	10.15	251	252 (8), 205 (100), 162 (28)	
20	1.00	152		
21	1.04	143		
22	12.50	267	268 (10), 221 (100), 206 (76), 163 (25)	
23	13.35	251	252 (15), 221 (100), 163 (32)	
24	2.05	200	201 (100), 186 (40), 171 (12)	

Table E.3 (continue).

compound	Retention time (min)	molecular weight (m/z)	molecular ion and fragmentations	photoproduct
25	5.25	150		
26	5.10	141		
27 (diuron)	3.51	233	234	

APPENDIX F**LIST OF PUBLICATIONS**

Sutaporn Meephon and Varong Pavarajarn. “Adsorption behaviors of diuron, linuron and 3,4-dichloroaniline on zinc oxide nanoparticles”. The 4th German-Thai Symposium on Nanoscience and Nanotechnology, Phitsanulok, Thailand, October 14-17, 2014.

Sutaporn Meephon and Varong Pavarajarn. “Comparative investigation on behavior of phenyl urea herbicides onto ZnO nanoparticles and nanorods”. The 15th AIChE Annual meeting, Salt Lake city, Utah, USA, November 8-13, 2015.

Sutaporn Meephon, Thanyada Rungrotmongkol, Nopporn Kaiyawet, Somchintana Puttamat and Varong Pavarajarn. “The influence of adsorption behavior on the formation of degradation intermediates: A case study of photocatalytic degradation of diuron on ZnO”. The 10th World Congress of Chemical Engineering, Barcelona, Spain, October 1-5, 2017.

Sutaporn Meephon, Thanyada Rungrotmongkol, Nopporn Kaiyawet, Somchintana Puttamat and Varong Pavarajarn. “Surface-dependence of adsorption and its influence on heterogeneous photocatalytic reaction: A case of photocatalytic degradation of linuron on zinc oxide”. Catalyst Letter (2018) 148:873-881.

VITA

Ms. Sutaporn Meephon was born in Bangkok, on December 26, 1989. She finished her high school from Thammasat Klongluang Wittayakom, Pathum Thani in 2008. She received her Bachelor's Degree in Chemical Engineering from King Mongkut's University of Technology Thonburi in 2012. She consecutively continued her Ph.D. in Chemical Engineering at Chulalongkorn University since May 2012.

